Electronic Theses and Dissertations

2022

A Non-Reacting Passive Scalar Comparison of StarCCM and OpenFOAM in a Supersonic Cavity Flame Holder

Thomas Nuese
South Dakota State University, thomas.nuese@jacks.sdstate.edu

A NON-REACTING PASSIVE SCALAR COMPARISON OF STARCCM AND

OPENFOAM IN A SUPERSONIC CAVITY FLAME HOLDER

BY:

THOMAS NUESE

A thesis submitted in partial fulfillment of the requirements of the

Master of Science

Major in Mechanical Engineering

South Dakota State University

2022

THESIS ACCEPTANCE PAGE

Thomas Nuese

This thesis is approved as a creditable and independent investigation by a candidate for

the master's degree and is acceptable for meeting the thesis requirements for this degree.

Acceptance of this does not imply that the conclusions reached by the candidate are

necessarily the conclusions of the major department.

Jeffrey Doom
 Advisor   Date

Yucheng Liu
Department Head   Date

Nicole Lounsbery, PhD
Director, Graduate School Date

ACKNOWLEDGEMENTS

TABLE OF CONTENTS

ABBREVIATIONS

V_0: Inlet velocity of the gas, m/s

P_0: Inlet Pressure of the gas, pa

T_0: Inlet Temperature of the gas, ºC

ρ_0: Density at Inlet of the gas, kg/m^3

c_p: Specific heat at constant pressure, J/kg K

c_v: Specific heat constant-volume, J/kg K

V^*: Carrier gas velocity at nozzle throat, m/s

P^*: Carrier gas pressure at nozzle throat, pa

T^*: Carrier gas temperature at nozzle throat, ºC

ρ^*: Density of the carrier gas at the nozzle throat, kg/m^3

A^*: Cross-sectional area at the nozzle throat, m^2

R: Gas constant, J/mol·K (8.314 J/mol·K)

ṁ: Mass flow rate, kg/s

M: Mach number

γ: Adiabatic Index

LIST OF FIGURES

ABSTRACT

A NON-REACTING PASSIVE SCALAR COMPARISON OF STARCCM AND

OPENFOAM IN A SUPERSONIC CAVITY FLAME HOLDER

THOMAS NUESE

2022

The scramjet engine equipped with a modern-day airliner would allow for very quick travel across the United States. The major problem is that designing such an engine and testing it to make sure it is safe would cost millions if not billions of dollars. Computational fluid dynamics allows for complex designs to be tested but can still take many days, weeks, or even months to complete. With the use of computational fluid dynamics (CFD), the scramjet engine can be analyzed to determine a quicker way to test and develop a reliable configuration in addition to analyzing the effects of different fuels on performance and efficiency. The current problem, when using CFD to analyze the scramjet engine, is that it cannot solve the simulation in a timely manner, which is very important in industry.

While there are solvers for CFD that have chemistry for combustion, they are extraordinarily complex and again take a large amount of time to converge on a solution. Even solvers that only include a small number of species, such as five to ten, require numerous days or even weeks to converge on a solution when using HPC. Using the passive scalar function within CFD programs, various fuels can be analyzed for mixing, combustion, and performance. The passive scalar mimics injecting dyed air into the geometry; the converged solution displays how the air (fuel) would distribute throughout the geometry as time passes on. In recent years, much research has been done on the

scramjet engine, but much more research and testing are needed before the scramjet engine can become widely accepted for use. Currently, scramjet engines are only utilized for military applications including aircrafts and missiles.

This thesis was conducted to research the effects of using passive scalar mixing to simplify the simulation process of combustion within a scramjet engine cavity. The simulations were performed using Reynolds Average Navier Stokes, Detached Eddy Simulations, and Large Eddy Simulation solvers in StarCCM. In addition, OpenFOAM utilized the sonicFOAM solver to perform simulations. The simulations were based on the Air Force Research Lab, AFRL, scramjet testing model. To assess the accuracy of the simulation results, it is crucial to validate the simulations against experimental data. Therefore, the simulation results were compared with David Peterson's simulation results ([5],[6],[7]) and agreed.

CHAPTER 1: INTRODUCTION

The scramjet engine is capable of very quick flight speeds. A flight speed of five times the speed of sound, or Mach 5 would easily be within its limits. The typical commercial airline flight cruising altitude is about 36,000 feet, or close to 11,000 meters. At this altitude, the air temperature is around negative 70 degrees Fahrenheit or 217 Kelvin. Under these conditions, the speed of sound is around 295 meters per second or 660 miles per hour. An airplane, equipped with a scramjet engine, cruising at Mach 5 would be flying at a speed of 1476 meters per second, or 3,300 miles per hour. The distance around the Earth's equator is about 25,000 miles; this would allow for a round trip of the Earth in just over 7.5 hours. Currently, a nonstop flight from New York to Los Angeles takes a little over 6 hours.

The scramjet, supersonic combustion ramjet, is based on the ramjet engine but combustion takes place in supersonic airflow rather than subsonic airflow. Ramjet engines are a form of jet engine that is equipped with a cone-shaped device protruding from the front of the engine, in order to compress the incoming air into the combustion chamber. The air entering the combustion chamber must have a speed that is less than the speed of sound for proper combustion to occur. Ramjet engines are not capable of producing thrust at zero speed, meaning some other form of engine must be equipped for takeoff. Ramjet engines are commonly seen for propelling missiles since they are a rather simple mechanism.

The ramjet engine begins to lose efficiency at high speeds due to high inlet air temperatures. As the inlet air temperature approaches the outlet air temperature, the amount of energy that can be extracted greatly reduces, causing the thrust to vastly reduce. A new type of engine, the scramjet engine, was developed to combat this problem.

History

The scramjet engine is a derivative of the ramjet engine, but the combustion takes place in supersonic flow rather than subsonic flow. Like ramjet engines, scramjet engines are not capable of producing thrust at zero speed, so an additional thrust-producing engine is necessary. The scramjet engine relies on high flight speeds to compress the incoming air before it is mixed with fuel for combustion.

Research and development of the scramjet engine began in the middle of the twentieth century. Testing of scramjet engines began in the early 1960s. The US and UK were the two main countries to perform this testing. In 1964, Antonio Ferri successfully demonstrated a function scramjet engine producing a net thrust, and later 517 pounds of force. The first patent for the scramjet engine was issued to Dr. Frederick Billig and Dr. Gordon Dugger in 1981 after an order of secrecy was lifted. The patent was submitted in 1964.

It was not until 1991 that the first successful supersonic scramjet flight test was achieved. The test was performed over the Soviet Union in a joint effort between NASA and the Central Institute of Aviation Motors (CIAM), based in the Soviet Union. During the test, the scramjet reached a top speed of Mach 5.5. Following this successful flight test, six more flight tests were performed between 1992 and 1998. The maximum speed was recorded at Mach 6.4 and was reached in 77 seconds. The tests yielded favorable results and gave promising evidence that autonomous hypersonic flight was possible.

After the turn of the century, much progress was made in scramjet engines. The first of these was the HyShot project which successfully demonstrated scramjet combustion in 2002 [1]. The goal of this project was only to demonstrate scramjet combustion, not to

power an aircraft. In 2004, the first flight test of scramjet equipped to an aircraft was successfully completed. This was achieved by the company Hyper-X and their X-43A aircraft [2]. The aircraft was carried by a B-52B to 95,000 ft when it was then released and demonstrated its scramjet engine capabilities. On its first flight, it reached a top speed of Mach 6.8 or close to 5,000 mph for a total of 11 seconds. On a later flight, the X-43A reached a top speed of Mach 9.6 or 6,800 mph. Both of these flights broke the world record for the top speed of an aircraft equipped with an air breathing engine. Figure 1 shows a picture of the X-43A.

Figure 1: NASA X-43A Aircraft [2]

The United States Air Force and the Defense Science and Technology Organization, out of England, formed the HIFire (Hypersonic International Flight Research Experimentation). The goal of this research program is to advance the study of hypersonic technology, in addition, to advance the technology of scramjet-powered aircrafts. The organization is working alongside Boeing to aid in the development of the Boeing X-51 scramjet aircraft

and hypersonic strike missiles. In 2009, Woomera was successful in its test flight of a hypersonic aircraft as part of HiFire.

In 2010, NASA and the US Air Force were successful in their flight test of the X-51A Waverider. Again, the X-51A was carried by a B-52 and released at a height of 70,000 ft. The X-51A used a solid rocket booster to reach a speed of Mach 4.5 and before the scramjet engine was fired up to propel the aircraft to a speed of Mach 5. The Waverider has been tested a few more times with some success and some failures due to various components.

In 2016, ISRO, India's space agency, was successful in the test flight of its twin scramjet aircraft called the Advanced Technology Vehicle, ATV. The ATV is equipped with a two-stage rocket that accelerates the vehicle up to speed before the scramjet engines are ignited. The ATV reached a top speed of Mach 6 at 20,000 m.

Figure 2: ISRO's Scramjet Engine [3]

Working Principle

The principle of scramjet engines is based on the principle of oxygen and combustion of fuel to produce thrust. The scramjet engine is comprised of three sections: a converging inlet, a combustor, and a diverging nozzle. The main purpose of the converging inlet is to compress the incoming, supersonic, atmospheric air before it enters the combustor. The main purpose of the combustor is to mix the fuel with compressed air to ignite the fuel. The main purpose of the diverging nozzle is to use the heat from the combustion of the fuel to generate thrust. Given this type of design, scramjet engines are favorable for supersonic flight as they operate much more efficiently than a jet engine and contain no moving parts. There are limits to this type of configuration, as the scramjet engine operates best in the hypersonic flight regime.

The scramjet engine offers advantages compared to other types of supersonic engines. Unlike rocket engines that carry both fuel and an oxygen agent on board, a scramjet engine relies on oxygen in the atmosphere mixed with fuel for propulsion. This is beneficial for keeping cost and weight lower but limits the scramjet to the suborbital flight regime due to the lack of oxygen in the outer orbital flight regime. The scramjet engine is more favorable than a ramjet engine due to its ability to keep the flow in the supersonic range as opposed to the subsonic range. By keeping the inlet flow speeds supersonic, the scramjet does not overheat as quickly as a ramjet would and is able to operate at much faster flight speeds.

Although the scramjet engine offers many advantages, it does include some disadvantages. One of the disadvantages is that it cannot produce thrust at zero speed. Due to its lack of thrust at zero speed, the aircraft or missile that uses scramjet propulsion must also be equipped with some other form of engine. Typically, a jet turbine engine or a rocket engine

provides the initial acceleration until the scramjet can be initialized. Another disadvantage of the scramjet engine is the cost associated with the testing and development. Since scramjets operate in the supersonic and hypersonic flow regimes, the equipment needed for performing tests is very expensive and highly sophisticated. Currently, CFD offers some help for testing but is not advanced enough to cover all ranges of tests and proves to be very time-consuming.

Figure 3: Test Bed for the X-51 Scramjet Engine [4]

CHAPTER 2: LITERATURE REVIEW

This chapter contains a literature review related to the advancements in simplifying the simulation process for fuel injection in a scramjet engine using the passive scalar. The study done in this thesis is aimed to add more knowledge on scramjet engine fuel combustion simulation and to solve potential problems or questions not answered by the literature available on scramjet engines.

The advancement in aircraft and defense technology has forced researchers to develop improved technologies for quicker methods to model and test new scramjet engine methods.

Wang et al. [8] performed LES simulations combined with a passive scalar method for numerical combustion methods. Simulation results of the passive scalar method were compared to H_2 and had a good agreement. The cavity had a simplified geometry but proved the passive scalar method could be promising in understanding combustion. Peterson et al. [5] performed simulations on a supersonic non-reacting flame holder using a RANS and hybrid RANS LES model. The simulation results were compared to experimental data, with the hybrid model being in better agreement, but still had difficulty in some regions.

Zang et al. [9] performed simulations to assess the validity of OpenFOAM's rhoCentralFoam solver. Various mesh sensitivities were analyzed, and the results were compared to ANSYS FLUENT simulations and proved to be in good agreement.

 Hassan et al. [10] assessed the ability of RANS, LES, and a hybrid RANS-LES modeling approach for supersonic crossflow with injector angles of 30 and 90 degrees. The results

were compared to experimental data, and it was determined that the hybrid model was a good compromise between accuracy and time. The hybrid model also improved results for harder-to-model injection angles.

Brodetsky et al. [11] performed simulations of the supersonic flow around truncated cones with various half angles and flow speeds. It was concluded the internal shock wave origination determines the character of the pressure distribution around the truncated cone. Whether the shock wave appears or not, the pressure measured from the end face approaches an asymptotic value. It was shown that the known boundaries of flow regimes measured for axisymmetric flow around the cones can be used to predict flow regimes in the vertical plane of symmetry of the truncated cone at incidence.

Ruan et al. [12] assessed the ability of LES to predict the compressible flow of multi-species reacting as well as studied the characteristics of reacting zones in a cavity-based scramjet. It was concluded that the LES model has successful and accurate kinetics but are reduced. The combustion was found to take place in the subsonic flow region in the mixing layer above the cavity. The combustion mostly occurred within a range of the residence time between 0.2 and 1.3 milliseconds.

Sebastian et al. [13] performed simulations on the supersonic flow around a spanwise-inclined jet in crossflow at Mach 2.5. A monotonically integrated LES (MILES) was used for analysis. It was determined that spanwise-inclined jet injection into a supersonic boundary layer causes oblique and barrel shocks to form. This led to separation regions both downstream and upstream from the injection site. Near-wall turbulence returned to normal at 20D from the injection site.

 Peltier and Carter [14] simulated the response of a cavity flame holder to a shock-induced distortion. It was determined that fuel injection upstream of the cavity leads to non-uniform combustion within the recirculation region. Direct cavity fueling through the ramp face produced more consistent combustion. It was shown by imaging that at Mach 2, the flame is primarily located at the bottom surface of the cavity for low fuel level injection. As the fuel injection rate increases, the flame moves up the cavity ramp toward the top of the cavity near the shear layer at elevated levels of fuel injection. Further research needs to be done to optimize the fuel injection strategy for a cavity flame holder.

 Qi et al, [15] performed simulations to determine the optimum fuel injection parameters and injection angles of cold kerosene in supersonic scramjets. Various injection angles were used. It was determined that penetration height, span expansion area, and shock wave angle of kerosene fuel droplets all increased with injection angle. As the injection angle increased, the kerosene was more prone to atomization.

Xiong et al. [16] simulated the effects of water content and energy on scramjet engine performance. Along with this, the effects of water injection on the max fuel equivalency ratio were also studied. It was concluded that the specific thrust of a scramjet engine can be increased with the addition of water, but the fuel impulse is decreased. It was further concluded that the maximum fuel equivalency ratio and specific thrust increase with water content at high Mach numbers and decrease at low Mach numbers.

 Li et al. [17] performed a simulation using a RANS model to analyze the effects of fuel injection from single and multiple walls, fuel equivalency ration, and axial injection position on engine performance. It was concluded that a single-wall fuel injection should be used for low Mach numbers and a multiple-wall fuel injection for high Mach numbers.

It was also determined that moving the fuel injector forward on two-stage fuel injection decreased engine performance.

Kummitha [18] simulated passive techniques to improve fuel and air mixture in scramjets. These three techniques were: a uniform zigzag surface, small parabola shape cavities, and bumps at the lower wall of the combustion chamber. It was concluded that parabola cavities are helpful to reduce the ignition delay and increase the tendency for early ignition and act as a flame holder. Parabola shape bumps are helpful for the creation of bow shocks and boundary layer separation. Lastly, the uniform zigzag surface (wavy wall) technique gave the best highest mixing and combustion efficiency.

Cao et al. [19] investigated various fuel injection schemes using ethylene. In the first case, all the ethylene is injected upstream of the cavity, in the second case 75% is injected upstream, and the remaining 25% into the cavity floor. It was concluded that combustion in the cavity region is weak when all fuel is injected upstream. When fuel is injected into both regions, there is better combustion efficiency.

Most of the recent research that has been conducted, has looked at several ways to improve fuel injection by using a diverse range of different methods. Other research has looked at using RANS, LES, or some modified form of a hybrid RANS-LES model for accurately predicting the fluid flow and mixing of fuel and air. Alternatively, numerous fuels, in a solid or gaseous state, have been researched for potential use in powering scramjet engines. There still remains room for improvement in simplifying simulations to accurately model the mixing of fuel and air and the combustion process. The current issue still remains that scramjet engine simulations take massive amounts of time and computation ability.

Research Objective

Despite these new critical findings, several vital problems still present themselves to be further investigated. Much of the current research on scramjet engines is still quite difficult. Whether it be testing, which is immensely expensive, or computing CFD simulations which are vastly time-consuming. Little research has been conducted on simplifying the fuel injection and combustion process of CFD simulations using the passive scalar. The goal of this current study further investigates the passive scalar to determine if it can be used to simplify the CFD simulation process. This will be done using StarCCM+ and OpenFOAM. The results of the two programs will be compared to check their validity.

CHAPTER 3: METHOD AND APPROACH

The methods and techniques used in the modeling and simulation of scramjet engine combustion chambers and the corresponding CFD analysis are discussed in this chapter.

Methodology

- Problem Statement
- Geometry
- CAD Model Generation
- Discretization
- Physics
- Solution
- Visualization
- Validation

Problem statement

The problem addressed in this research is:

Is the passive scalar capable of predicting the theoretical combustion location in a

supersonic cavity flame holder for both StarCCM and OpenFOAM?

Geometry

The geometry used to conduct the simulations consisted of a supersonic combustion chamber. The chamber is comprised of an inlet nozzle, an isolator, and a test section. The inlet provides constant airflow at Mach 2. The test section contains the flame holder cavity, which is where fuel is injected from the 11 equally spaced injectors. To simplify and speed up the simulation process, only one injector was included. Figure 4 shows a further explanation of the supersonic combustion chamber geometry.
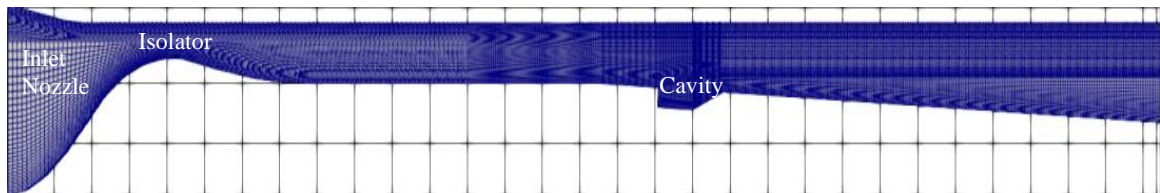
Figure 4: Combustion Chamber Geometry

<u>Plotted Geometry</u>
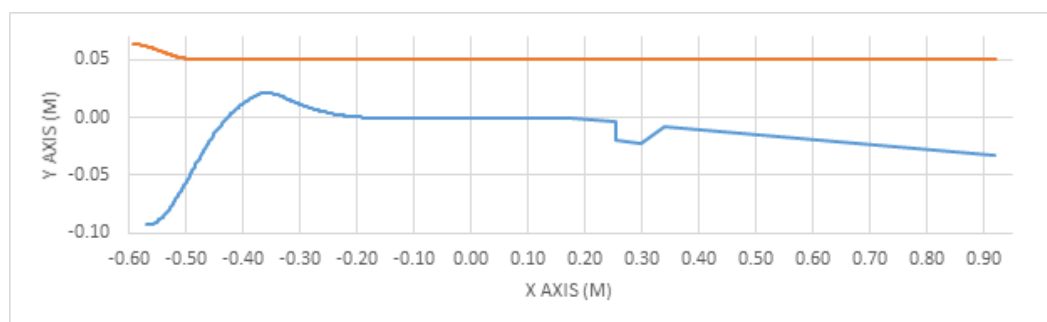
Figure 5: Plotted Combustion Chamber Geometry

Figure 5 shows a plot of the combustion chamber geometry. The geometry-shape was obtained from the Air Force Research Lab (AFRL). This is the same geometry as their actual test combustion chamber. The geometry was plotted in excel and imported into StarCCM+ and OpenFOAM.
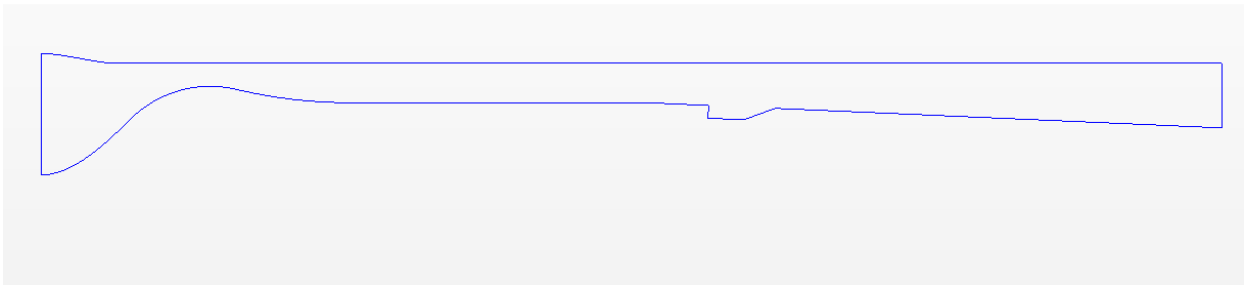
Figure 6: Geometry
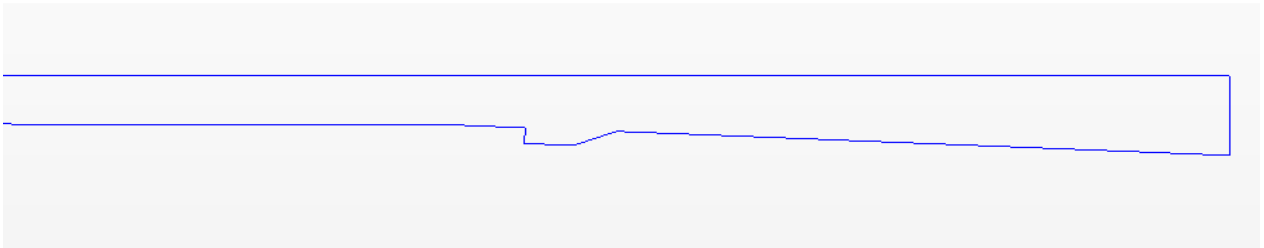
Figure 7: Modified Geometry

Figure 6 shows the geometry after the lines generated in excel were imported into StarCCM+ and OpenFOAM. Figure 7 shows the modified geometry that was used in the simulation process.

CAD Model Generation

CAD Models of the geometries provided in the geometry section were generated using the StarCCM+ software and OpenFOAM software. The procedure for CAD Modeling in StarCCM+ is briefly provided in the Appendix section. Figures 8 and 9 shows the CAD models for both StarCCM and OpenFOAM.

Figure 8: StarCCM+ CAD Model of Supersonic Combustion Chamber

Figure 9: OpenFOAM Model of Supersonic Combustion Chamber

For the simplicity of the simulations, the inlet nozzle and isolator section of the geometry were left off, and boundary conditions were imposed to ensure accuracy. By removing these two sections, the total number of cells could be reduced while still providing the same degree of accuracy. This also sped up the simulation process.

Discretization

Discretization can be done through many different methods, but the two main methods are mesh, or grid methods, and mesh-free methods. The easier and more frequently used of the two methods is the mesh method. When using the meshing method, the region of interest is portioned into smaller sections. Depending on the meshing method used, these sections can have various shapes. For two-dimensional geometries, sections are broken into squares or triangles. When a three-dimensional geometry is meshed, it is further broken into tetrahedrons or hexahedrons. Then, governing equations are discretized over the mesh. These consist of the Finite Difference Method, the Finite Element Method, and the Finite

Volume Method in Computational Fluid Dynamics for discretization methods. In this particular case, the geometry of interest was a 3D body.

Meshing models used for the simulation

- Extruder

- Prism Layer Mesher

- Surface Wrapper

- Surface Remesher

- Trimmer

Detailed instructions for performing the meshing operation are provided in the Appendix section.

Shortened Supersonic Combustion Chamber Mesh

Figure 10 shows the mesh of the shortened supersonic combustion chamber. Figure 11 shows a closer view of the mesh specifically looking close at the flame holder cavity.
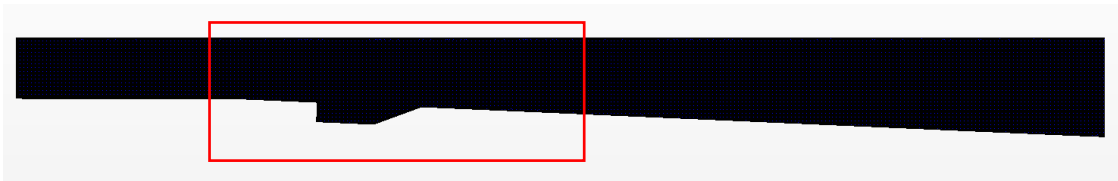
Figure 10: StarCCM Mesh
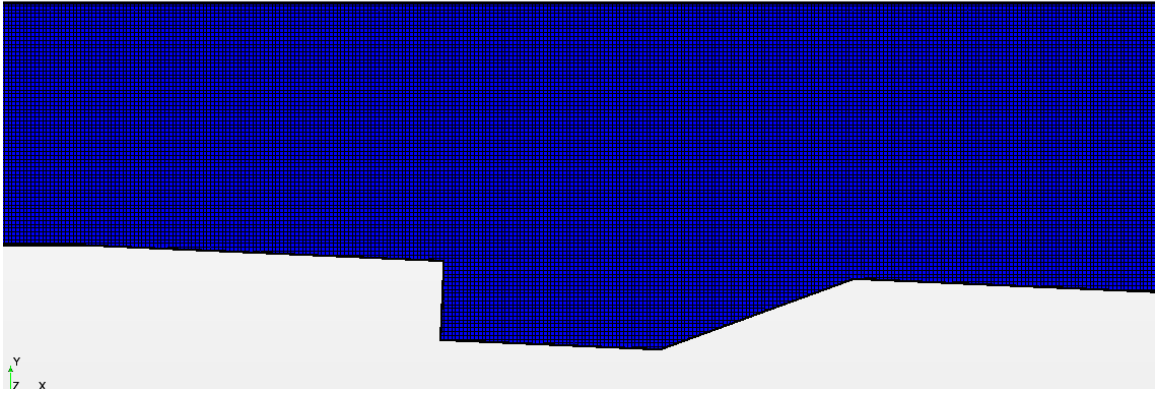
Figure 11: Zoomed in StarCCM+ Mesh

The total number of cells for the mesh came out to be 996,762. The total number of faces for the mesh was 2,937,144.

For the OpenFOAM mesh, the default blockMesh tool was used to generate a hexahedral mesh. The mesh was slightly modified to contain more cells in the flame holder cavity. The meshed geometry as well as a zoomed-in mesh can be seen in Figures 12 and 13.
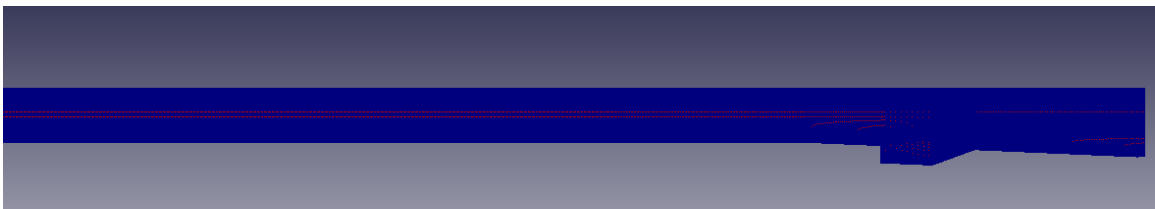
Figure 12: OpenFOAM Mesh
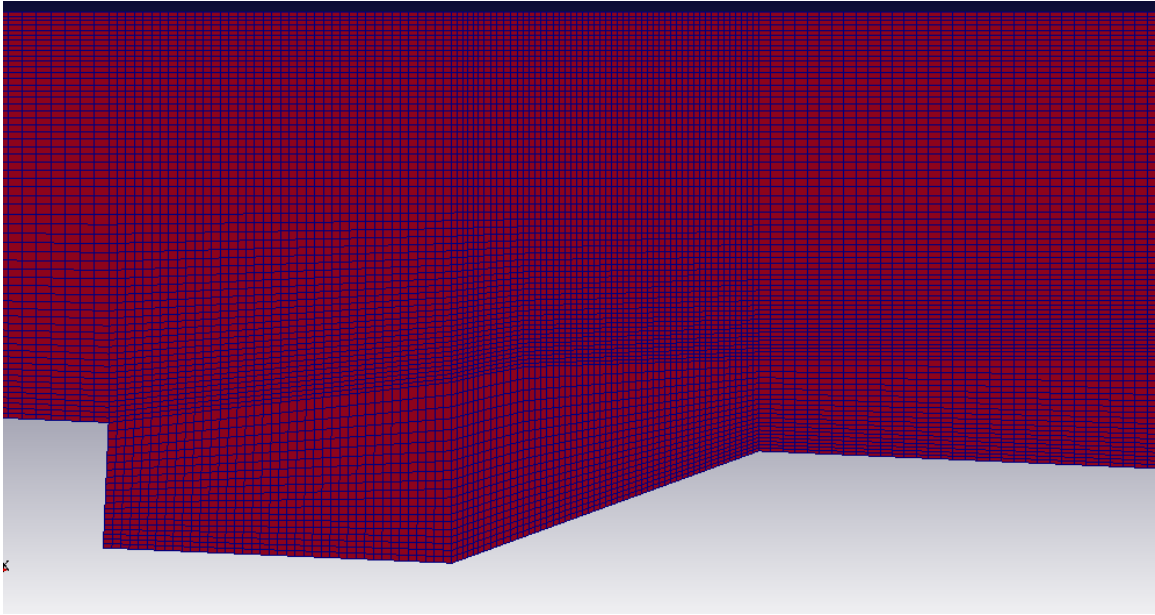
Figure 13: Zoomed in OpenFOAM Mesh

Physics

Some initial calculations were performed using the following equations below to determine boundary conditions of the geometry inlet, as the incoming air is accelerated to reach supersonic speeds.

Nozzle throat is referred to the smaller cross-section area of the converging/diverging nozzle. The inlet air temperature at nozzle throat (T^*) is defined as

$$\frac{T_0}{T^*} = 1 + \frac{\gamma - 1}{2}$$

$$T^* = \frac{T_0}{1 + \frac{\gamma - 1}{2}}$$

Inlet air velocity at nozzle throat (V^*) is defined as

$$V^* = \sqrt{\gamma R T^*}$$

The mass flow rate (ṁ) of the fuel can be defined by

$$\rho^* = \frac{\dot{m}}{V^* A^*}$$

The inlet air pressure at the nozzle throat can be determined using the ideal gas law:

$$P^* = \rho^* R T^*$$

The stagnation pressure at the nozzle throat can be defined using the isentropic relations

$$\frac{P_o}{P^*} = \left(\frac{T_0}{T^*}\right)^{\frac{\gamma}{\gamma-1}}$$

$$\frac{P_o}{P^*} = \left(1 + \frac{\gamma-1}{2}\right)^{\frac{\gamma}{\gamma-1}}$$

$$P_0 = P^* \left(1 + \frac{\gamma-1}{2}\right)^{\frac{\gamma}{\gamma-1}}$$

Once the parameters at the throat are defined, it is possible to determine these quantities along the diverging section of the nozzle. When the variation of the nozzle cross-sectional area is specified, the corresponding Mach number (M) can be determined using the following equation

$$\frac{A}{A^*} = \left(\frac{1}{M}\right)\left[\left(\frac{2}{\gamma+1}\right)\left(1 + M^2 \frac{\gamma-1}{2}\right)\right]^{\frac{\gamma+1}{[2(\gamma-1)]}}$$

Once the Mach number is obtained at a given cross-sectional area of the diverging nozzle section, the remaining corresponding values can be determined by using the following isentropic relations

$$\frac{P}{P^*} = \left(\frac{\gamma + 1}{2 + (\gamma - 1)M^2}\right)^{\frac{\gamma}{\gamma-1}}$$

$$P = P^*\left(\frac{\gamma + 1}{2 + (\gamma - 1)M^2}\right)^{\frac{\gamma}{\gamma-1}}$$

$$\frac{T_o}{T} = 1 + \frac{\gamma - 1}{2}M^2$$

$$T = \frac{T_o}{1 + \frac{\gamma - 1}{2}M^2}$$

$$\frac{\rho_o}{\rho} = \left(1 + \frac{\gamma - 1}{2}M^2\right)^{\frac{1}{(\gamma-1)}}$$

$$\rho = \frac{\rho_o}{\left(1 + \frac{\gamma - 1}{2}M^2\right)^{\frac{1}{(\gamma-1)}}}$$

Governing equations

The flow in the supersonic combustion chamber was considered to be supersonic turbulent flow. The governing equations are the unsteady, compressible, Navier-Stokes equations, which can be broken down into three equations, and the passive scalar equation.

- Continuity equation,

- Momentum equation,

- Energy equation, and

- Passive Scalar Equation

Continuity equation:

$$\frac{\partial \rho}{\partial t} + \frac{\partial}{\partial x_i}(\rho u_j) = 0$$

Momentum Equation:

$$\frac{\partial(\rho u_i)}{\partial t} + \frac{\partial(\rho u_i u_j)}{\partial x_j} = -\frac{\partial P}{\partial x_i} + \left[\frac{\partial \tau_{ij}}{\partial x_j}\right]$$

$$\tau_{ij} = \mu\left[\frac{\partial u_i}{\partial x_j} + \frac{\partial u_j}{\partial x_j} - \frac{2}{3}\frac{\partial u_k}{\partial x_k}\delta_{ij}\right]$$
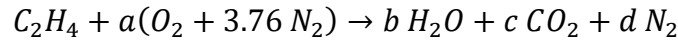
Energy Equation:

$$\frac{\partial \rho E}{\partial t} + \frac{\partial}{\partial t}(\rho E + P) = \frac{\partial \tau_{ij}}{\partial x_j}u_i + \frac{\partial}{\partial x_j}\left(k\frac{\partial T}{\partial x_j}\right)$$

Passive Scalar Equation:

$$\frac{\partial \rho Z}{\partial t} + \frac{\partial \rho Z u_j}{\partial x_j} = \frac{\partial}{\partial x_j}\left(\rho D\frac{\partial Z}{\partial x_j}\right)$$

In addition, the chemical reaction of ethylene is important for determining where combustion will occur. The chemistry equation can be seen below.

$$C_2H_4 + a(O_2 + 3.76\ N_2) \rightarrow b\ H_2O + c\ CO_2 + d\ N_2$$

To solve this equation, a MATLAB code was developed to balance the equation as well as to calculate the other necessary parameters needed for the analysis of the results. These values can be seen in Figure 14.

```
MW = 28.000 [Molecular Weight],
a = 3.00 [O2 + 3.76N2],
b = 2.00 [H2O],
c = 2.00 [CO2],
d = 11.28 [N2],
Mole Fraction CH = 0.0700 [CH],
Mole Fraction O2 = 0.2101 [O2],
Mole Fraction N2 Reactant = 0.7899 [N2 R],
Mass Fraction O2 = 0.2331 [O2],
Mass Fraction N2 Reactant = 0.7669 [N2 R],
Mass Fraction Fuel = 1.0000 [FC2H4],
Mass Fraction N2 Reactant = 0.7669 [N2 R],
AFst = 14.7900 [Air Fuel],
s = 3.4286 [s],
phi = 14.7086,
Zst = 0.06366,
```

Figure 14: Ethylene Calculation Values

The value of most importance in this output is the Z_{st} value. This corresponds to the mixture fraction of ethylene and air. This is the theoretical value at which ethylene and air should be "most reactive" when mixed. When viewing simulation results, this is the value to look for in both mixture fraction and passive scalar scenes.

Solver Settings

Fluid motion equations are overly complex and mostly require computational ways to solve. The CFD program solves the Navier-Stokes equations for compressible flow. In this study, CFD simulations were performed using StarCCM and OpenFOAM to predict the gas flow field.

Selected Physics Models for the simulation

- All y+ Wall Treatment

- Three Dimensional

- Steady State/ Unsteady

- Fluid: Gas (Ethylene)

- Ideal Gas

- Multi-Component Gas

- Reynolds Averaged Navier Stokes (RANS)/ Large Eddy Simulation (LES)/ Detached Eddy Simulation (DES)

- Coupled Flow

- Coupled Energy

- Coupled Species

- Non-reacting/Reacting

- Gradients

- Turbulent Flow

- SST K – Omega

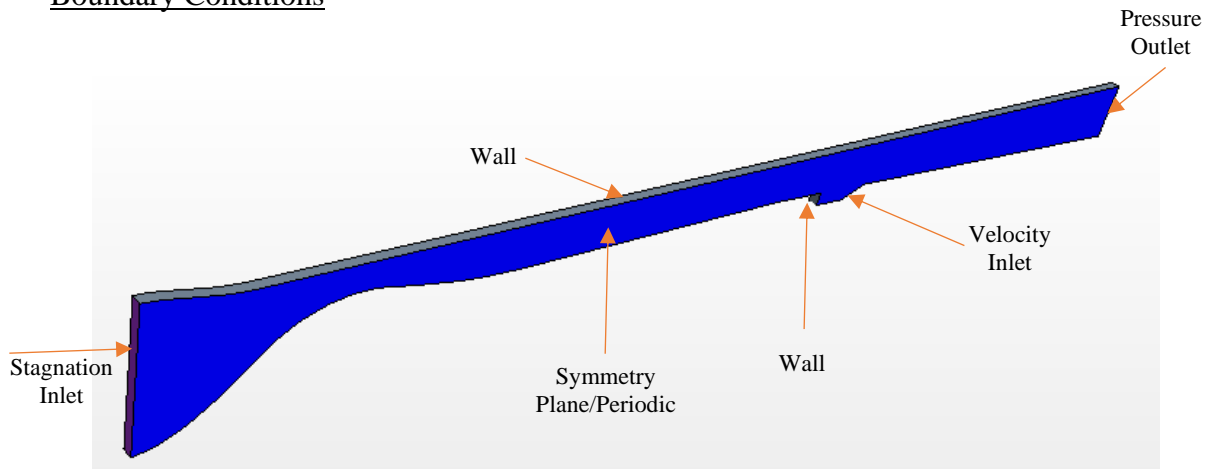- Passive Scalar

- Wall Distance

Further explanation of selecting physics models can be found in the Appendix section.

For the OpenFOAM case, the sonicFOAM solver was used for the non-reacting case.

<u>Primary Input variables</u>

- Air Inlet Pressure: 483,000 Pa

- Air Inlet Temperature: 589 K

- Fuel gas type: Ethylene

<u>Boundary Conditions</u>

Figure 15: Model with Boundary Conditions

Summary of Boundary Conditions used for various nozzles

Figure 15 shows the boundary conditions that were used for the simulations. The inlet was set to a stagnation, or pressure, inlet with a total pressure of 483,000 Pa. The outlet was set to a pressure outlet. The top and bottom of the geometry were defined as walls. Lastly, the front and back of the geometry were defined as symmetry planes initially and later changed to be set to a periodic boundary condition for better validity of results. OpenFOAM simulations were run after the StarCCM simulations, so the boundary in OpenFOAM was always periodic.

CHAPTER 4: RESULTS AND DISCUSSION

In this chapter, the calculated results obtained from the numerical simulations are visualized, and the results are validated. For visualization, a scalar cross-section view along with an XY plot at the center axis with various scalar fields are provided. The data obtained from the simulations are plotted and compared to experimental data as well as other previous simulation data from the AFRL. A MATLAB code was developed to plot the data.

Initially, simulations by Dave Peterson ([5],[6],[7]) were studied and replicated to ensure that this research work would be possible. As with any new research, existing findings needed to be replicated before new research could be studied. As a result, a simple flame holder cavity has initially modeled in StarCCM using the dimensions given. Results for this initial verification can be seen below. The simulations were run at Mach 2 with no fuel injection and no passive scalar enabled. Figures 16-19 show the simple model and initial results.
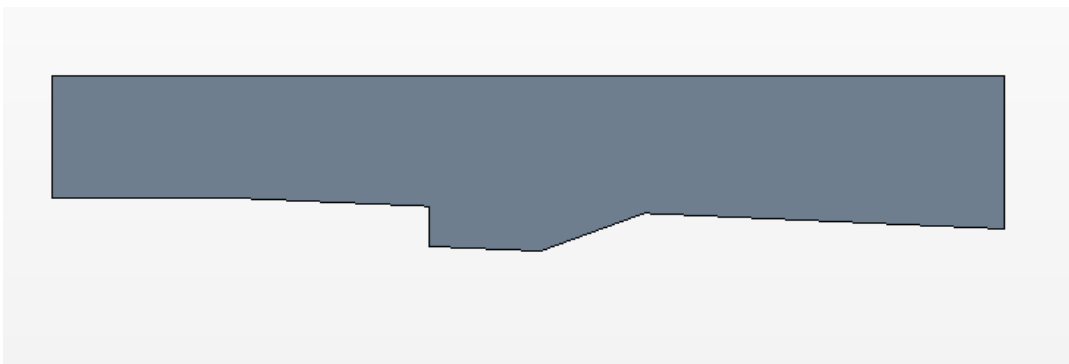
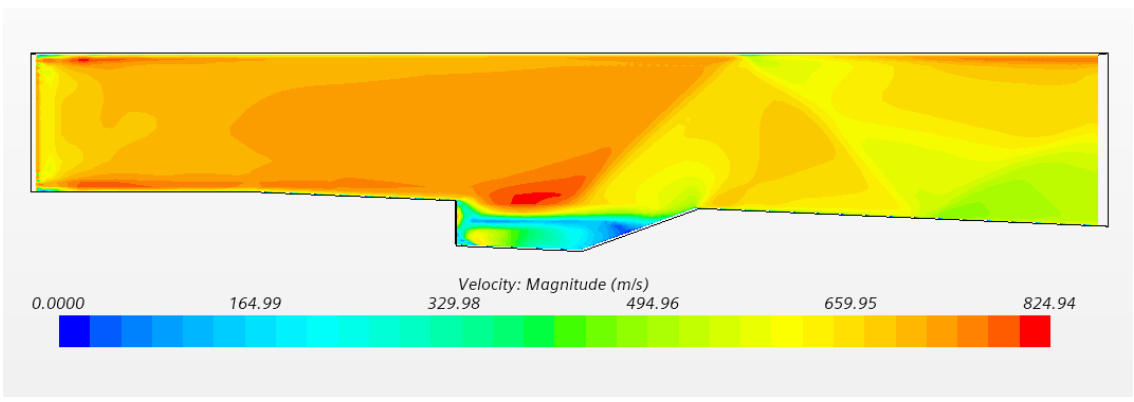*Figure 16: Geometry of Simple Flame Holder Cavity*

Visualization

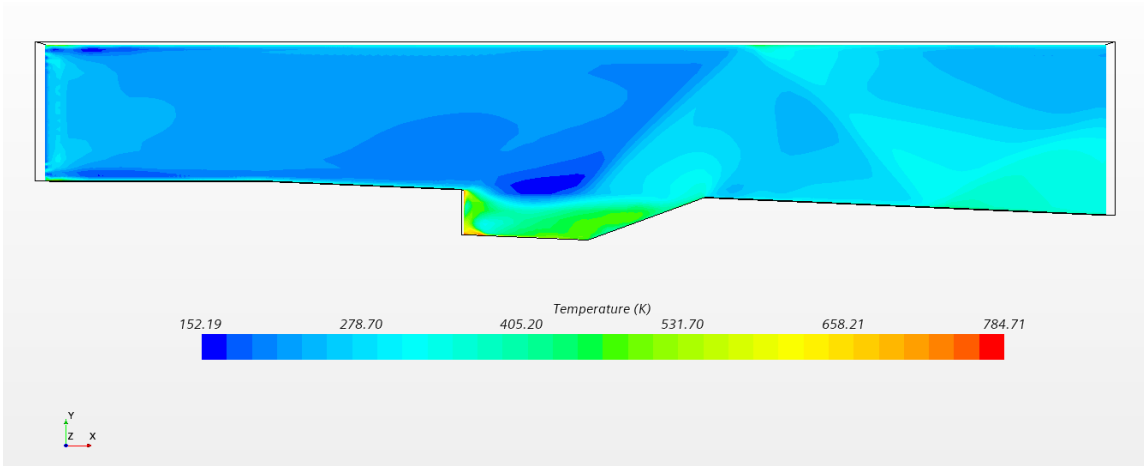*Figure 17: Velocity Scene of Simple Flame Holder Cavity*

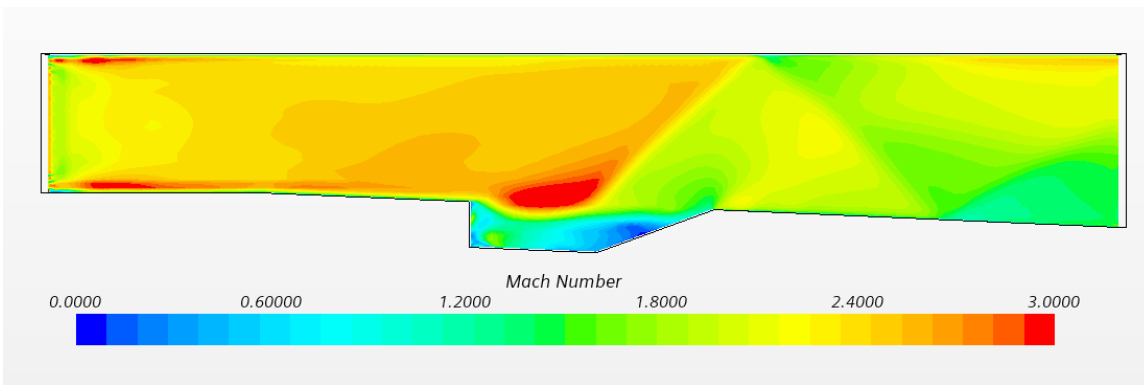*Figure 18: Temperature Scene of Simple Flame Holder Cavity*

Figure 19: Mach Number Scene of Simple Flame Holder Cavity

Upon completion of the simulations, data was extracted from the cavity region to be compared to previous findings. The plots for this can be seen below. The normalized x component of the velocity is plotted, on the x-axis, as a function of the freestream velocity within the cavity. The y axis is the vertical distance within the cavity. Four separate locations within the flame holder cavity were studied: 26.5 cm, 28.4 cm, 30.2 cm, and 32.0 cm. These values are the distance from the start of the geometry right after the isolator.
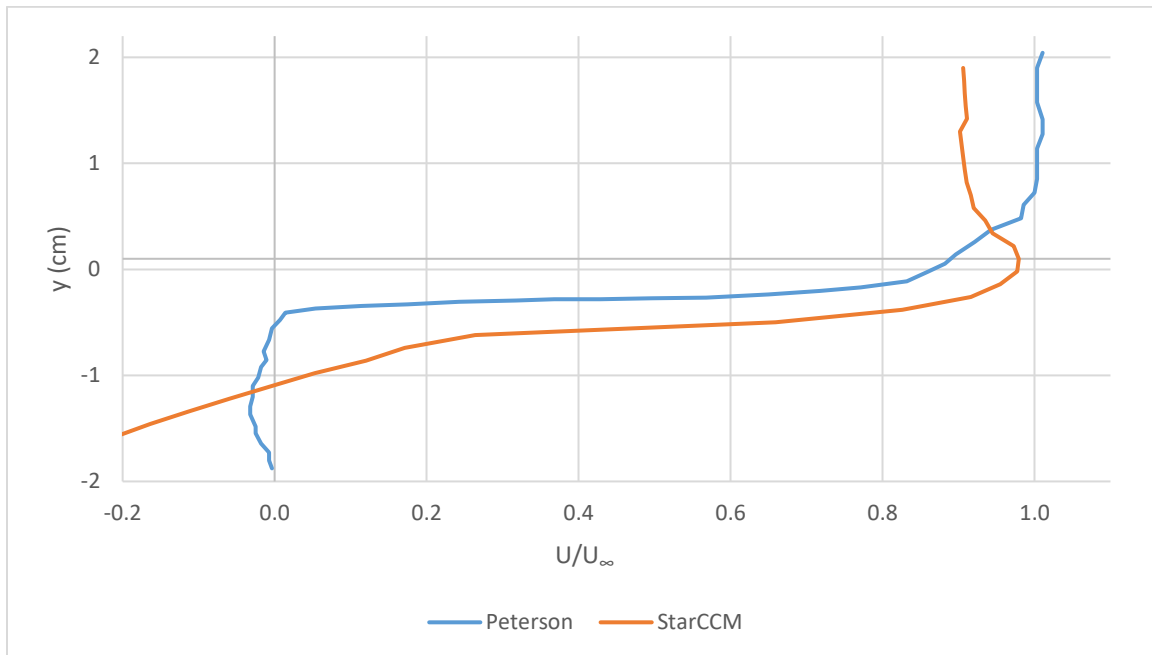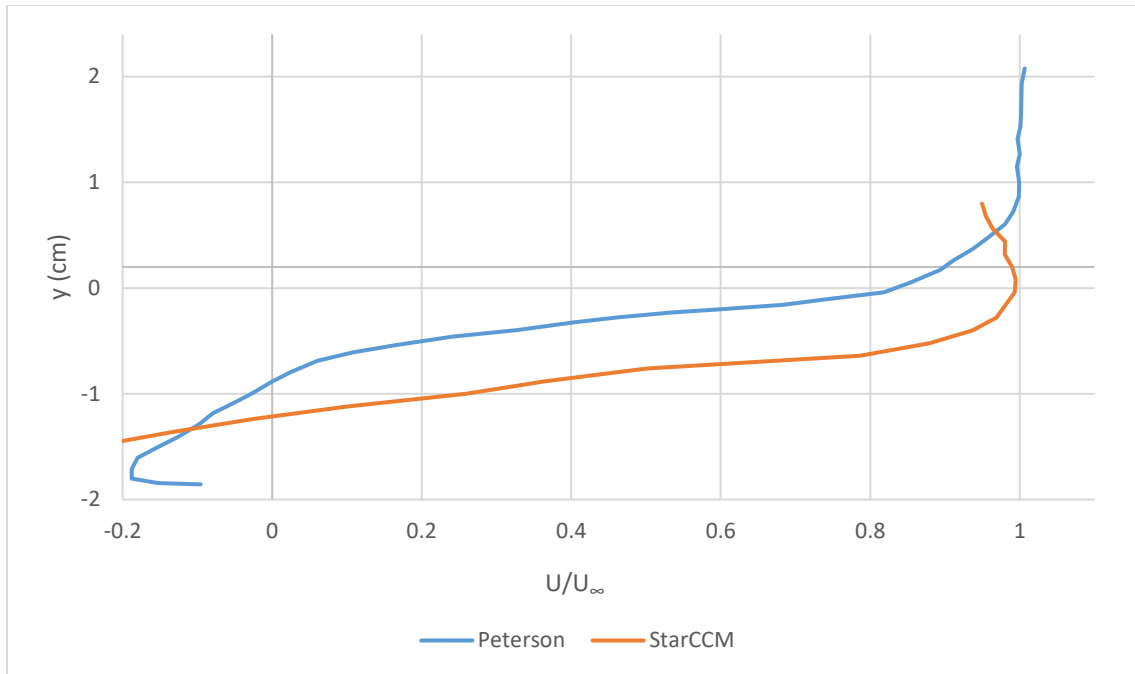

Figure 20: 26.5 cm Data
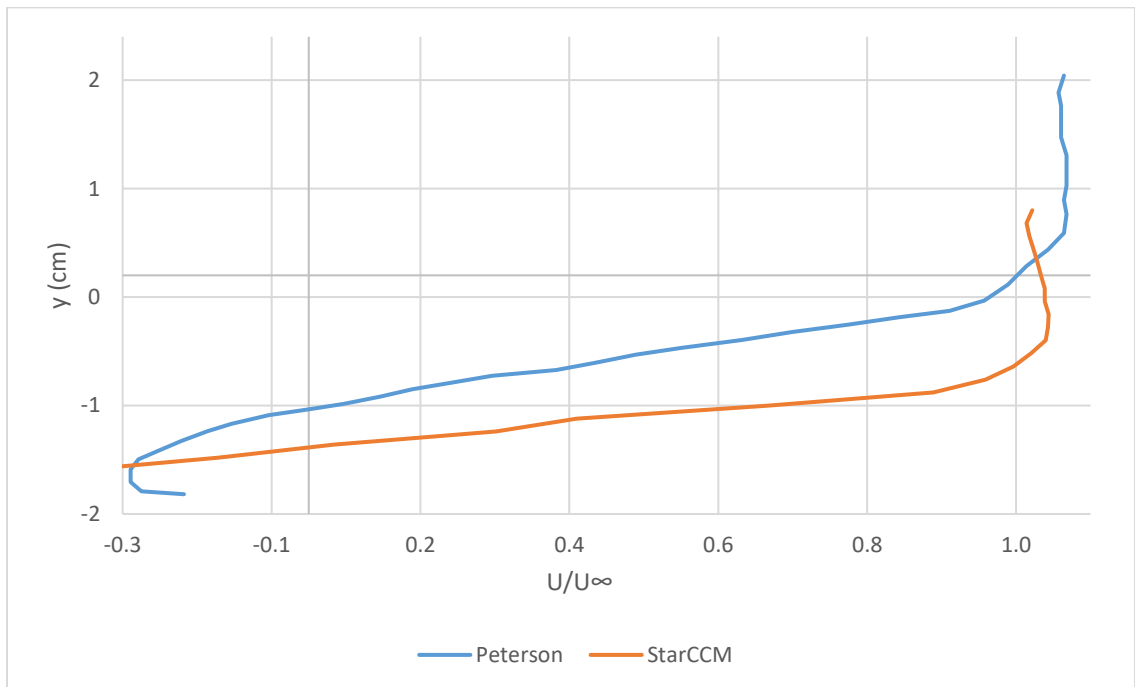
Figure 21: 28.4 cm Data

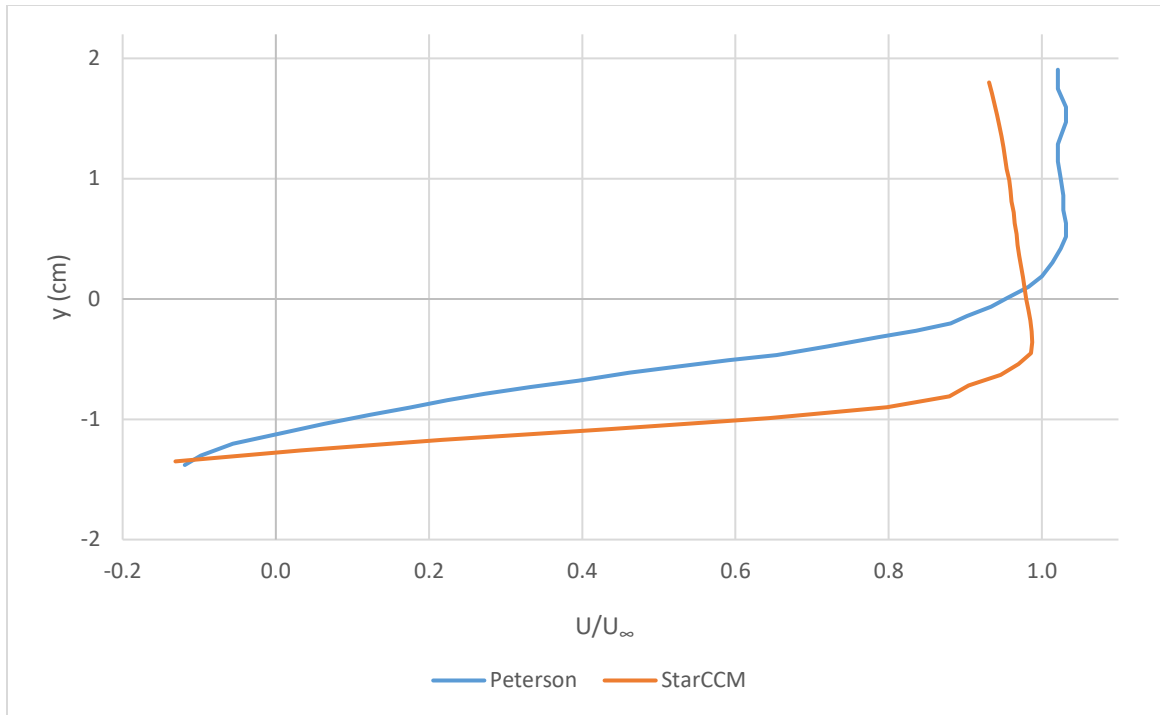

Figure 22: 30.2 cm Data

Figure 23: 32.0 cm Data

As seen in Figures 20-23, the simulations agree with previous simulations. The small values of the x-axis of the StarCCM data are in some disagreement due to no injection being used in the simulations that were run. Other causes of deviations within the data are due to a much smaller number of mesh cells being used to speed up simulation times.

Upon completion of the initial validation, the actual cavity that is used at the AFRL for research was used for the rest of the research.

After trying numerous different mesh sizes and a few different mesh techniques, the above meshing models worked the best, but still had substantial amounts of trouble when trying to perform simulations at a Mach 2 inlet speed. The simulation would work at subsonic speeds, but once supersonic speeds were set, the simulation would fail. The supersonic combustion chamber was also shortened, to try and aid in the stability of the simulation,

but this proved to be unsuccessful as well. The simulation ran for a few hundred iterations, but still failed and gave the error message seen in Figure 24.
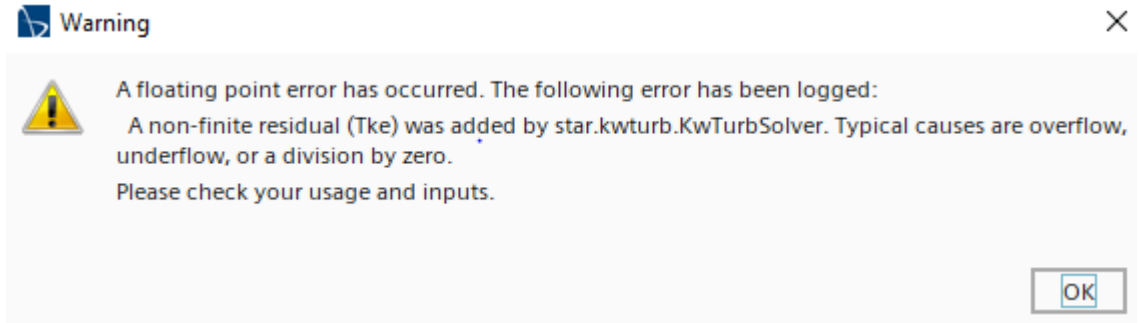
Figure 24: Error Message from StarCCM+

After a further explanation from the Air Force Research Lab, it was concluded that a stagnation inlet boundary condition might fix the error. The inlet was switched from a velocity inlet to a stagnation inlet with a total pressure of 483,000 Pa and a total temperature of 589 K. The simulation was initialized following the swap from a velocity inlet to pressure or stagnation inlet.

RANS Case with No Fuel Injection

To begin, the first set of simulations using the actual AFRL geometry was the simplest case. This included running RANS, or Reynolds Averaged Navier Stokes, simulations. The injector was initially left out of the simulations to verify that it was possible to get accurate simulation results. The simulation proved to be successful, and the results can be seen in the next few pages.
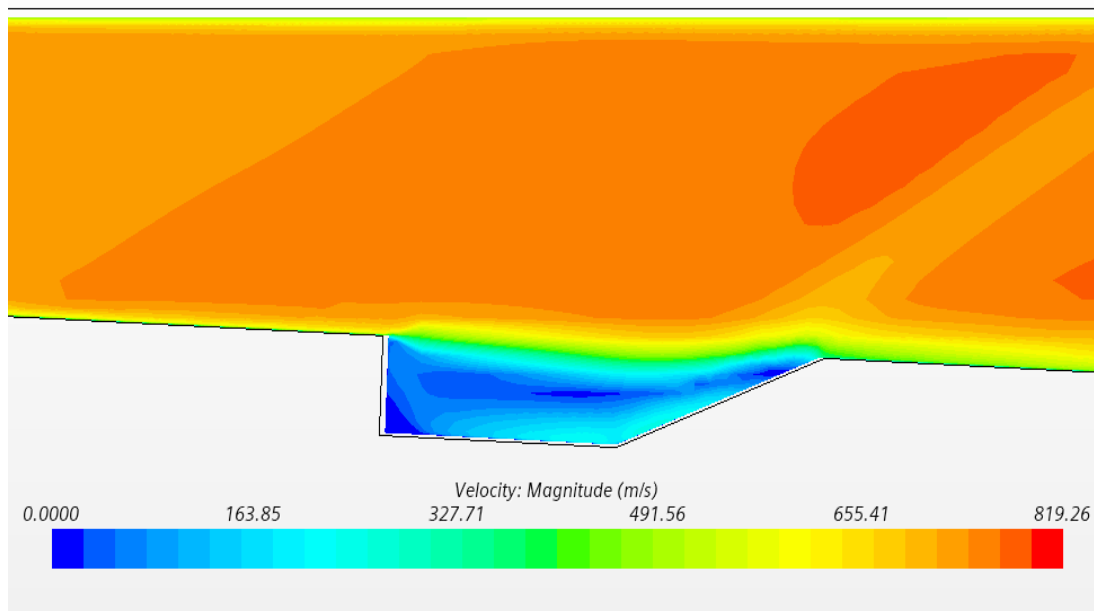
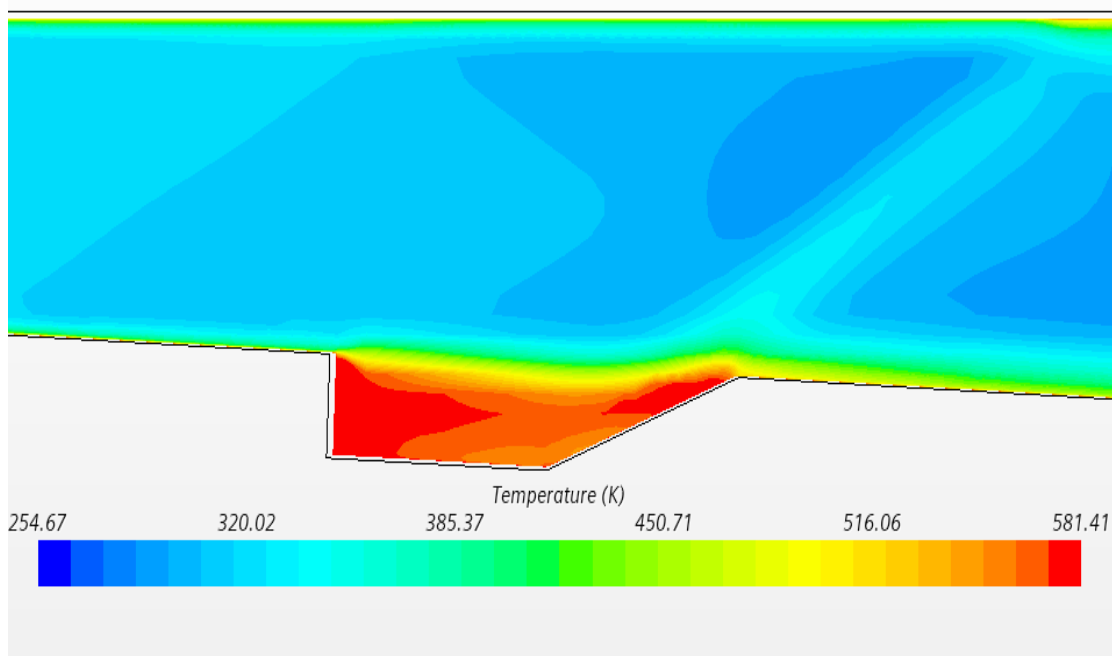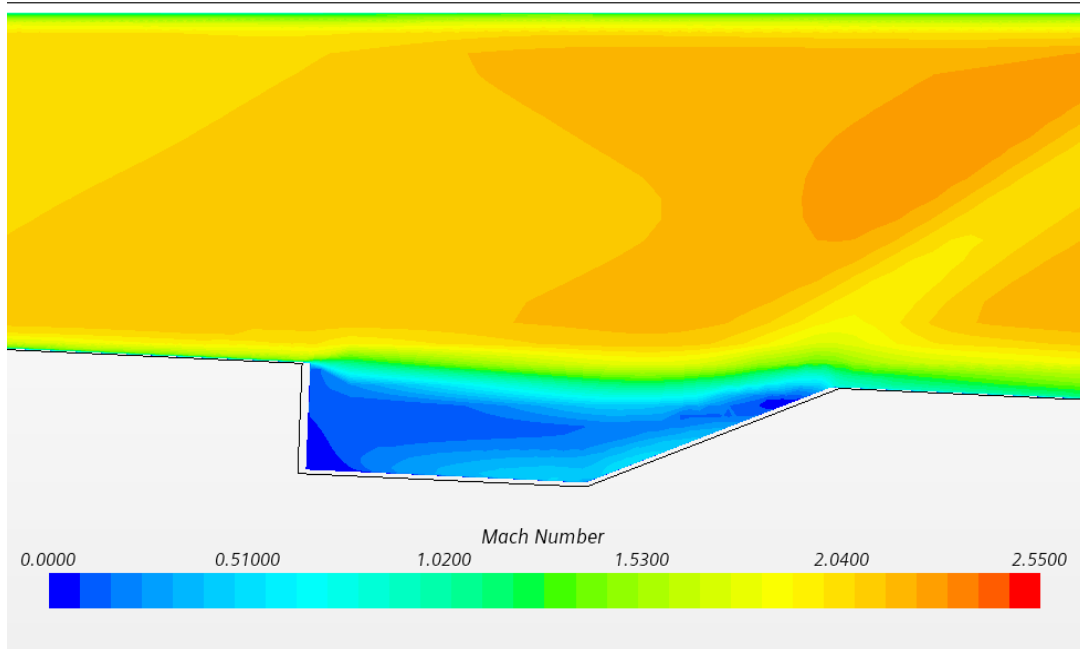*Figure 25: RANS No Injector Velocity Scalar Scene*

Figure 26: RANS No Injector Temperature Scalar Scene

Figure 27: RANS No Injector Mach Number Scalar Scene

Looking at Figures 25-27 for velocity, temperature, and Mach number, it can be seen that the results agree. The cavity region has the lowest velocity of anywhere else in the geometry. This low-velocity region helps to promote a better air-fuel mixture while allowing enough time for combustion to occur. The cavity also has the highest temperature anywhere in the geometry. This increased temperature is due to the low velocity and Mach number in this cavity region; the air within this region is compressed as it decreases in speed causing the temperature to rise, as wanted. The remaining airflow above the flame holder cavity is right around Mach 2, which is the desired speed for these simulations, which once again verifies the results.
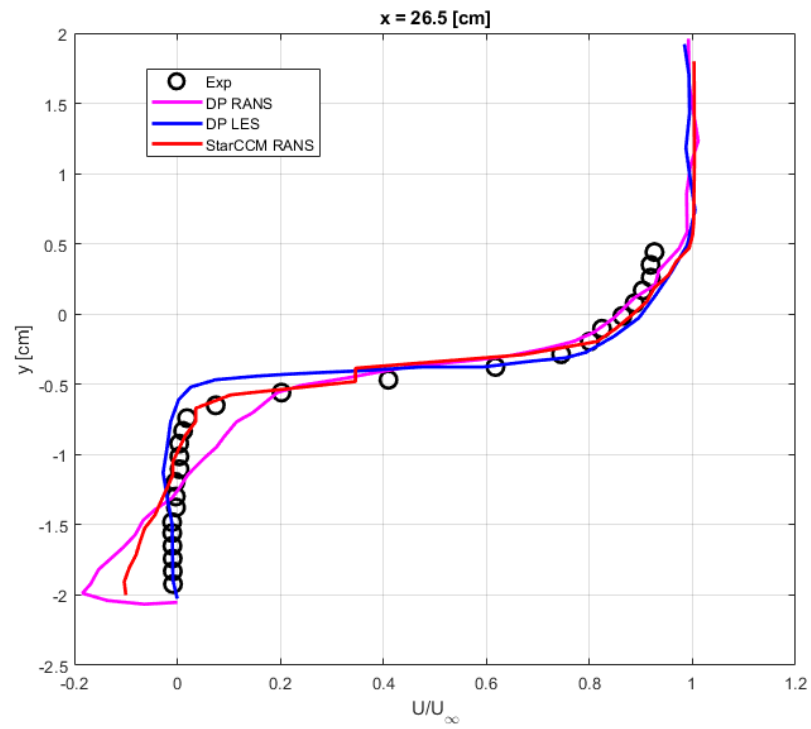
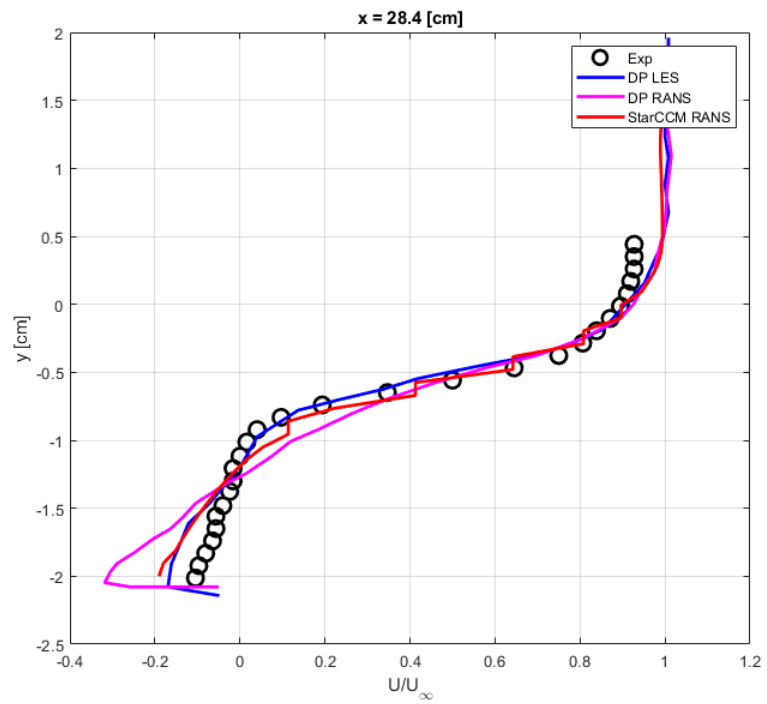*Figure 28: 26.5 cm Data for RANS with No Injection*

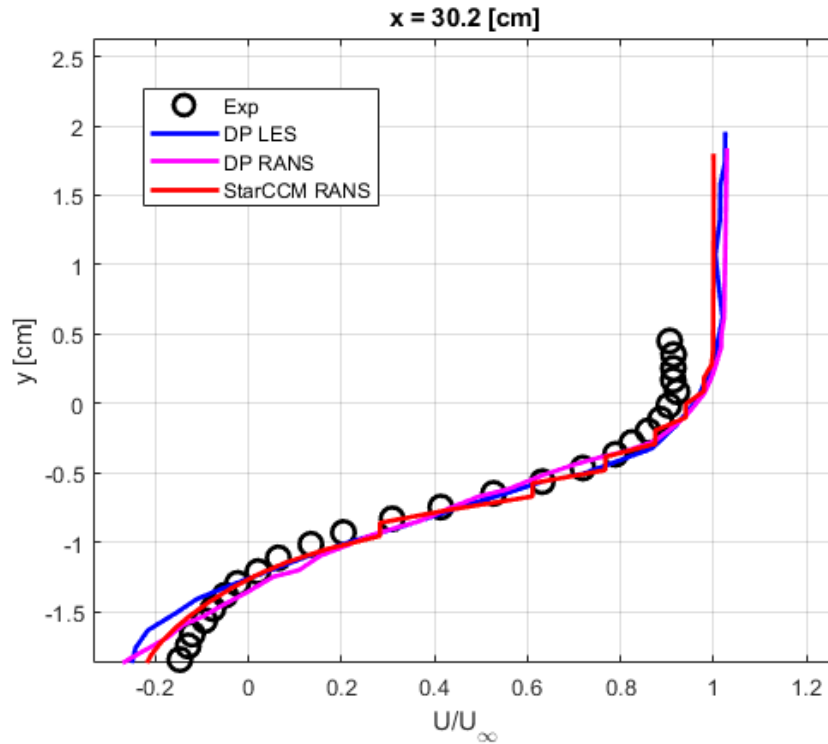*Figure 29: 28.4 cm Data for RANS with No Injection*

Figure 30: 30.2 cm Data for RANS with No Injection

Data was extracted from the simulation results to be compared to published data from Peterson's results ([5],[6],[7]). Looking at the three separate locations within the flame holder cavity, the simulations agree with the experimental data as well as the published data from Peterson. The StarCCM simulations performed better than those from Peterson for the RANS. Through the simulation visual scenes and plots comparing the simulations to published and experimental data, it was decided the simulation was successful and the next steps could be completed. Upon the successful completion of the RANS simulations with no fuel injection, an LES, Large Eddy Simulation, case was performed within StarCCM.
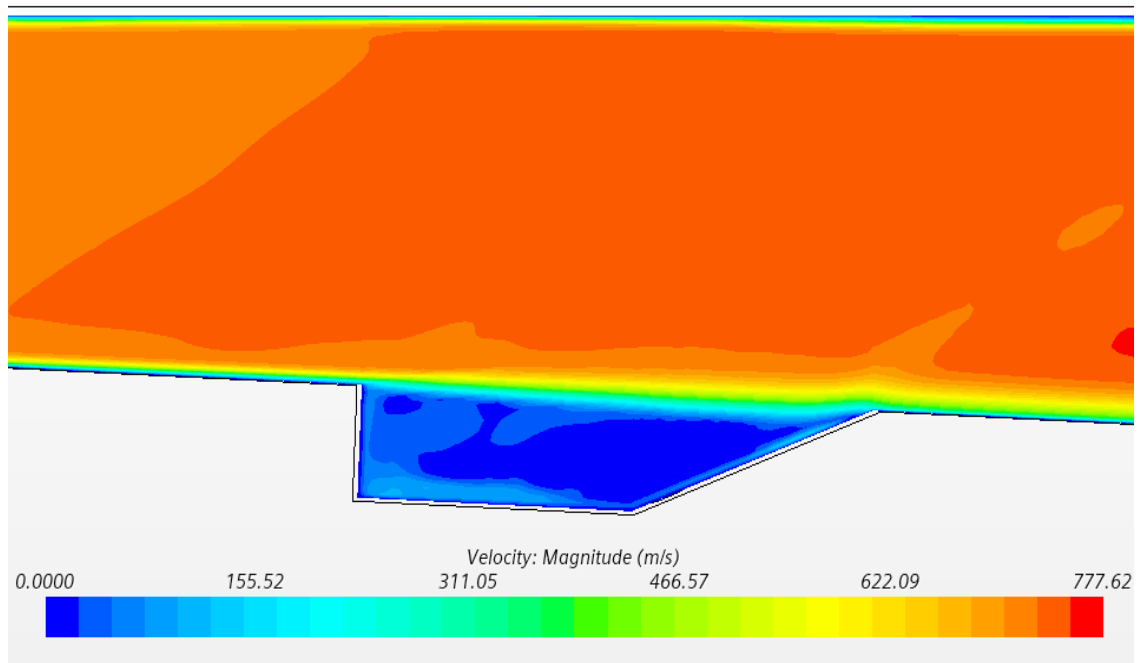
LES Case with No Fuel Injection

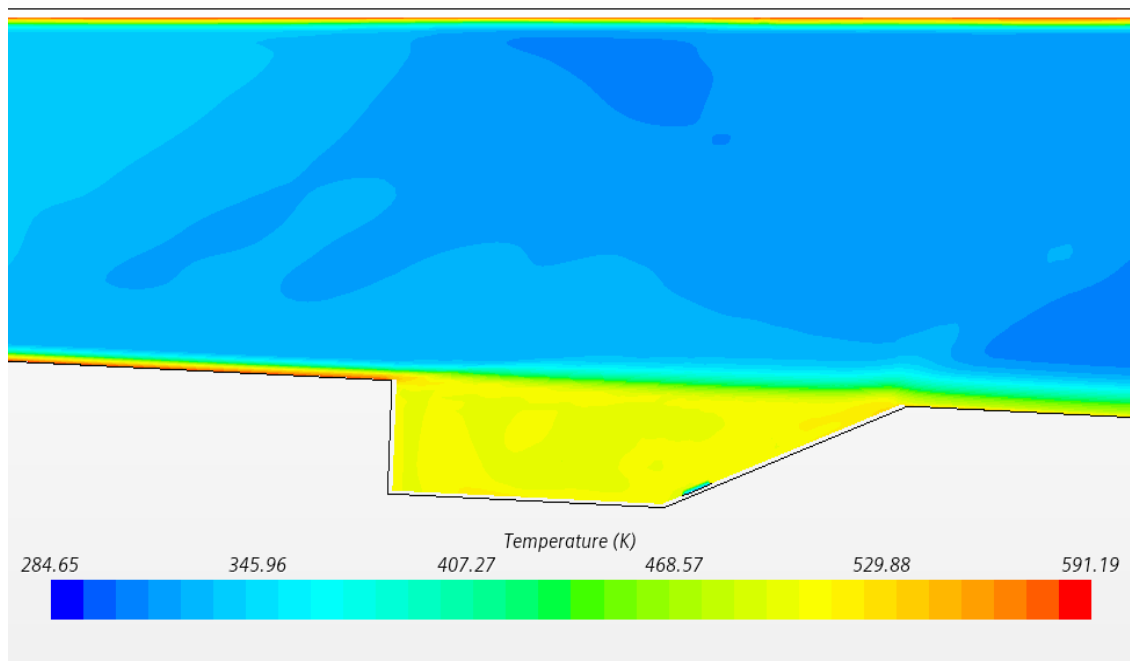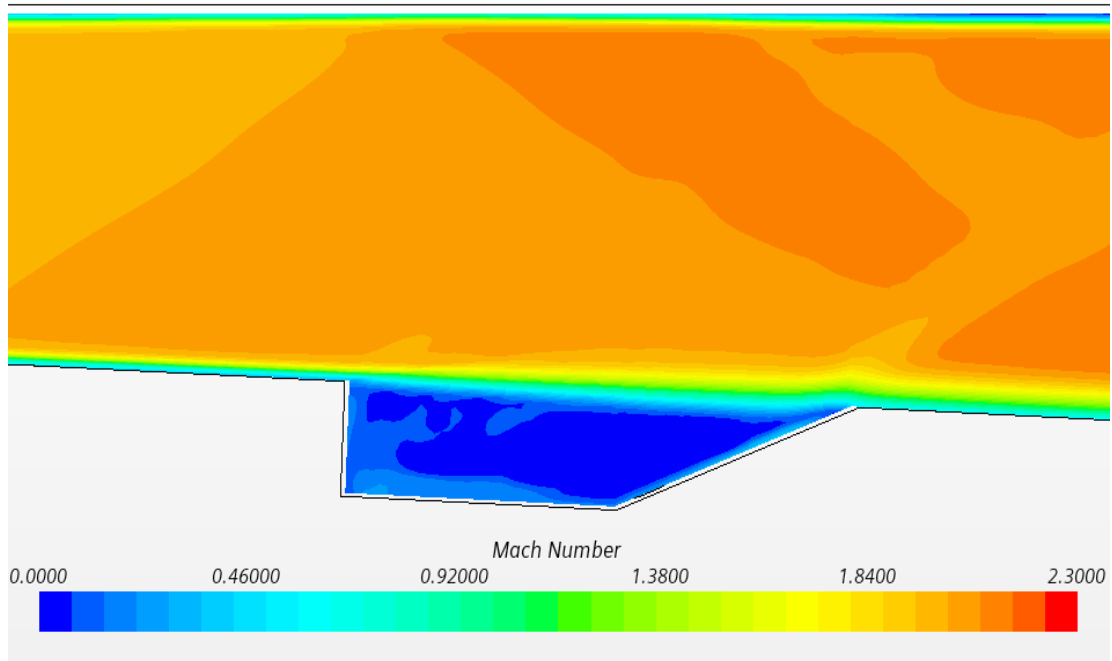*Figure 31: LES No Injector Velocity Scalar Scene*

Figure 32: LES No Injector Temperature Scalar Scene

Figure 33: LES No Injector Mach Number Scalar Scene

Looking at Figures 31-33 for velocity, temperature, and Mach number, it can be seen that the results agree. The cavity region, again, has the lowest velocity of anywhere else in the geometry. The cavity also has the highest temperature anywhere in the geometry. The temperature within the cavity for the LES simulation appears to be slightly lower than that of the RANS simulations. The RANS had a temperature close to 560 K whereas the LES simulation predicts a temperature of closer to 500 K. This could be partly due to the fact that LES simulations start right at time zero whereas the RANS tries to reach steady state. The velocity and Mach number from the LES simulations agree with those from the RANS simulations.
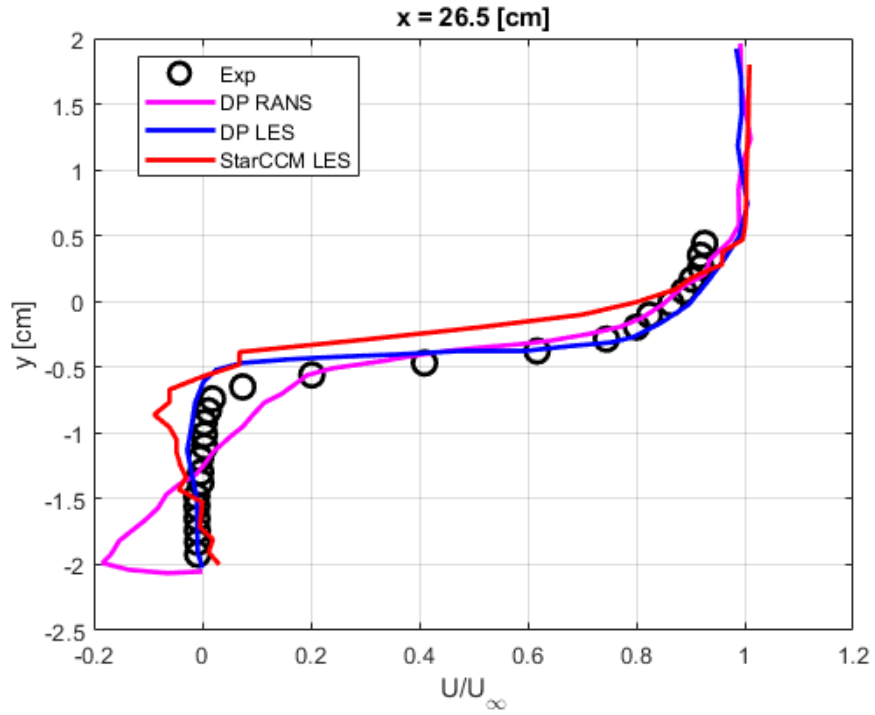
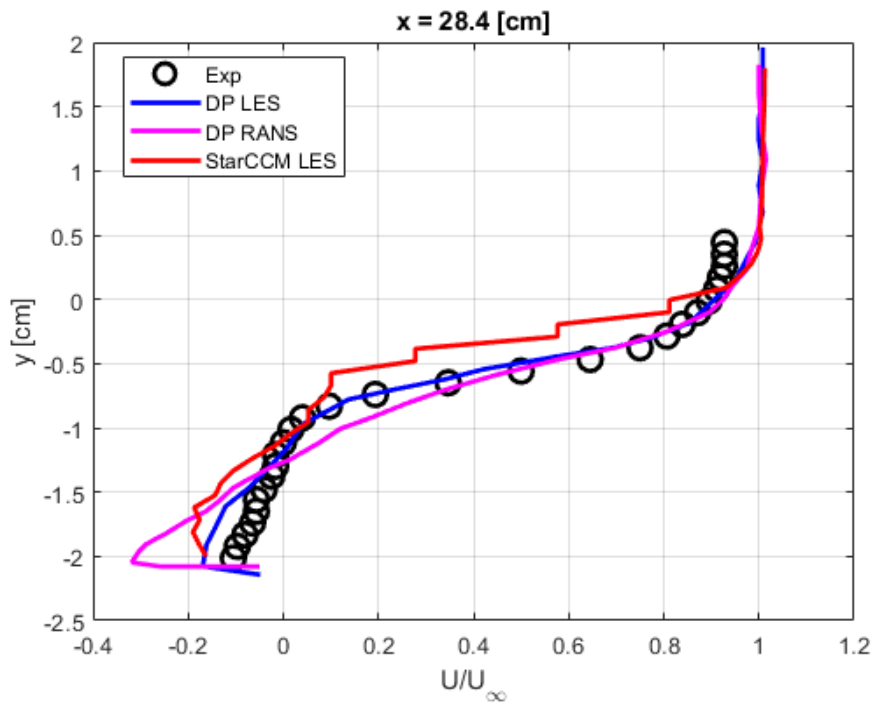*Figure 34: 26.5 cm Data for LES with No Injection*

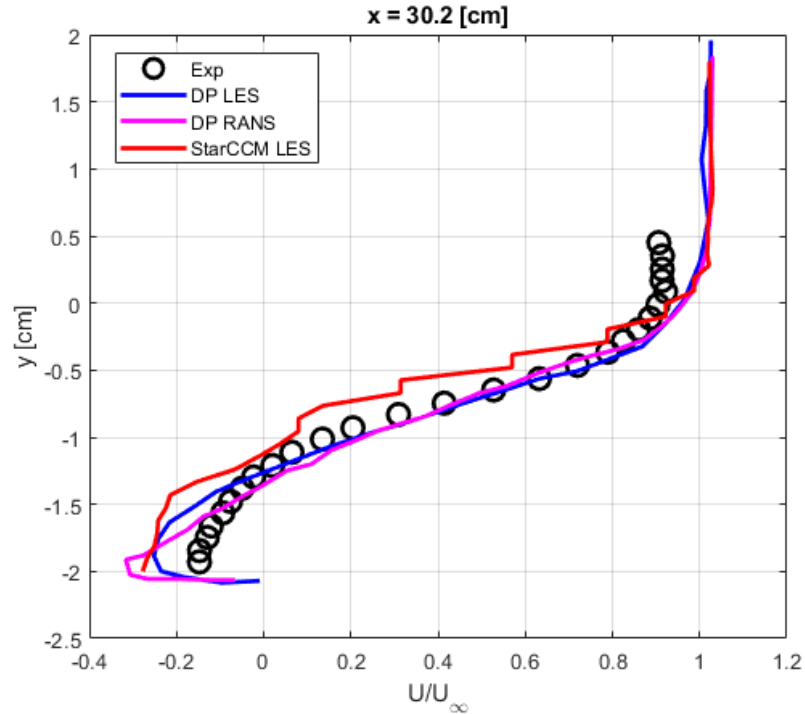*Figure 35: 28.4 cm Data for LES with No Injection*

Figure 36: 30.2 cm Data for LES with No Injection

Data was again extracted from the simulation results to be compared to published data from

Peterson's results ([5],[6],[7]). Figures 34-36 show data from three separate locations

within the flame holder cavity; the simulations agree with the experimental data as well as

the published data from Peterson. The StarCCM simulations do have some issues with

matching the experimental data within the -1 cm to 0 cm range. This could be due to a few

different things. Firstly, StarCCM has some jagged jumps in the velocity visualization.

Even when trying to add more points when extracting data, these stairstep jumps were

present. Secondly, this region is remarkably close to where the flame holder cavity meets

with the rest of the combustion chamber, so there are massive changes in velocity in this

region. Through the simulation visual scenes and plots comparing the simulations to

published and experimental data, it was decided the simulation was successful and the next

steps could be completed. Upon the successful completion of the LES simulations with no

fuel injection, an injector was added to the geometry. At this point, it was also decided that enough initial verification had been completed and OpenFOAM could be implemented into the simulation process. The next step was to run a URANS Non-Reacting Case with injection.

RANS Non-Reacting Case with Ethylene Injection

For the non-reacting case, the geometry was kept the same except for fuel injection was added in the flame holder cavity. The fuel being injected was ethylene, which has remarkably comparable properties to air. The temperature of the ethylene was assumed to be 327 K. The velocity of the ethylene was set to be around 28 m/s in the negative x-direction. This gives a mass flow rate of fuel close to 0.0001 kg/s. In addition to the geometry staying similar, the boundary conditions were all kept the same for this case. The physics models were kept pretty much the same. Again, RANS is what was used for turbulence modeling. In addition, the non-reacting physics model was selected as well as having the passive scalar enable for the simulations. Only air and ethylene were enabled for the non-reacting physics model, with the air entering from the stagnation inlet and the ethylene entering the fuel injector located in the flame holder cavity. The next few pages show the simulation results that were obtained from both StarCCM and OpenFOAM simulations. Velocity, temperature, and the passive scalar scenes are shown in the following Figures 37-44.
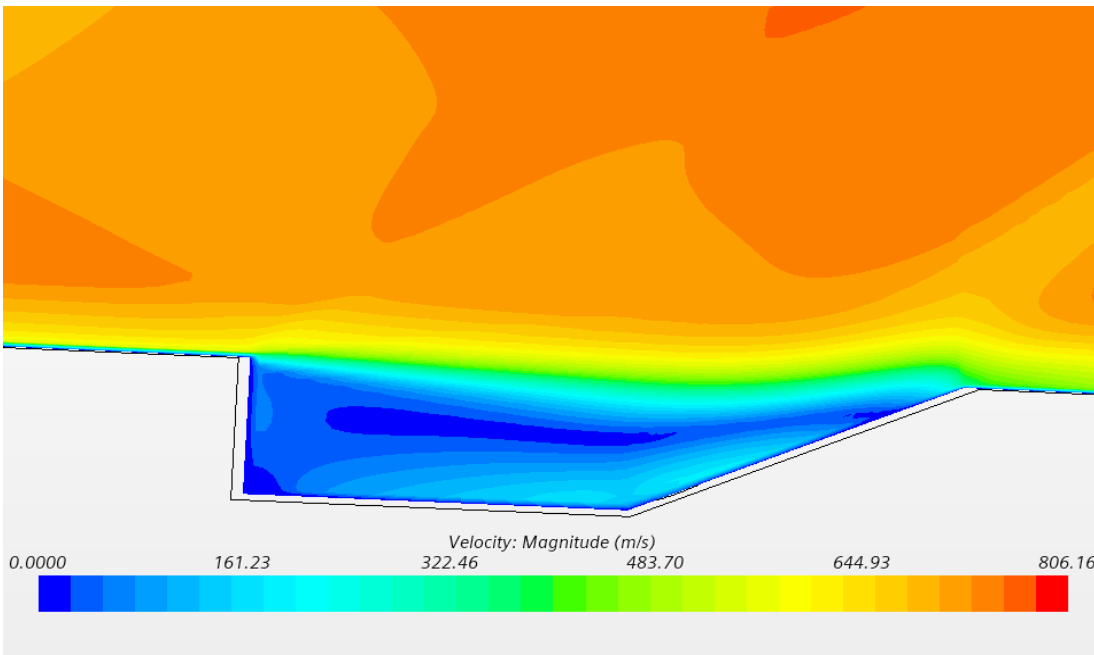
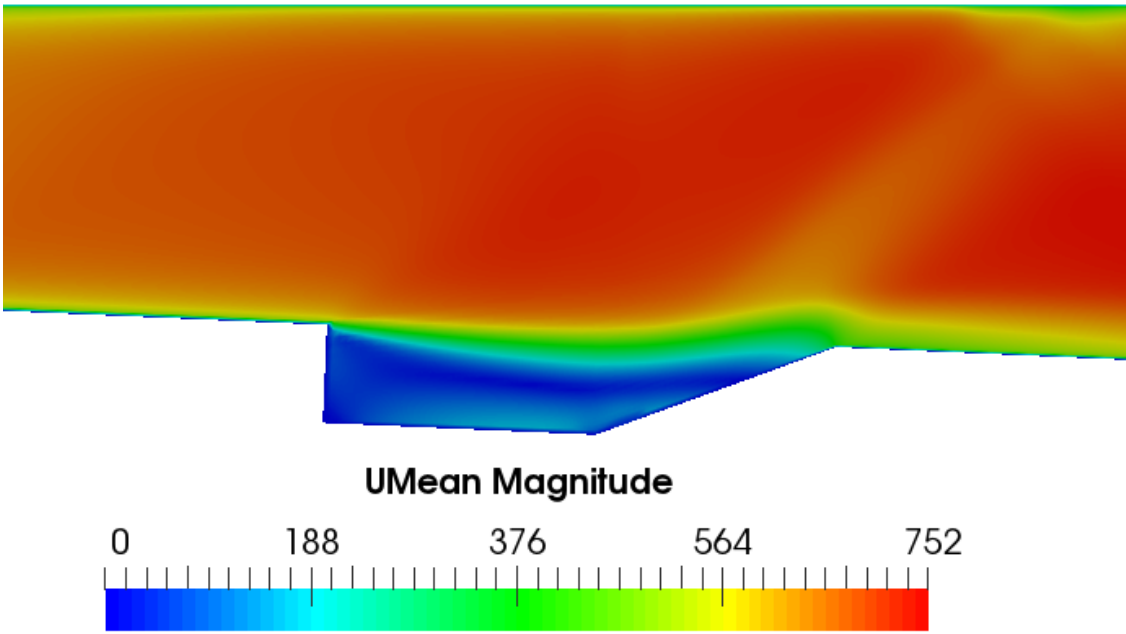*Figure 37: Non-Reacting RANS StarCCM Velocity Scene*

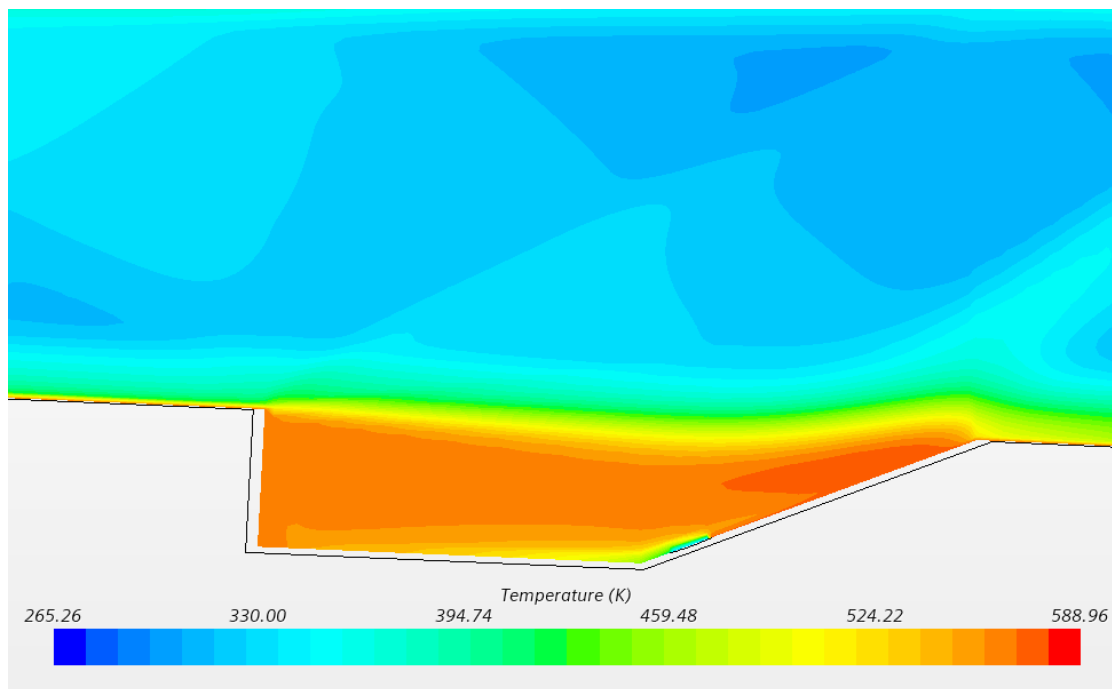*Figure 38: Non-Reacting RANS OpenFOAM Velocity Scene*

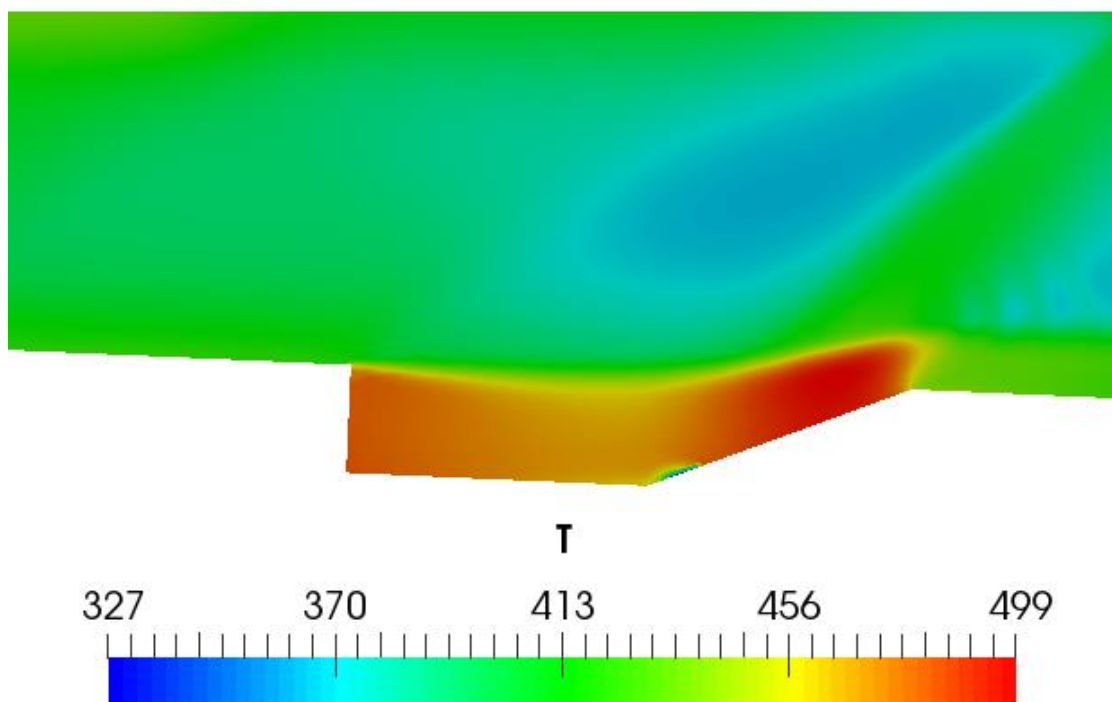*Figure 39: Non-Reacting RANS StarCCM Temperature Scene*

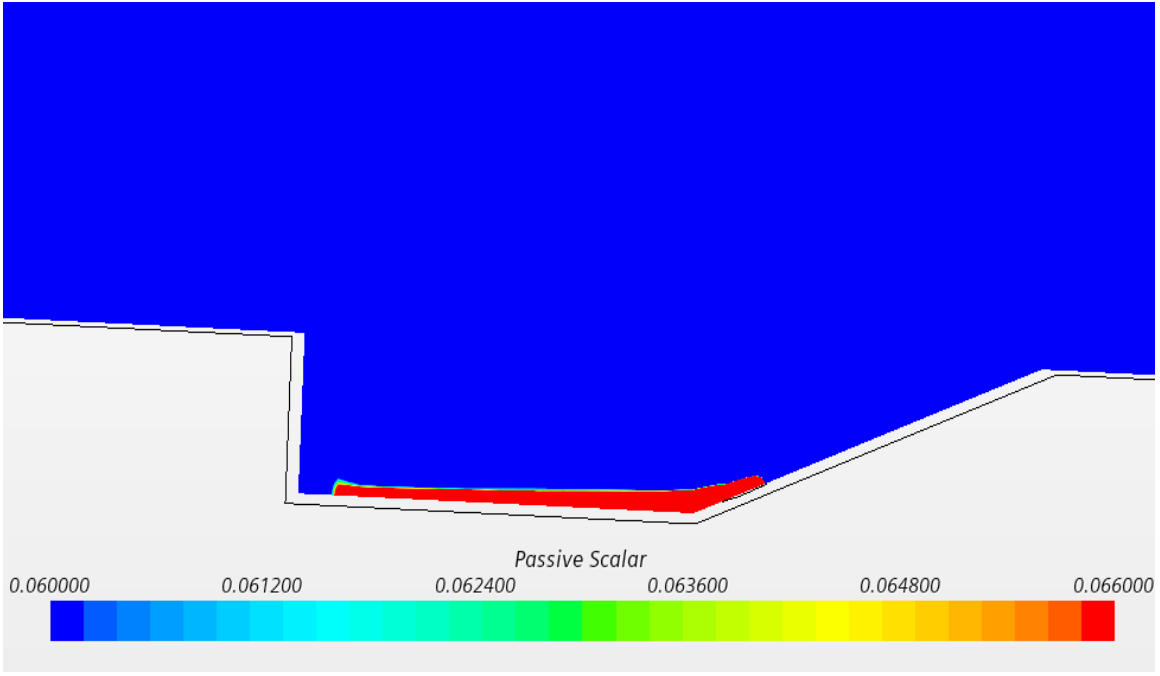*Figure 40: Non-Reacting RANS OpenFOAM Temperature Scene*
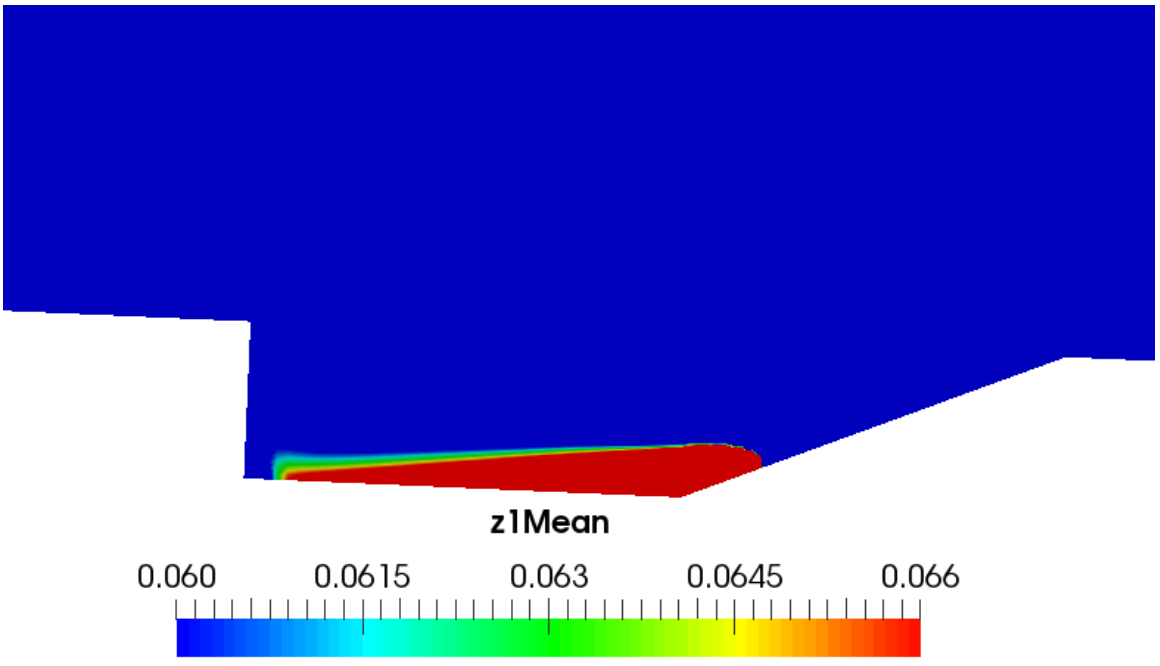
Figure 41: Non-Reacting RANS StarCCM Passive Scalar Scene

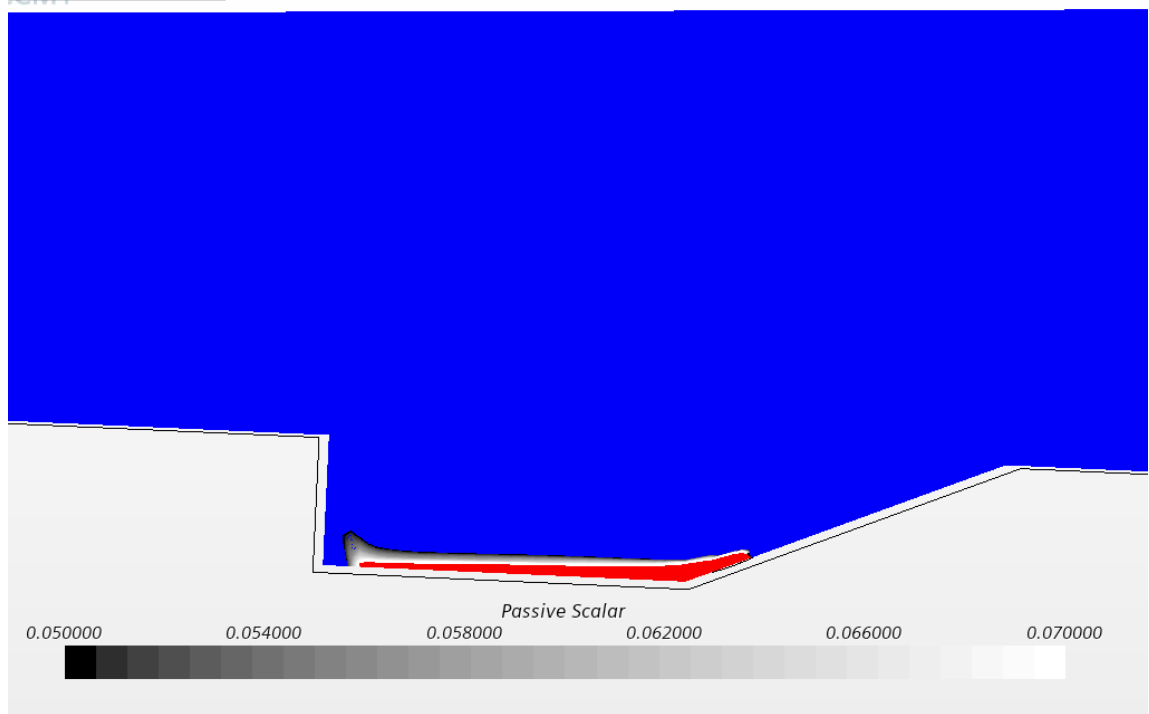*Figure 42: Non-Reacting RANS OpenFOAM Passive Scalar Scene*

Figure 43: Non-Reacting RANS StarCCM Imposed Passive Scalar Scene
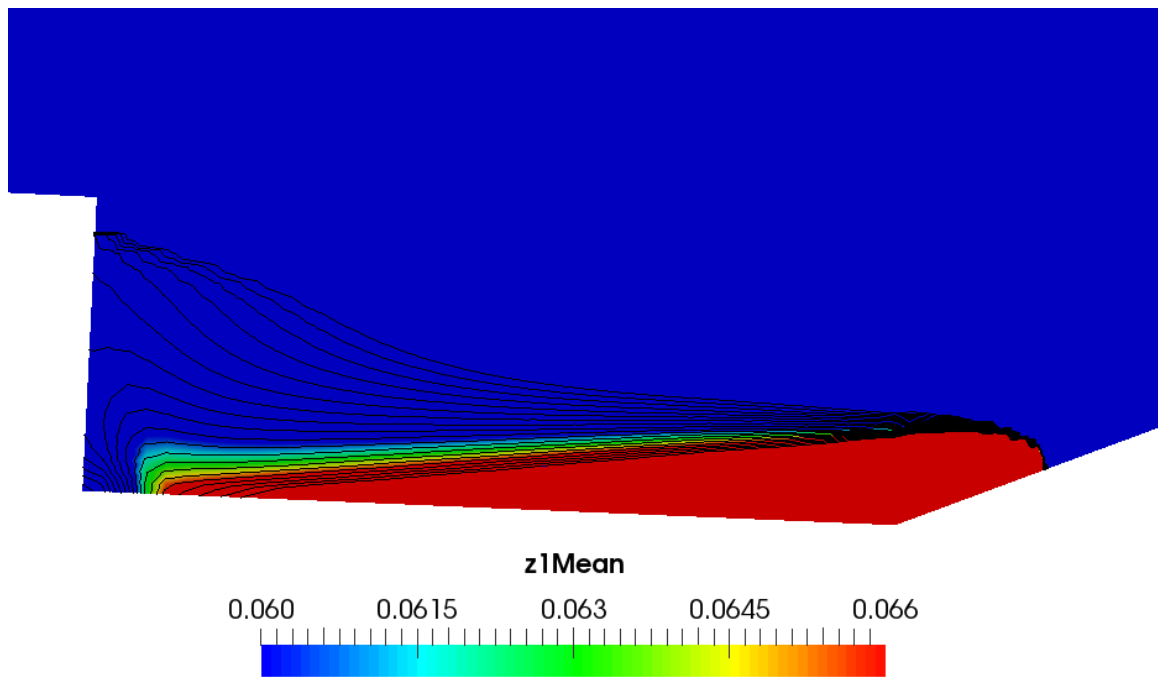

Figure 44:N on-Reacting RANS OpenFOAM Imposed Passive Scalar Scene

The simulations agree with the experimental data as well as the published data from Peterson. When comparing the velocity scenes from both StarCCM and OpenFOAM, seen in Figures 37 and 38, both give remarkably similar visual results and velocity profiles. Looking at the temperature scenes both in Figures 39 and 40, the results agree with each other giving terribly similar temperature profiles and ranges. Lastly, looking at the passive scalar scenes from both, seen in Figures 41 and 42, there are a few slight differences. Precisely looking at a passive scalar value of 0.0636, OpenFOAM has a higher concentration on the leftmost side of the cavity compared to the StarCCM simulation. As seen in Figures 43 and 44, the imposed lines show where theoretical combustion will occur. The black is the lowest concentration, and the white is the highest concentration for StarCCM. OpenFOAM has streamlines ranging from the 0.05 to 0.07 values of the passive scalar. This scalar field range was derived from the work from Mastorakos et al [20]. This range is defined as the "most reactive" mixture fraction, which is discussed in more detail from Mastorakos et al. Ethylene's most reactive mixture fraction is 0.06375. It is evident that OpenFOAM predicts much more combustion to occur on the backside of the cavity. This may partly be because it is a non-reacting case. The OpenFOAM simulations may have a longer run time leading to more fuel being injected. The profiles also appear slightly different but remarkably similar to each other.

Upon completion of the simulations, data was again extracted from the simulation results to be compared to published data from Peterson's results ([5],[6],[7]). At this point, to gain more validity, seven distinct locations within the flame holder cavity were analyzed. This time locations were taken every centimeter or less within the cavity. An x-distance of zero corresponds to where the geometry starts after the isolator. The distance of 25.6 cm would

correspond to the leftmost side of the cavity. The x-axis represents the normalized velocity

components, and the y-axis represents the vertical distance within the cavity. Figures 45-

58 show the plotted results. The first set of graphs shows the normalized x, or U, velocity

component, and the second set shows the normalized y, or V, velocity component.
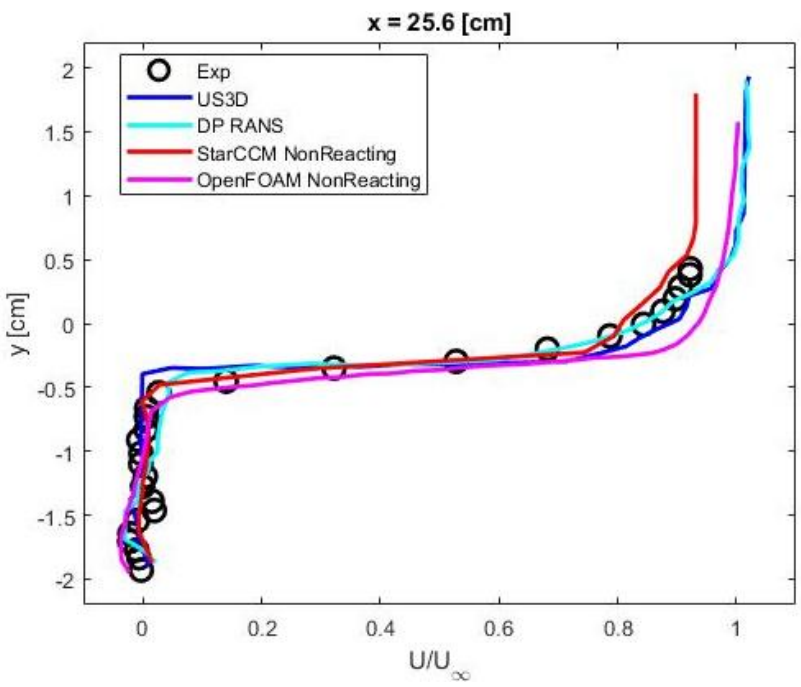
Normalized X-Component RANS Graphs

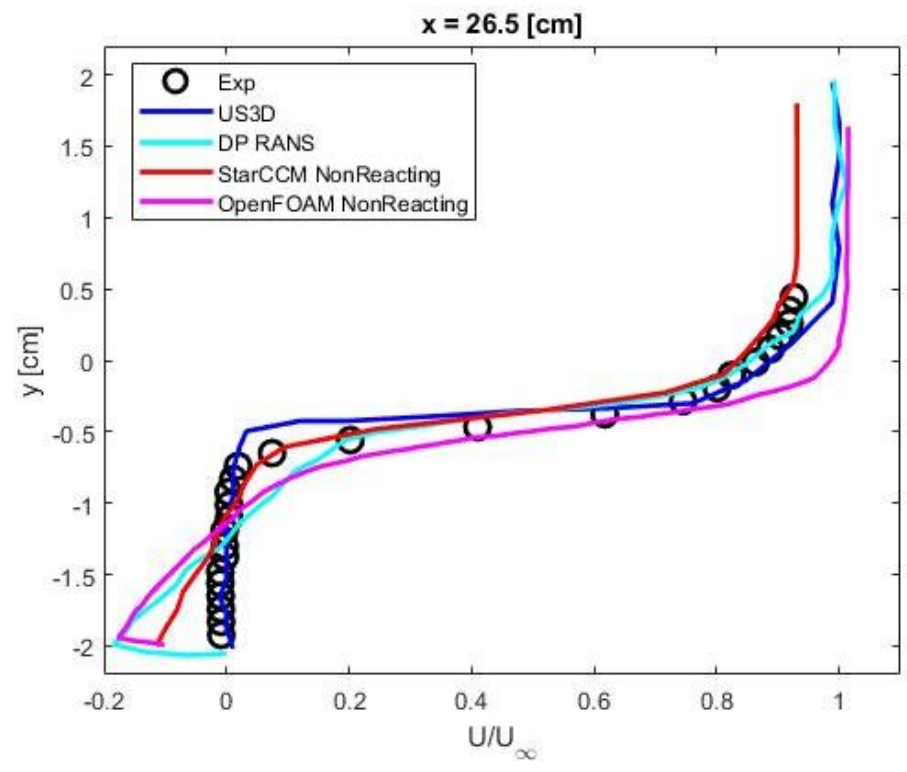*Figure 45: 25.6 cm X-Component Data for Non-Reacting RANS*

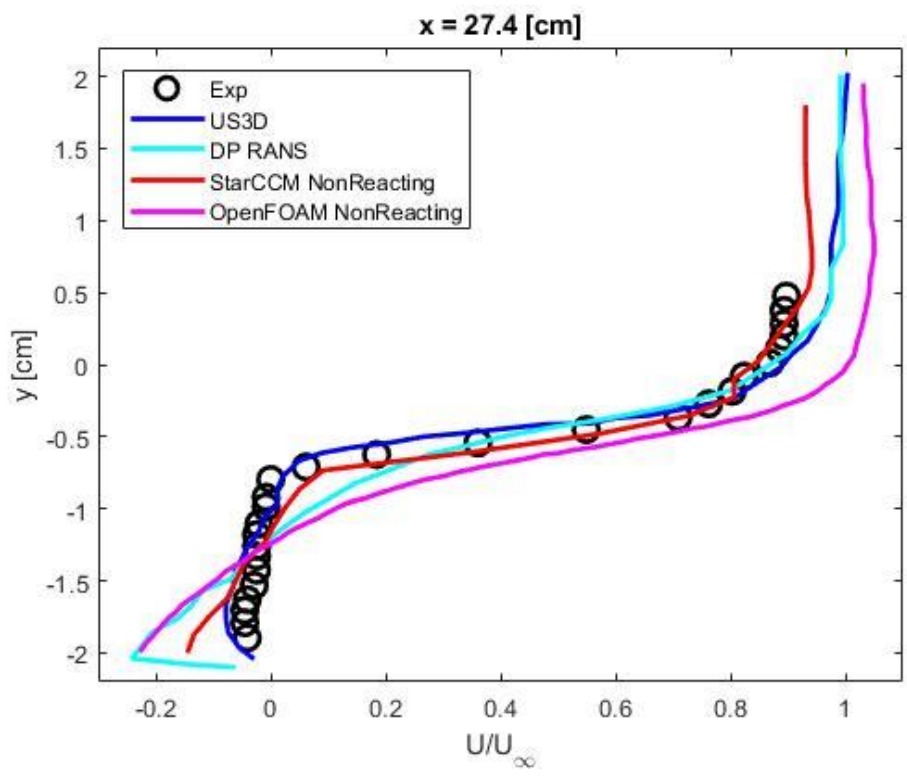*Figure 46: 26.5 cm X-Component Data for Non-Reacting RANS*

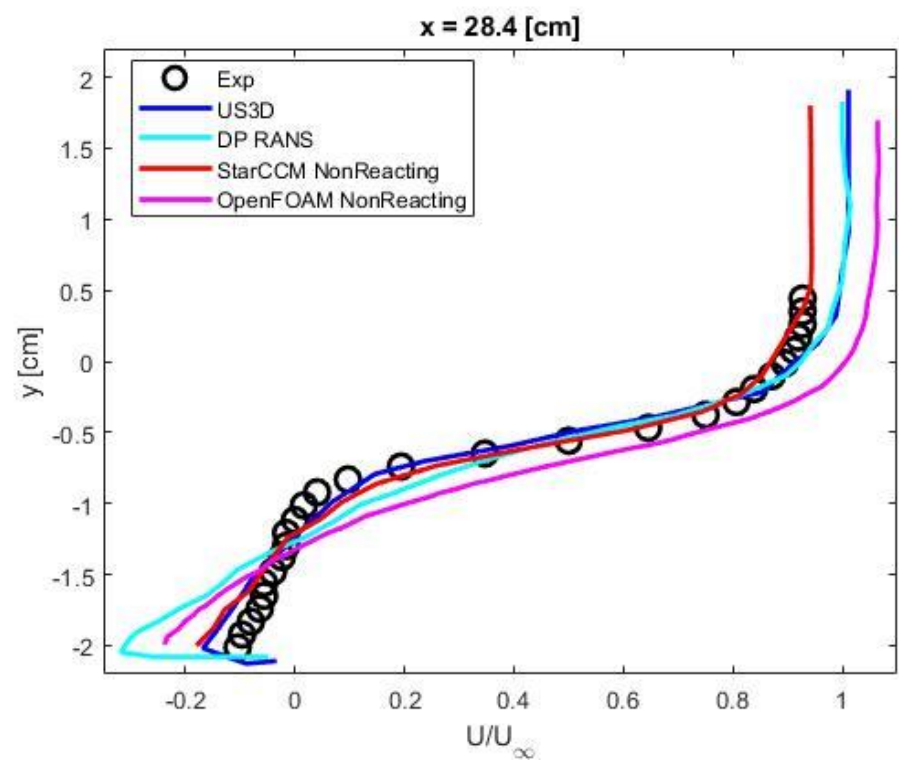*Figure 47: 27.4 cm X-Component Data for Non-Reacting RANS*

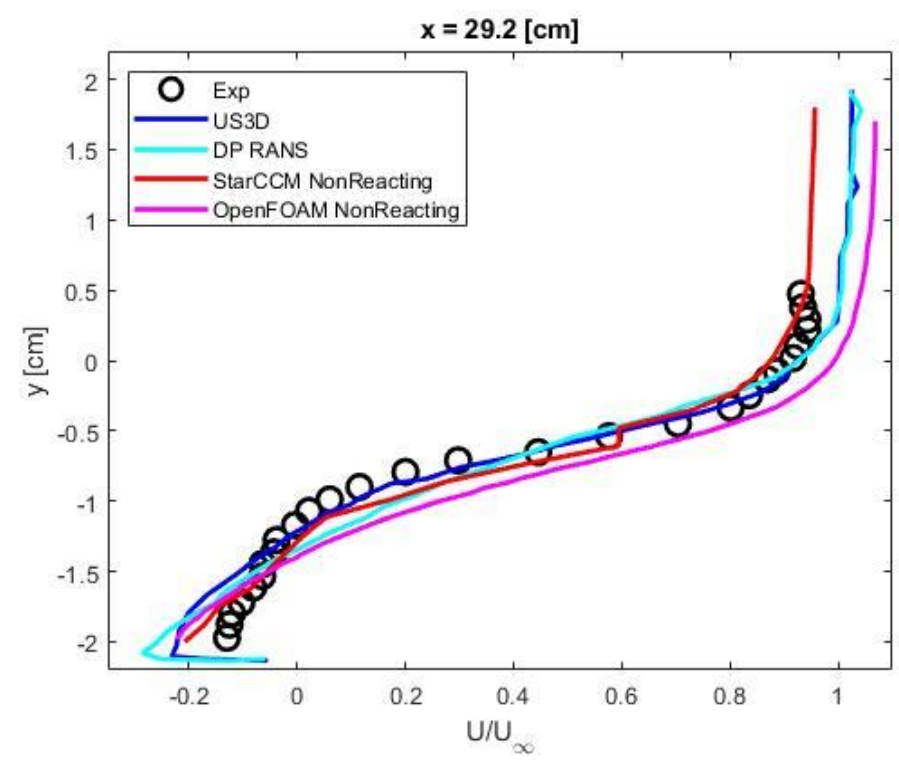*Figure 48: 28.4 cm X-Component Data for Non-Reacting RANS*

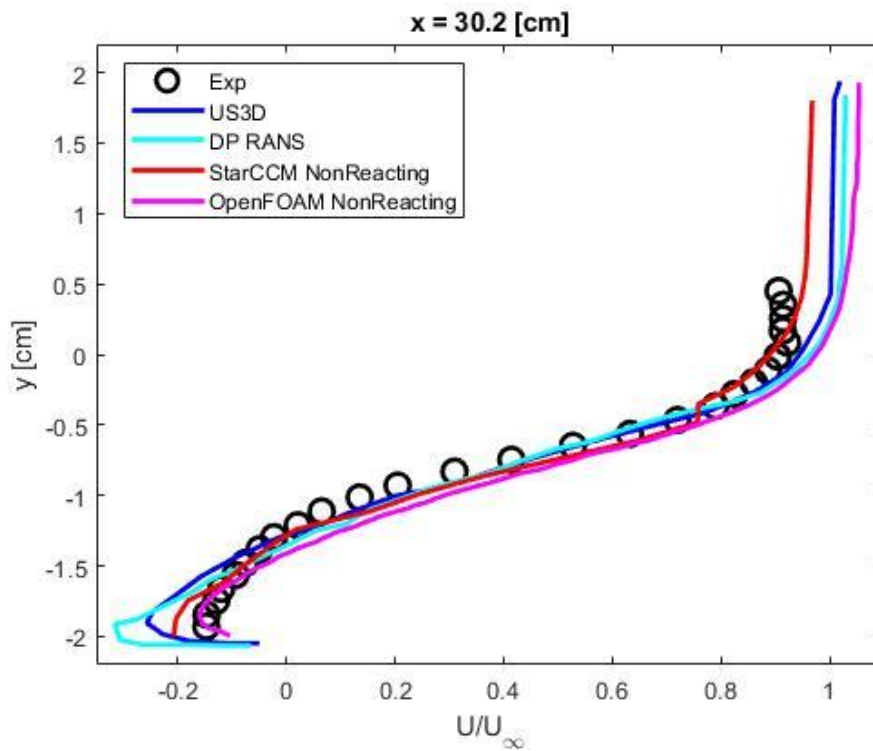*Figure 49: 29.2 cm X-Component Data for Non-Reacting RANS*

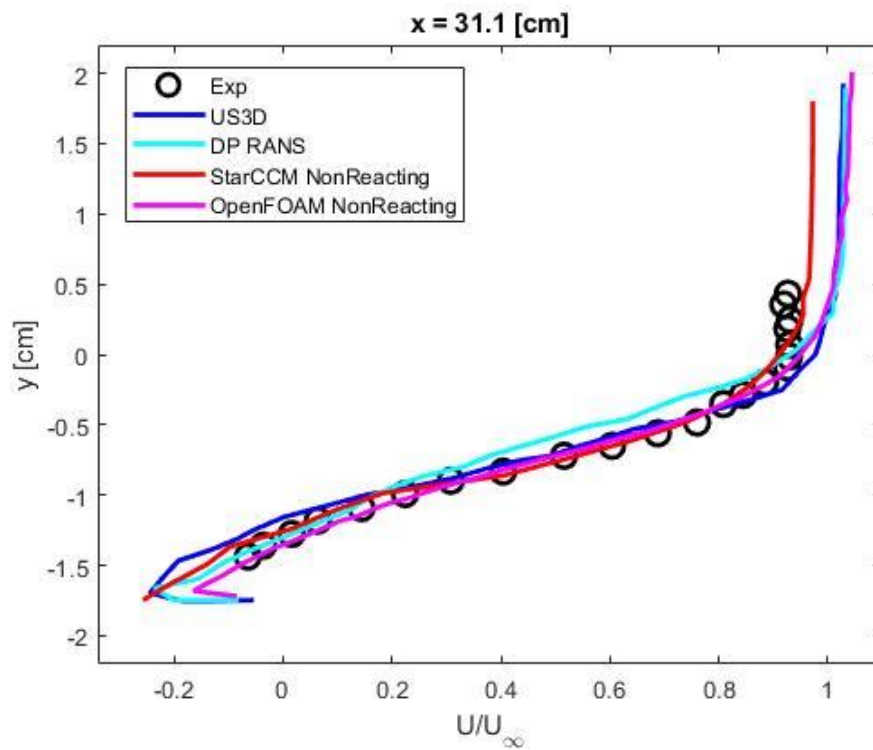*Figure 50: 30.2 cm X-Component Data for Non-Reacting RANS*

Figure 51: 31.1 cm X-Component Data for Non-Reacting RANS

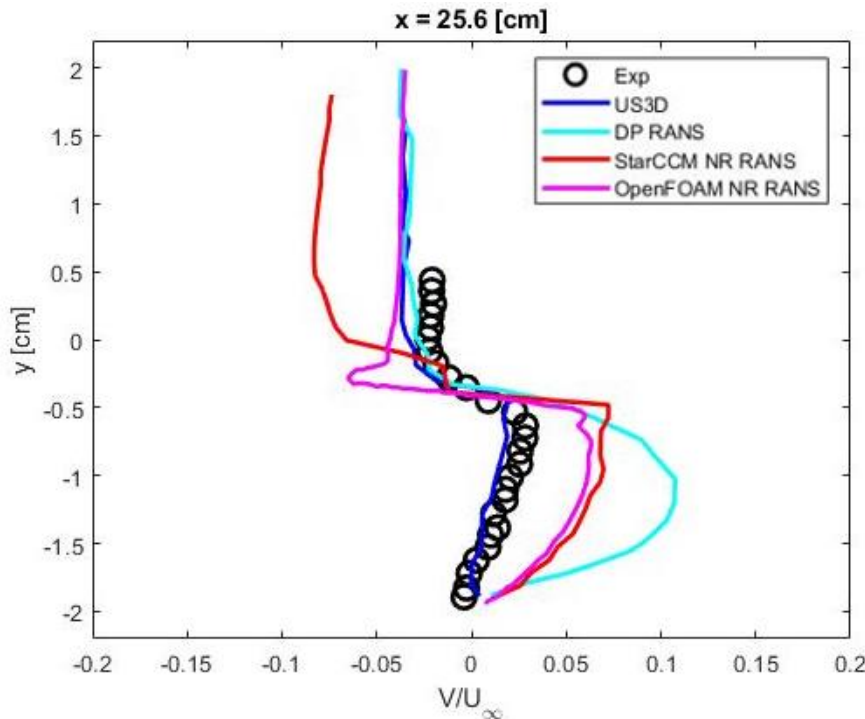Normalized Y-Component RANS Graphs

Figure 52: 25.6 cm Y-Component Data for Non-Reacting RANS
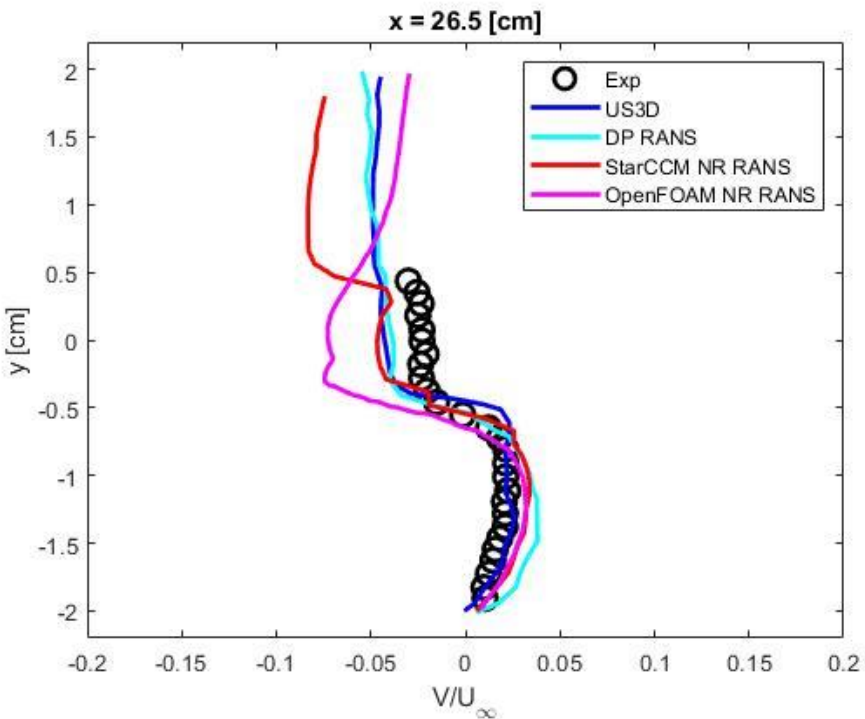

Figure 53: 26.5 cm Y-Component Data for Non-Reacting RANS
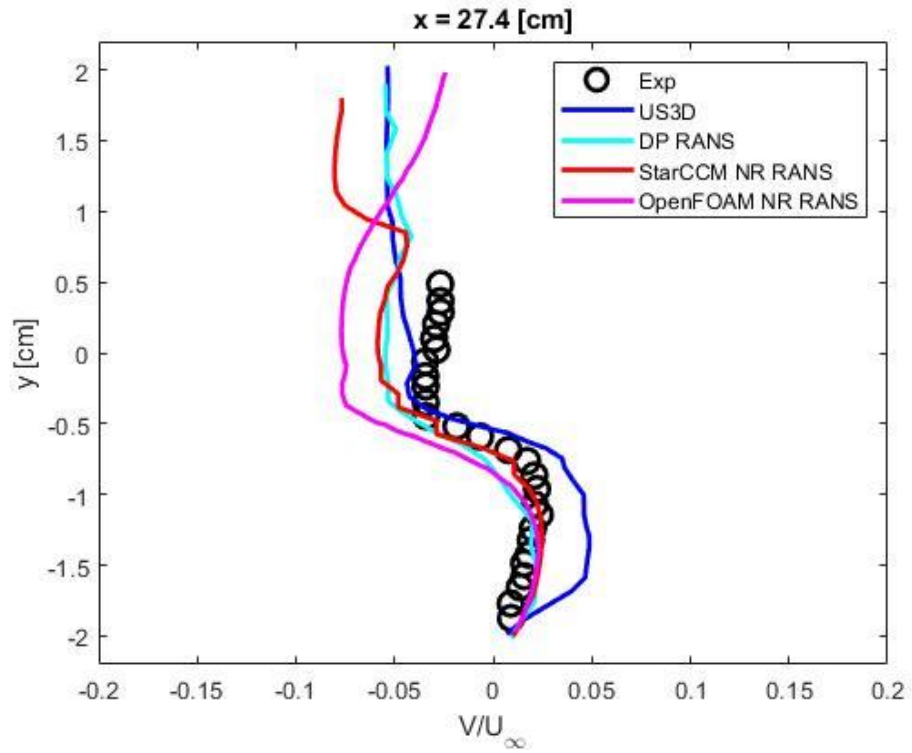
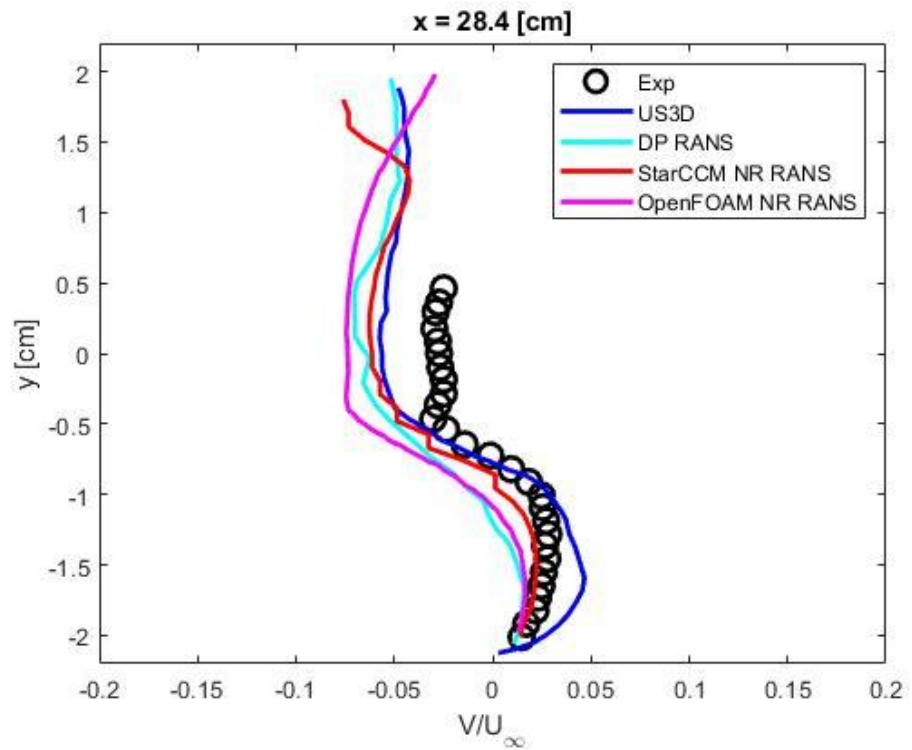*Figure 54: 27.4 cm Y-Component Data for Non-Reacting RANS*

Figure 55: 28.4 cm Y-Component Data for Non-Reacting RANS
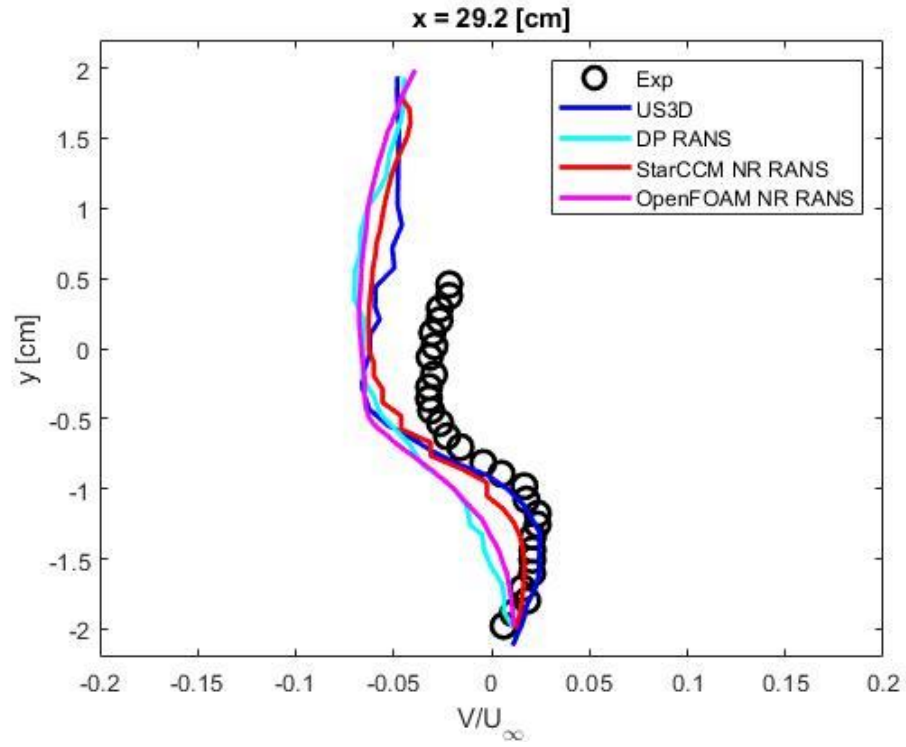
Figure 56: 29.2 cm Y-Component Data for Non-Reacting RANS
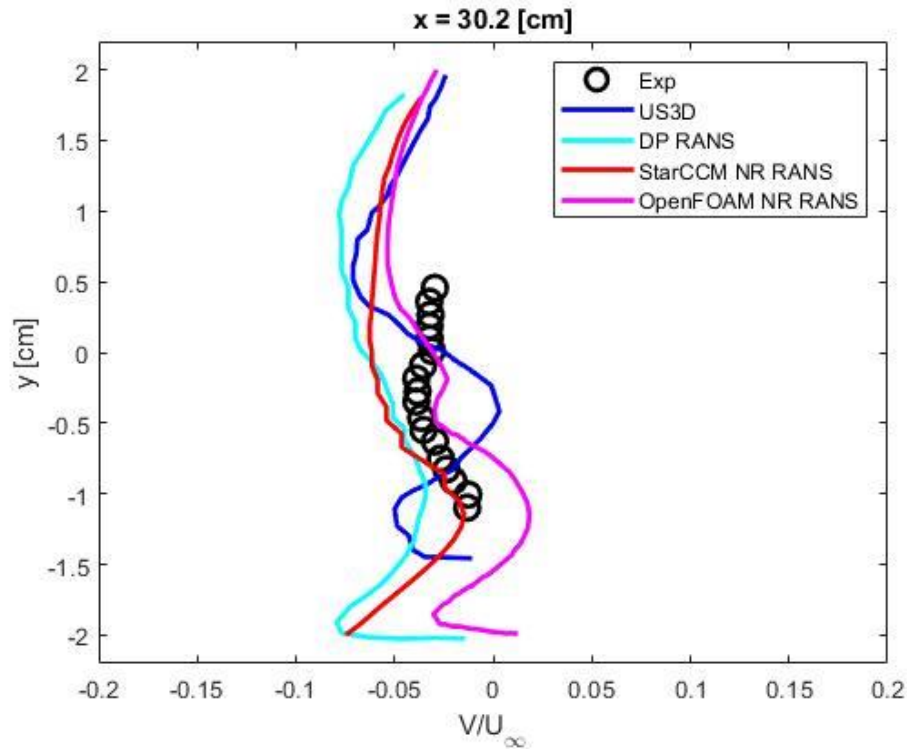
Figure 57: 30.2 cm Y-Component Data for Non-Reacting RANS
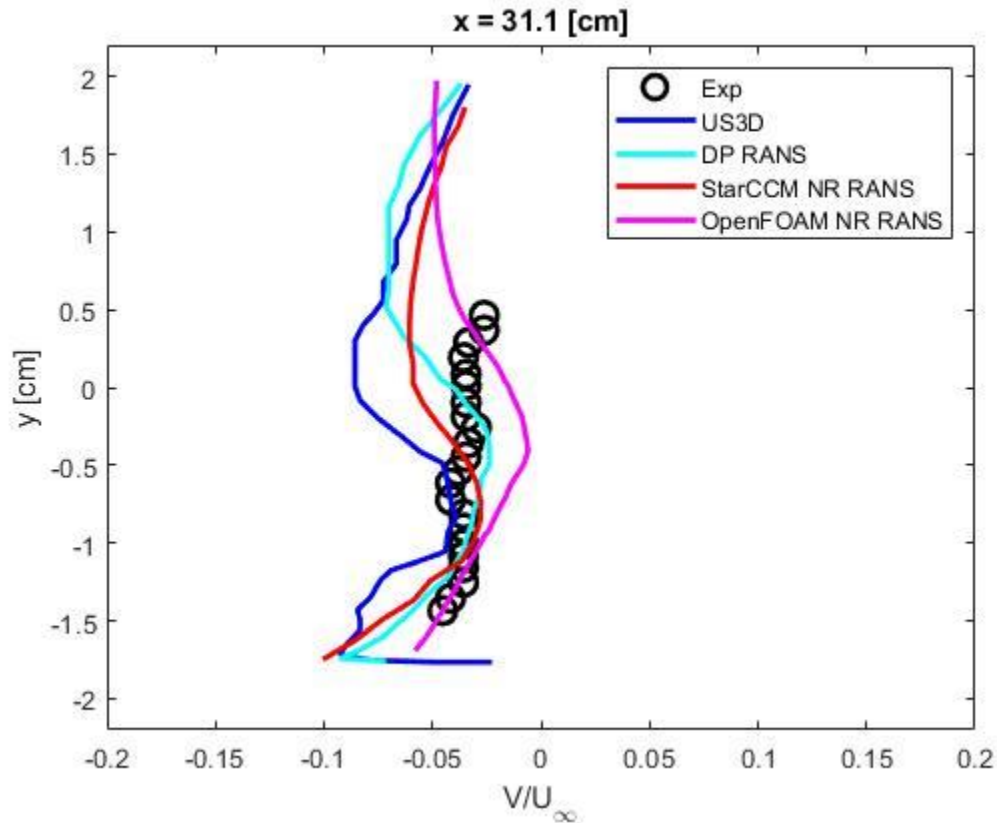
Figure 58: 31.1 cm Y-Component Data for Non-Reacting RANS

The simulations agree with the experimental data as well as the published data from Peterson. When comparing the velocity scenes from both StarCCM and OpenFOAM, seen in Figures 37 and 38, both give remarkably similar visual results and velocity profiles. Looking at the temperature scenes both in Figures 39 and 40, the results agree with each other giving terribly similar temperature profiles and ranges. Lastly, looking at the passive scalar scenes from both, seen in Figures 41 and 42, there are a few slight differences. Precisely looking at a passive scalar value of 0.0636, OpenFOAM has a higher concentration on the leftmost side of the cavity compared to the StarCCM simulation. As

seen in Figures 43 and 44, the imposed lines show where theoretical combustion will occur. It is evident that OpenFOAM predicts much more combustion to occur on the backside of the cavity. This may partly be because it is a non-reacting case. The OpenFOAM simulations may have a longer run time leading to more fuel being injected. The profiles also appear slightly different but similar to each other.

The StarCCM simulations appear to better match the experimental and published data when compared to the OpenFOAM results. Specifically, when looking at the data that is on the high end of the normalized x-velocity and the higher end of the vertical location within the cavity. The StarCCM data more closely follows the experimental data in addition to outperforming the published data. For greater x-distances within the flame holder cavity, specifically, where x = 30.2 and x = 31.1, OpenFOAM does a better job at matching the experimental data at low values of normalized velocities and low values of vertical location. This specific location corresponds closely to where the fuel is being injected.

Looking at the normalized y component graphs, StarCCM and OpenFOAM agree with the experimental and published data, specifically for locations in the middle region of the cavity. For regions x = 25.6 cm, x = 30.2 cm, and x = 31.2 cm there is some deviation present. The experimental data shows more uniform velocity distributions when compared to the simulation velocity distributions. Further research needs to be conducted on grid resolution as well as turbulence modeling to accurately capture and model the physics that is taking place right near the walls in the cavity region.

Through the simulation visual scenes and plots comparing the simulations to published and experimental data, it was concluded the simulations were successful and the next steps

could be completed. The next step was to run an LES Non-Reacting Case with injection. All other conditions from the previously used RANS simulations were held constant. The turbulence modeling was just switched from RANS to LES.

LES Non-Reacting Case with Ethylene Injection

The following simulation results were determined to be incorrect when comparing StarCCM to OpenFOAM. It was determined that the OpenFOAM case was not run long enough, which gave much greater temperatures than should be present. Another thing that was learned was that it is necessary to look at the passive scalar mean instead of the instantaneous passive scalar. Figures 59-61 below are some of the mistakes that were made and their corresponding corrections.
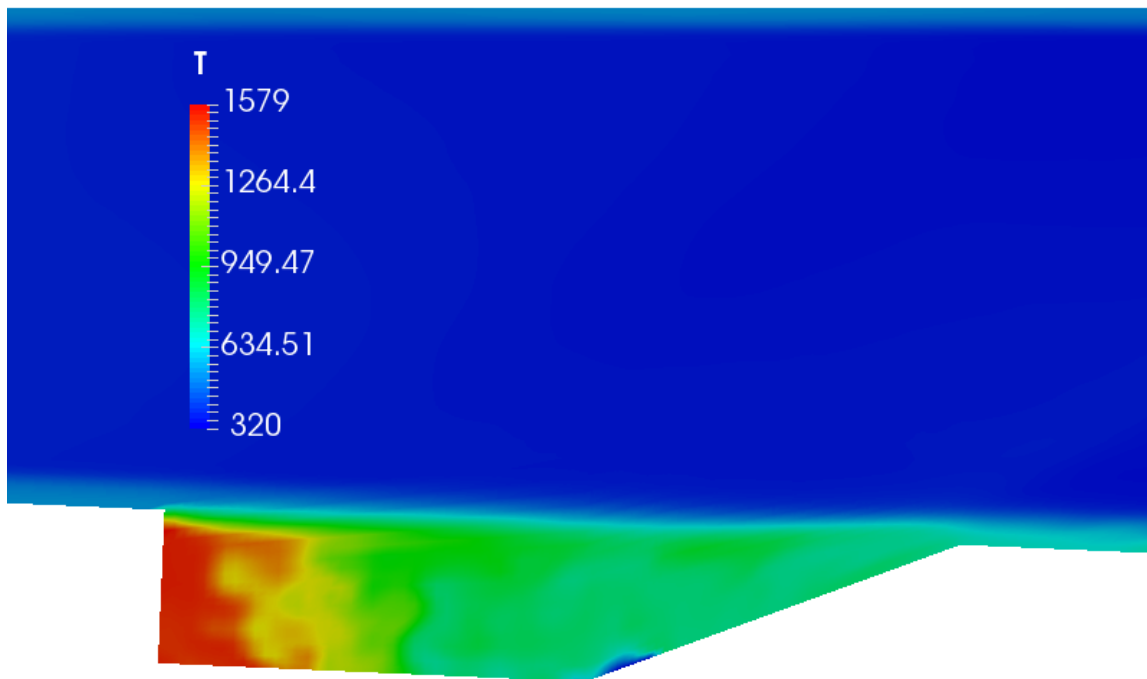

Figure 59: OpenFOAM Temperature Scene for 0.01 Second LES Case

In Figure 59, the OpenFOAM LES case was run for a total of 0.01 seconds. The maximum temperature was close to 1600 K. At temperatures this high, the ethylene is close to ignition. It takes time for the high-temperature zones to be eliminated when the simulation is first initialized. It was later determined that this was too short of a total time. The total time of the simulation was increased to 0.055 seconds.
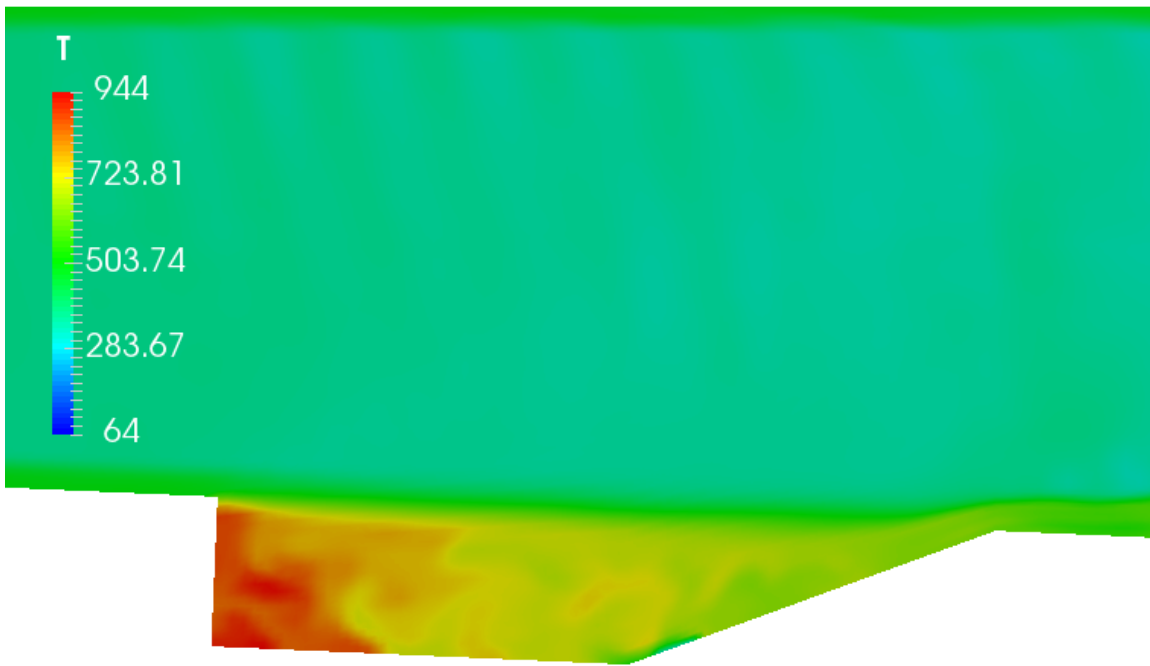
Figure 60: OpenFOAM Temperature Scene for 0.04 Second LES Case

In Figure 60, the OpenFOAM LES case was run for 0.055 seconds. After running the OpenFOAM LES case for a longer total time, the temperature scene was still giving close to a 300 K difference. It was decided that 0.2 seconds was still too short of a time. Finally, the case was for a total time of 0.2 seconds.
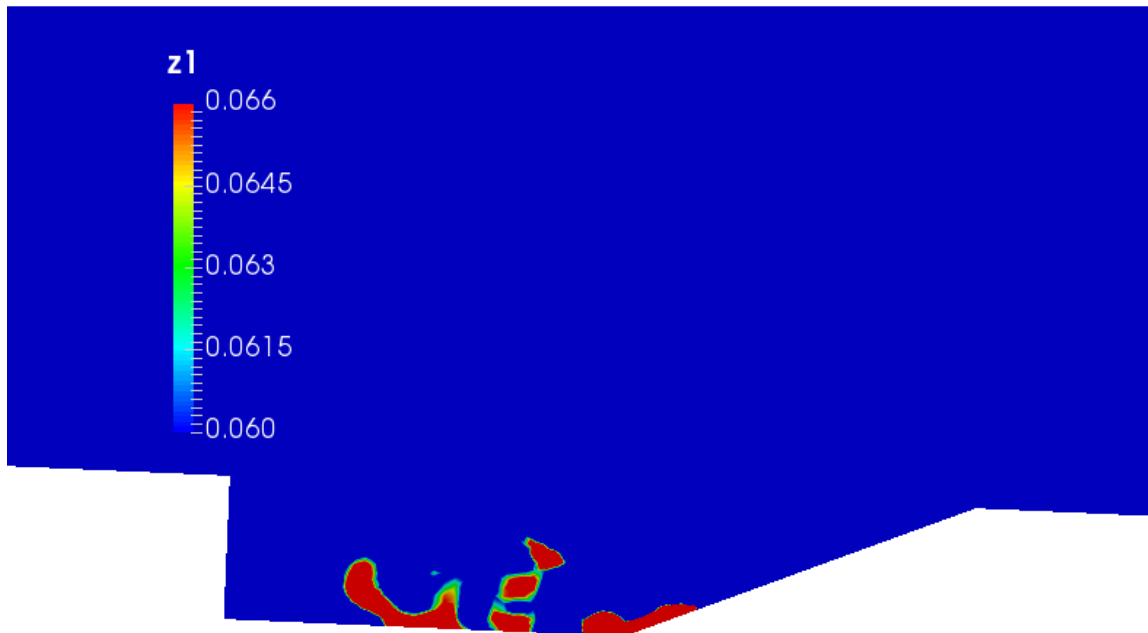
Figure 61: Instantaneous Passive Scalar Scene for LES OpenFOAM Case

Figure 61 depicts the instantaneous passive scalar scene for the non-reacting OpenFOAM LES case. After viewing the results, it was determined that the passive scalar mean needs to be viewed rather than the instantaneous passive scalar function. When working with LES, more fluctuation is present when compared to RANS. After learning from these mistakes, changes were implemented, simulations were corrected, and more accurate results were achieved. Figures 62 through 69 show the finalized results for the non-reacting LES case with fuel injection. The figures display both the OpenFOAM and StarCCM results for the velocity scene, the temperature scene, and the mean passive scalar scene.
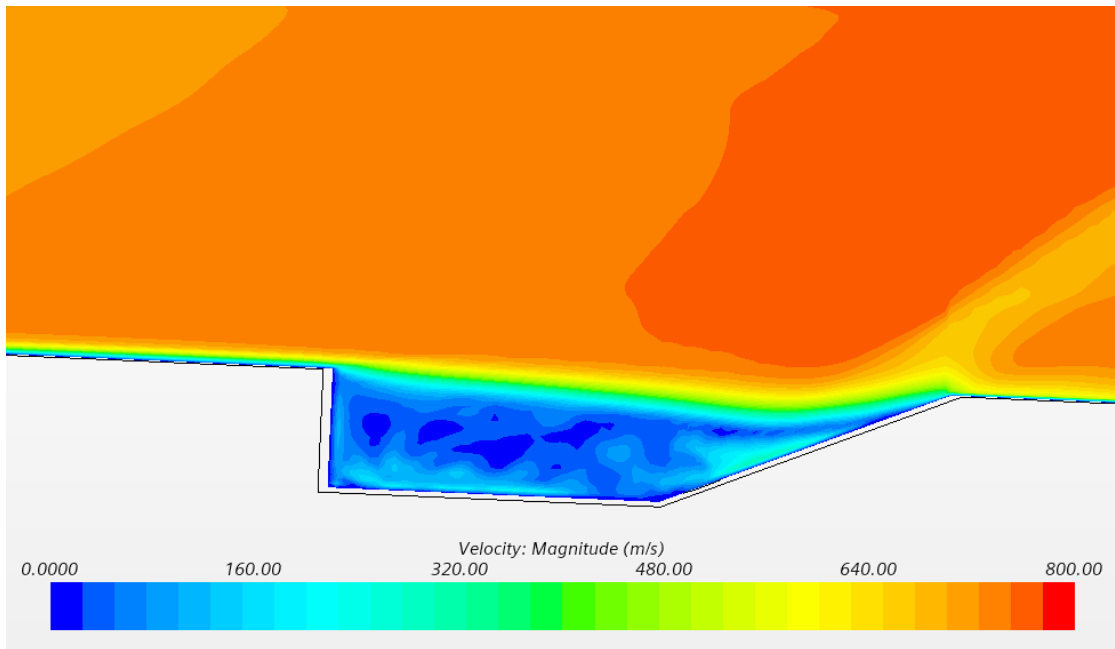
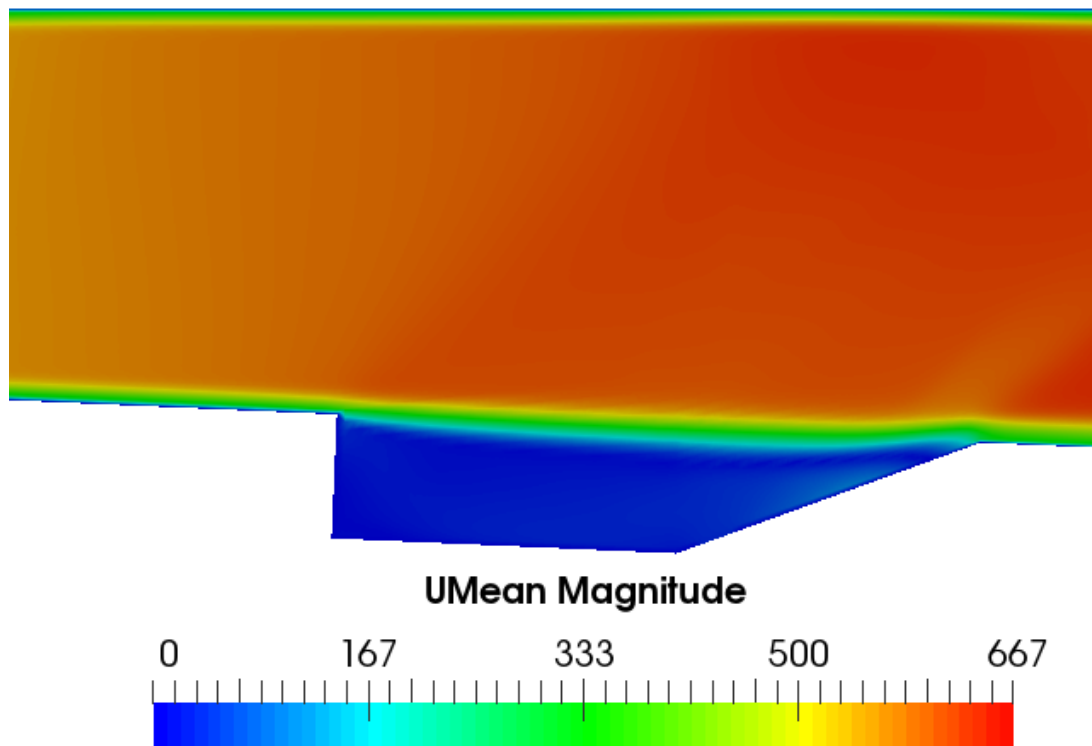*Figure 62: Non-Reacting LES StarCCM Velocity Scene*

Figure 63: Non-Reacting LES OpenFOAM Velocity Scene
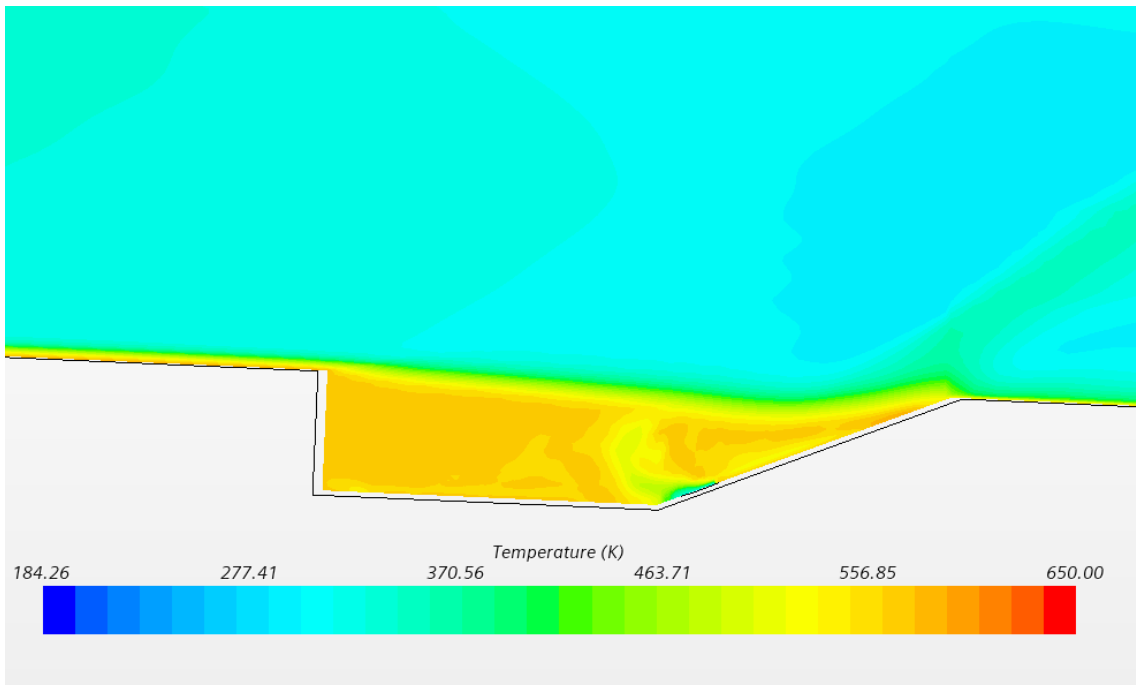
Figure 64: Non-Reacting LES StarCCM Temperature Scene
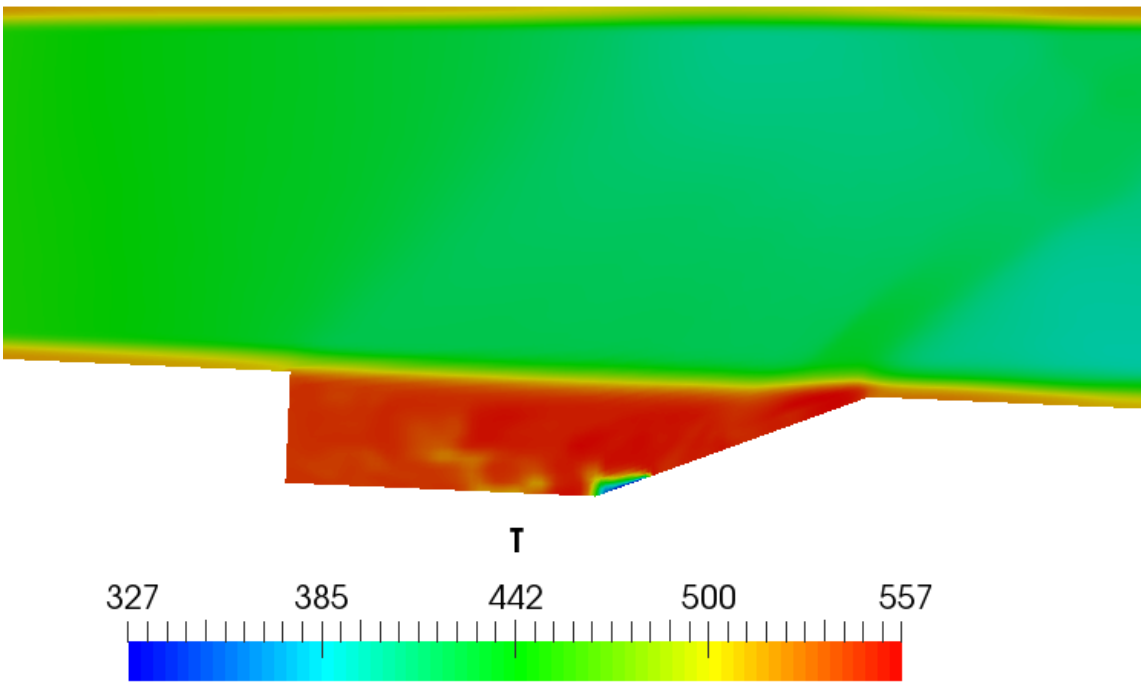
Figure 65: Non-Reacting LES OpenFOAM Temperature Scene

Mean of Passive Scalar

Figure 66: Non-Reacting LES StarCCM Mean Passive Scalar Scene
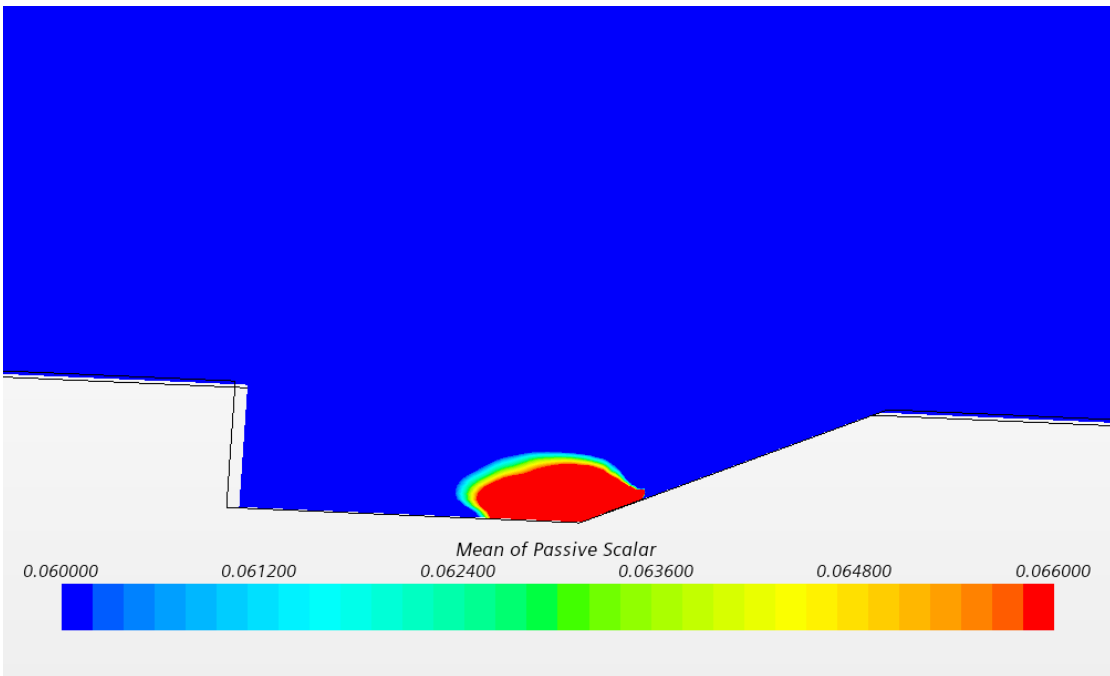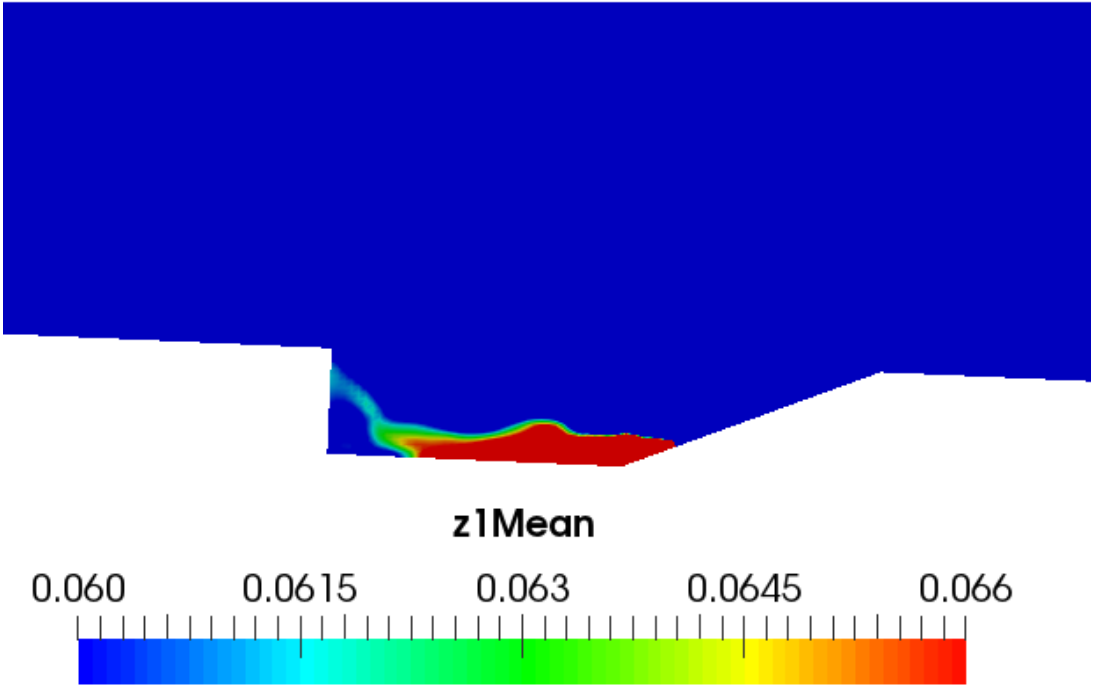

z1Mean

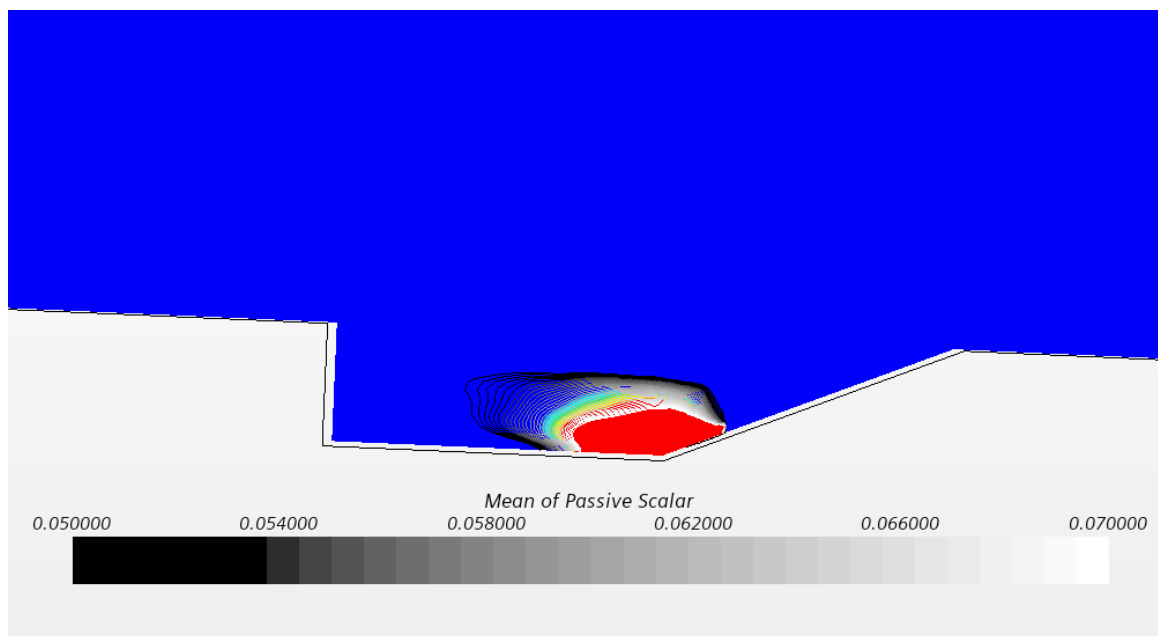*Figure 67: Non-Reacting LES OpenFOAM Mean Passive Scalar Scene*

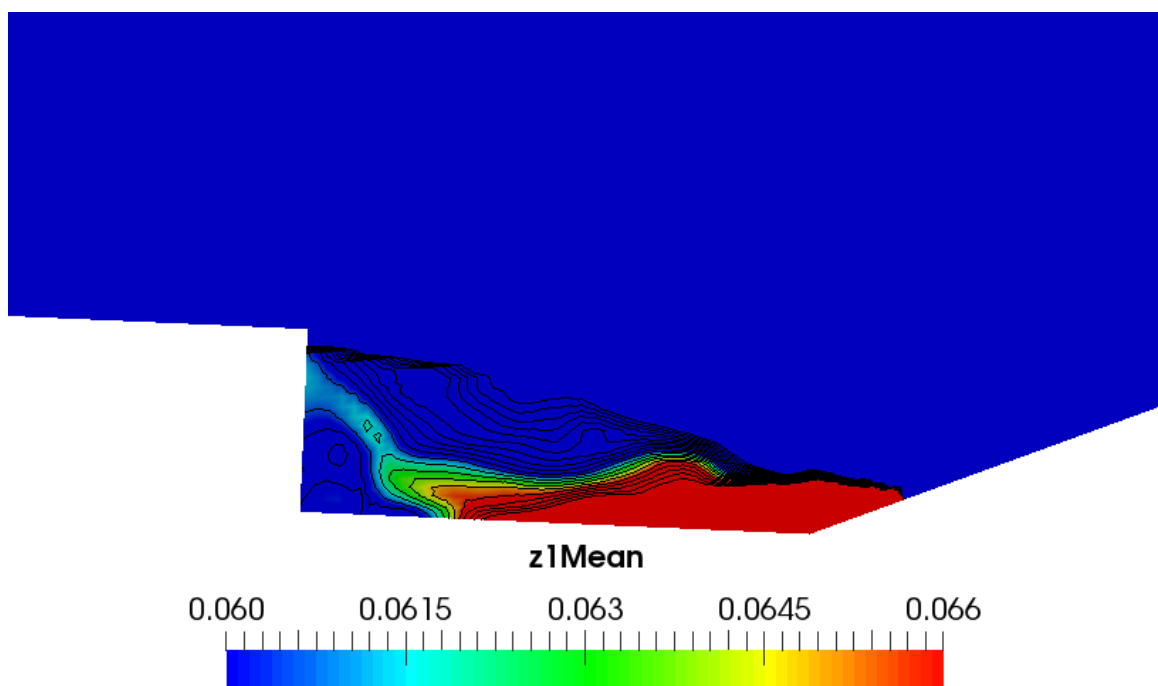*Figure 68: Non-Reacting LES StarCCM Imposed Mean Passive Scalar Scene*

Figure 69: Non-Reacting LES OpenFOAM Imposed Mean Passive Scalar Scene

The simulations agree with the experimental data as well as the published data from Peterson. When comparing the velocity scenes from both StarCCM and OpenFOAM, seen in Figures 62 and 63, both give remarkably similar visual results and velocity profiles. Looking at the temperature scenes from both in Figures 64 and 65, the results agree with each other giving terribly similar temperature profiles and ranges. Lastly, looking at the passive scalar scenes from both, seen in Figures 66 and 67, there are a few slight differences. Precisely looking at a passive scalar value of 0.0636, OpenFOAM has a higher concentration on the leftmost side of the cavity compared to the StarCCM simulation. As seen in Figures 68 and 69, the imposed lines show where theoretical combustion will occur. The black is the lowest concentration, and the white is the highest concentration for StarCCM. OpenFOAM has streamlines ranging from the 0.05 to 0.07 values of the passive scalar. It is evident that OpenFOAM predicts much more combustion to occur on the backside of the cavity. The OpenFOAM LES passive scalar scenes are very comparable to those obtained when running the RANS case in OpenFOAM, whereas StarCCM gives differing results. The profiles also appear slightly different but similar to each other. StarCCM should be considered to be the more accurate of the two as it is the commercial code and has been the more developed among the two. Some research has shown that OpenFOAM does have some problems accurately modeling LES.

Upon completion of the non-reacting LES simulations, data was again extracted from the simulation results to be compared to published data from Peterson's results ([5],[6],[7]). For this particular case, only three locations within the cavity could be extracted to be compared to experimental and published data. The three locations that had published data include the following: 26.5 cm, 28.4 cm, and 30.2 cm. Figures 70-75 show the plotted

results. The first set of graphs shows the normalized x, or U, component of velocity, and the second set of graphs show the normalized y, or V, component of velocity.

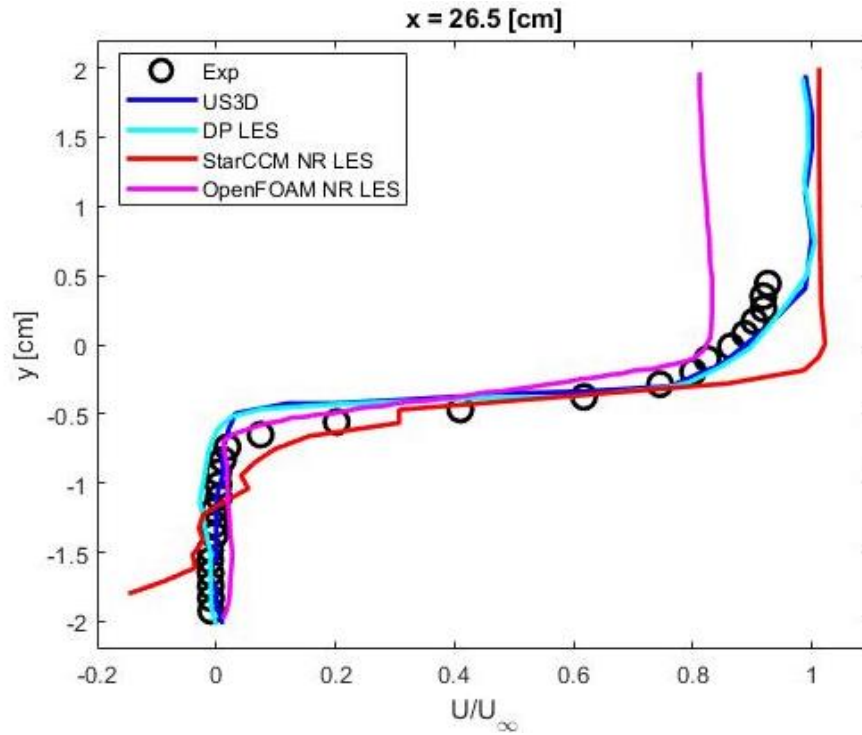Normalized X-Component RANS Graphs

Figure 70: 26.5 cm X-Component Data for Non-Reacting LES
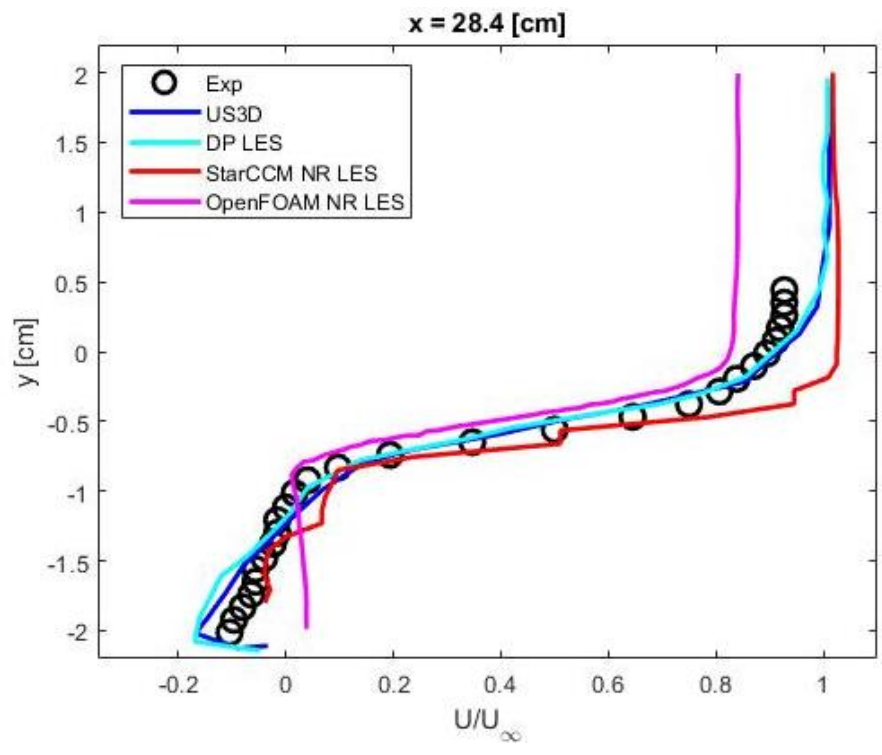
Figure 71: 28.4 cm X-Component Data for Non-Reacting LES

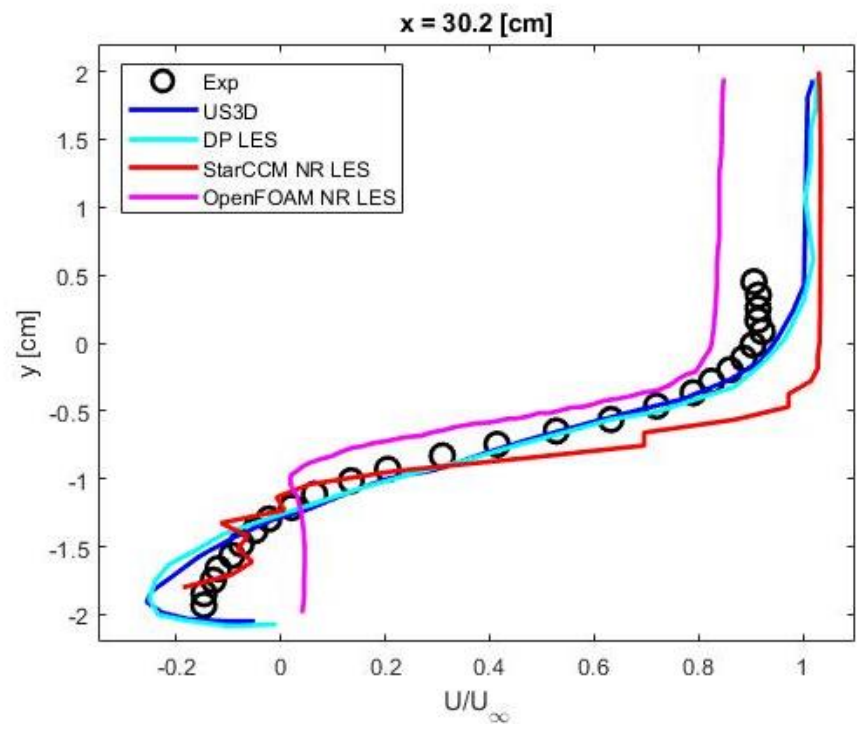*Figure 72: 30.2 cm X-Component Data for Non-Reacting LES*

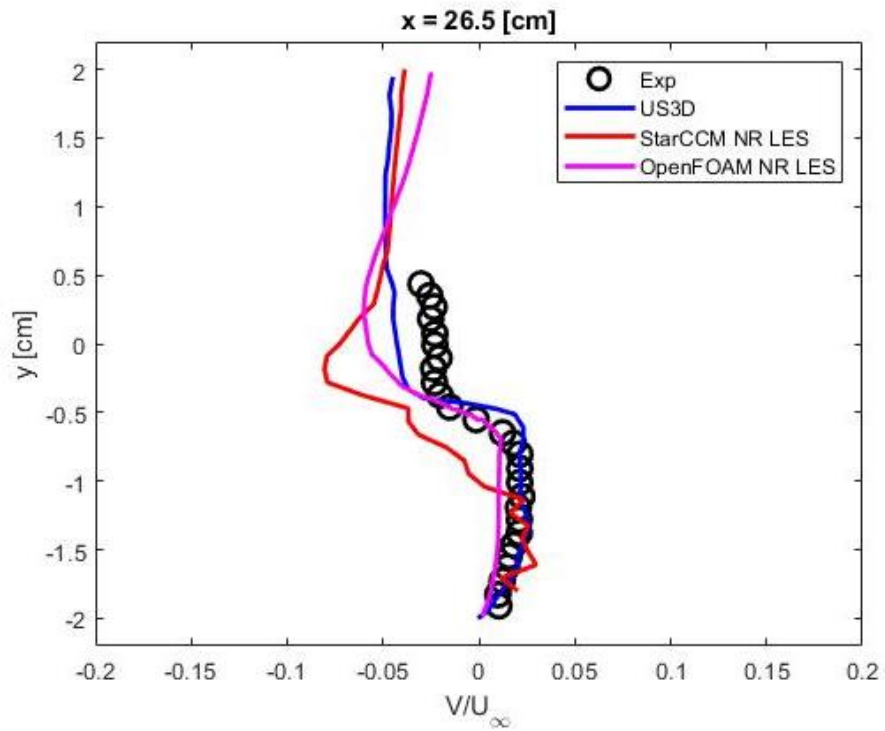Normalized Y-Component RANS Graphs

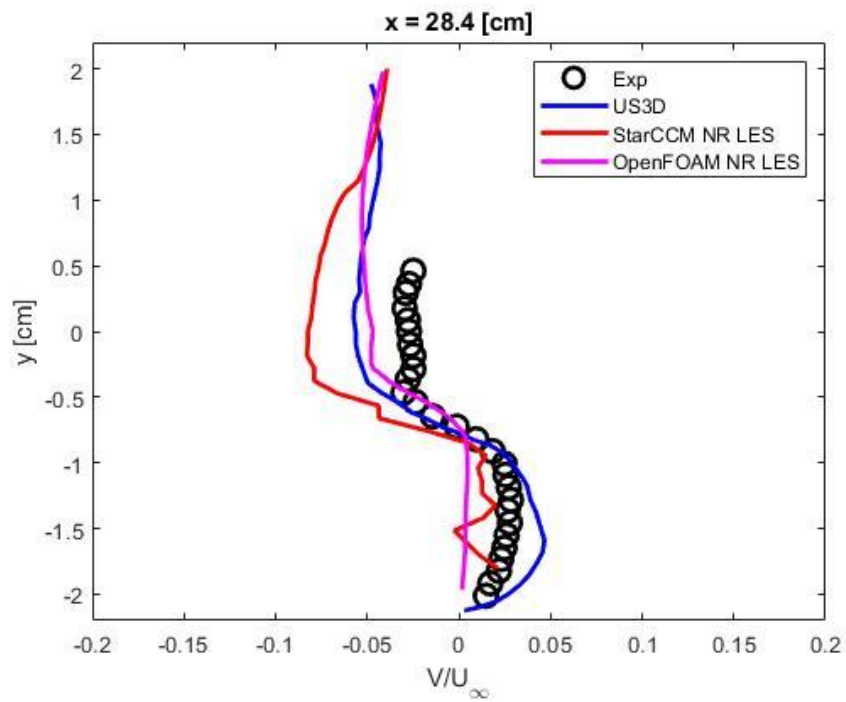*Figure 73:26.5 cm Y-Component Data for Non-Reacting LES*

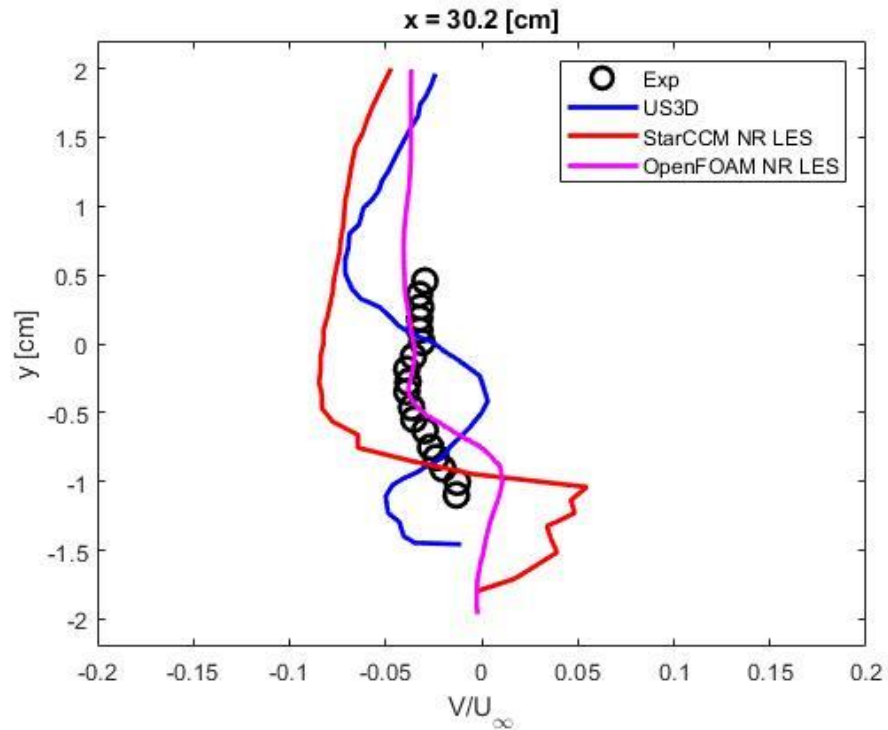*Figure 74: 28.4 cm Y-Component Data for Non-Reacting LES*

Figure 75: 30.2 cm Y-Component Data for Non-Reacting LES

The simulations have similar-appearing velocity and temperature profiles when comparing the visual results. OpenFOAM gives a lower freestream velocity, as well as a lower temperature. When assessing the scenes for the passive scalar, it can be seen that the two simulations give vastly different results. OpenFOAM predicts a greater dispersion of the fuel when modeling using LES. StarCCM predicts the fuel staying closer to the right side of the cavity, where the injection occurs. When assessing the validity of the two, the StarCCM results are the more accurate results. After talking with Peterson, it was determined that OpenFOAM needs improvement to its LES simulation capabilities.

When comparing the simulation results to the experimental and published data for the normalized x component graphs, it is evident that the OpenFOAM LES solver could use some further modifications and improvements. Looking at the x = 26.5 cm location data in figure 70, OpenFOAM outperforms StarCCM for regions lower in the cavity. OpenFOAM

agrees with the experimental and published data but underpredicts the freestream velocity. StarCCM struggles to accurately capture the physics for regions lower in the cavity but more closely predicts the freestream velocity. This is expected, as current LES modeling has a challenging time accurately modeling near-wall treatments. This was evident when looking at many published papers and speaking with Dave Peterson from the AFRL. Looking at figures 71 and 72, StarCCM more accurately models the physics within the middle regions of the cavity from lesser to greater values of x-distance, whereas OpenFOAM struggles to capture the correct velocities at lower y-value regions. Again, StarCCM slightly overpredicts the normalized velocities for y values from -0.5 to 0 cm. OpenFOAM does a better job of modeling these values when compared to StarCCM, but again, underpredicts the freestream velocity.

Looking at the normalized y component graphs, StarCCM and OpenFOAM agree, for the most part, with the experimental and published data for locations of x = 26.5 cm and x = 28.4 cm within the cavity. OpenFOAM does an excellent job of capturing the physics when specifically looking at the x = 26.5 cm location. It agrees with the experimental data for lower regions of the cavity and has a deviation closer to the freestream region. StarCCM does a respectable job for lower cavity regions as well but begins deviating from the experimental data as it approaches freestream velocities. StarCCM agrees when specifically looking at the x = 28.4 cm location. StarCCM agrees with the experimental data for lower regions of the cavity and has a deviation closer to the freestream region. OpenFOAM gives a more uniform normalized velocity that has more deviation from the experimental data at lower regions in the cavity and agrees when modeling y locations of -1.0 cm to -0.5 cm and has some further deviation present as it approaches freestream

velocities. When looking at the cavity location of x = 30.2 cm, both have some disagreement when compared to experimental data. Even the hybrid code developed by Peterson has difficulties capturing the physics. OpenFOAM appears to most accurately capture the physics when comparing it amongst simulation data but could still use further improvements. OpenFOAM greatly agrees with y locations of -0.5 cm to 0.5 cm. Some explanations for the large discrepancies include fuel injection causing solver problems, grid resolution, and turbulence modeling. Further work needs to be done to improve LES turbulence modeling for supersonic flows. Upon completion of the findings, it was decided to run a hybrid RANS-LES non-reacting case in Star-CCM.

Detached Eddy Simulation Non-Reacting Case with Ethylene Injection

A hybrid RANS-LES simulation was performed using a Detached Eddy Simulation, DES, along with the SST (Menter) K-Omega Detached Eddy solver in StarCCM. This solver is similar to the US3D solver that was developed by David Peterson with which much of the simulation data is compared. A hybrid RANS-LES model typically gives more accurate results than a RANS with the added benefit of having quicker simulation solving times than LES solvers. Research has shown that OpenFOAM has some difficulties running a hybrid model and achieving accurate results, so for this specific case, only StarCCM was used when running simulations and comparing to experimental and published flame holder cavity data. Figures 76-79 show the DES results.
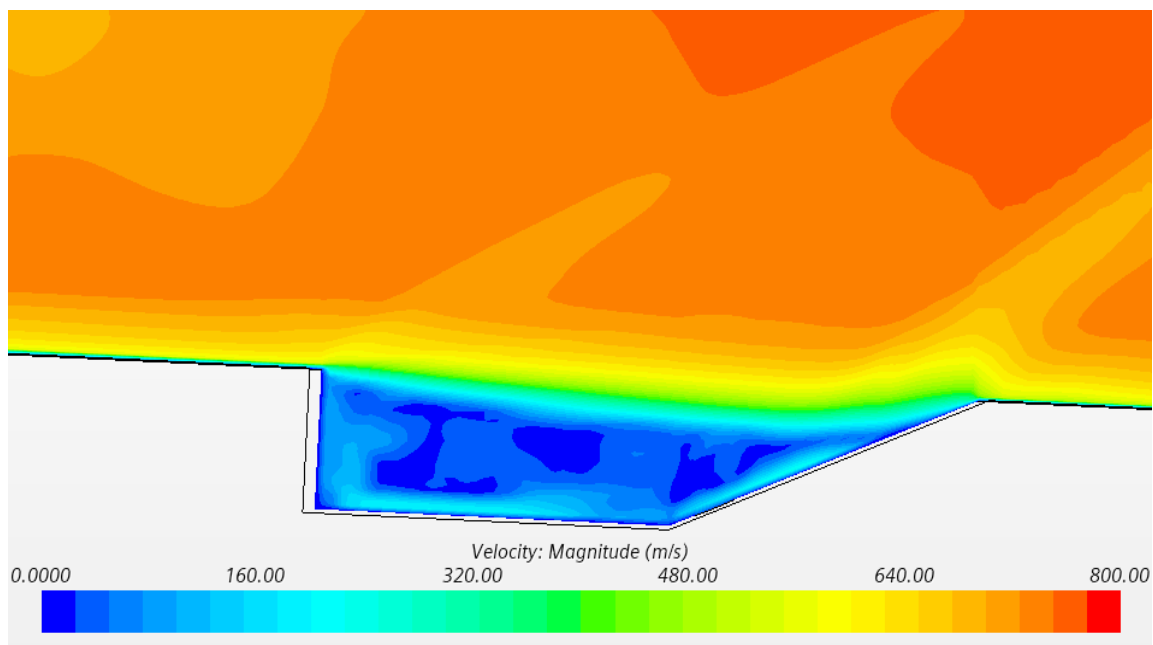
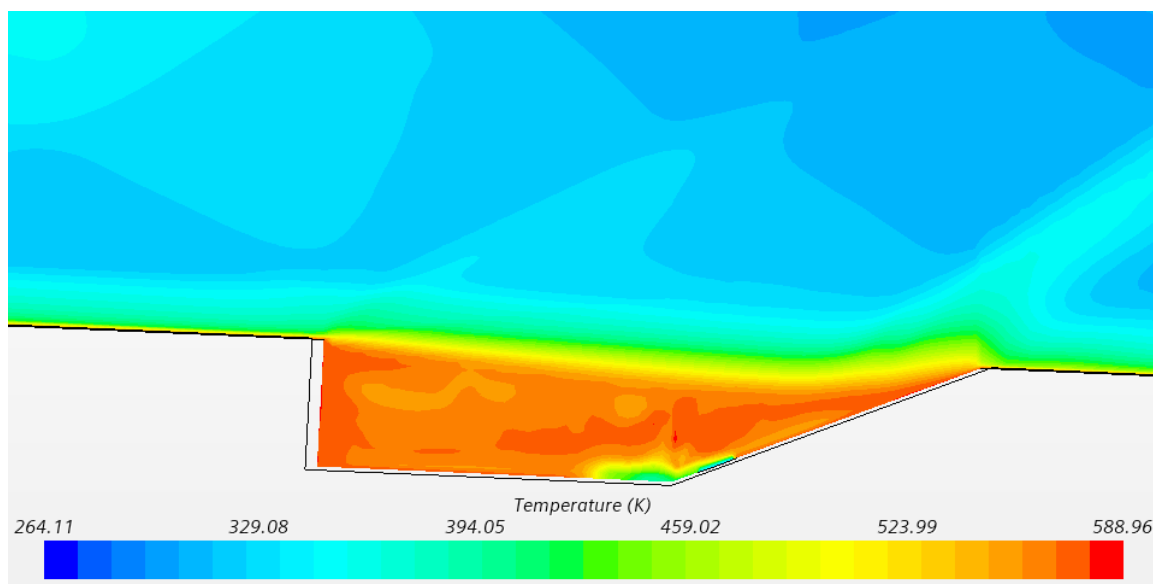*Figure 76: Non-Reacting DES StarCCM Velocity Scene*

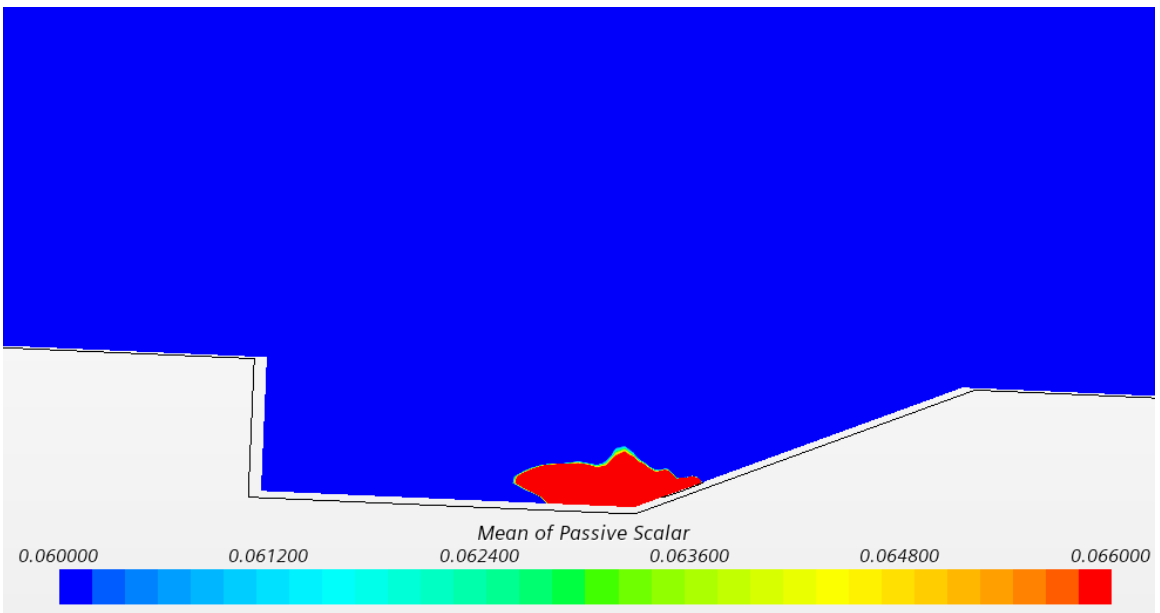*Figure 77: Non-Reacting DES StarCCM Temperature Scene*

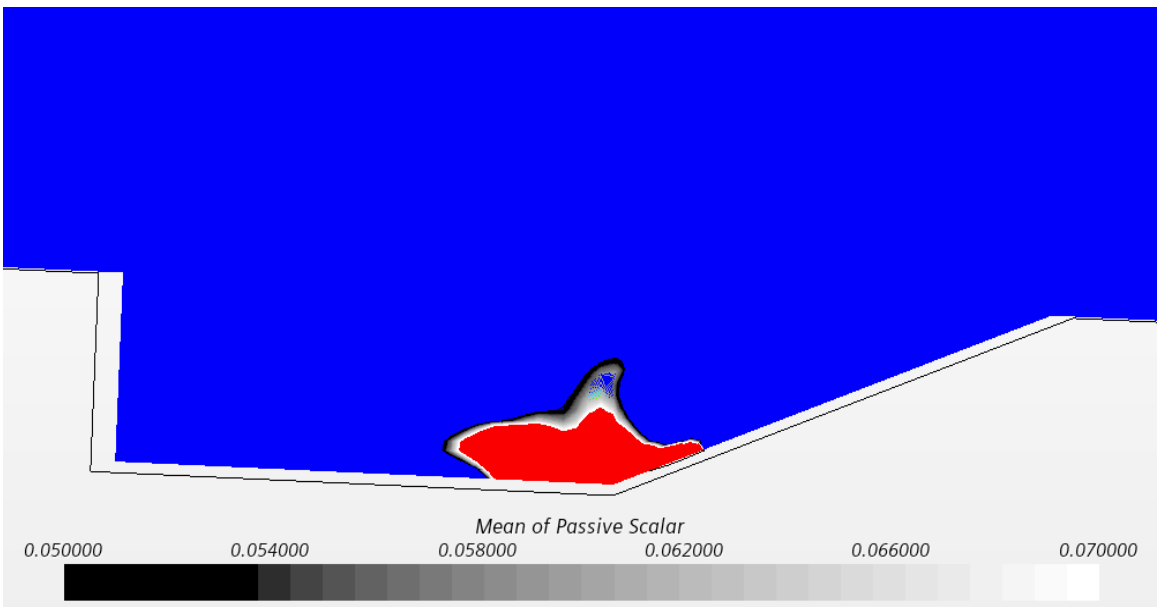*Figure 78: Non-Reacting DES StarCCM Mean Passive Scalar Scene*

Figure 79: Non-Reacting DES StarCCM Imposed Mean Passive Scalar Scene

Upon completion of the non-reacting DES simulations, extracted data was compared to Peterson's results ([5],[6],[7]). For this particular case, the StarCCM simulations were

compared to the US3D hybrid RANS-LES developed by Peterson, experimental data, and lastly to the previously performed non-reacting RANS and LES StarCCM simulations. DES simulations should give results between RANS and LES since it is a hybrid of the two. Figures 80-93 show the plotted results.
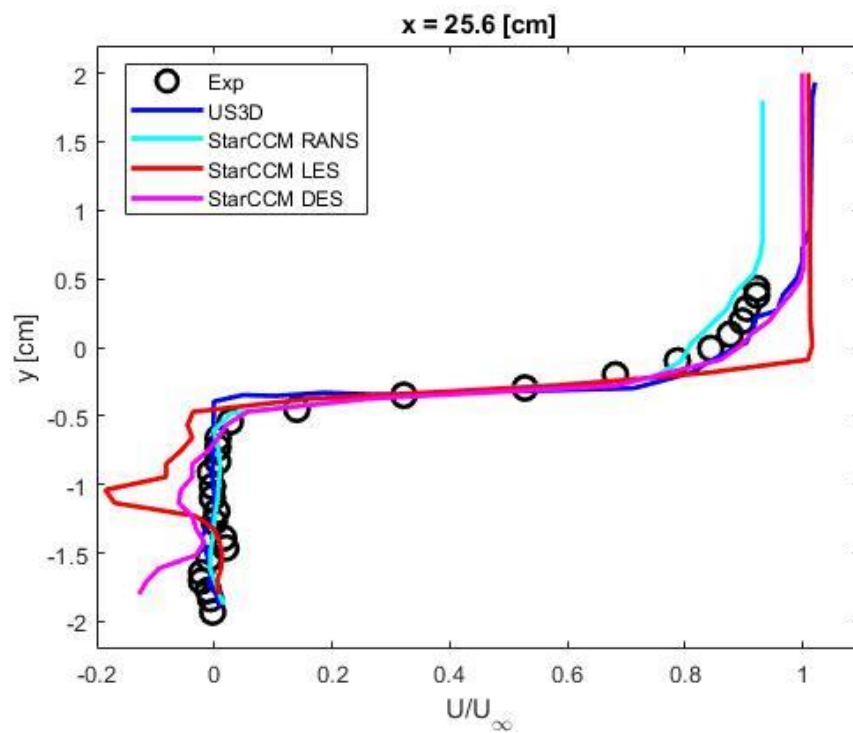
Normalized X-Component RANS Graphs

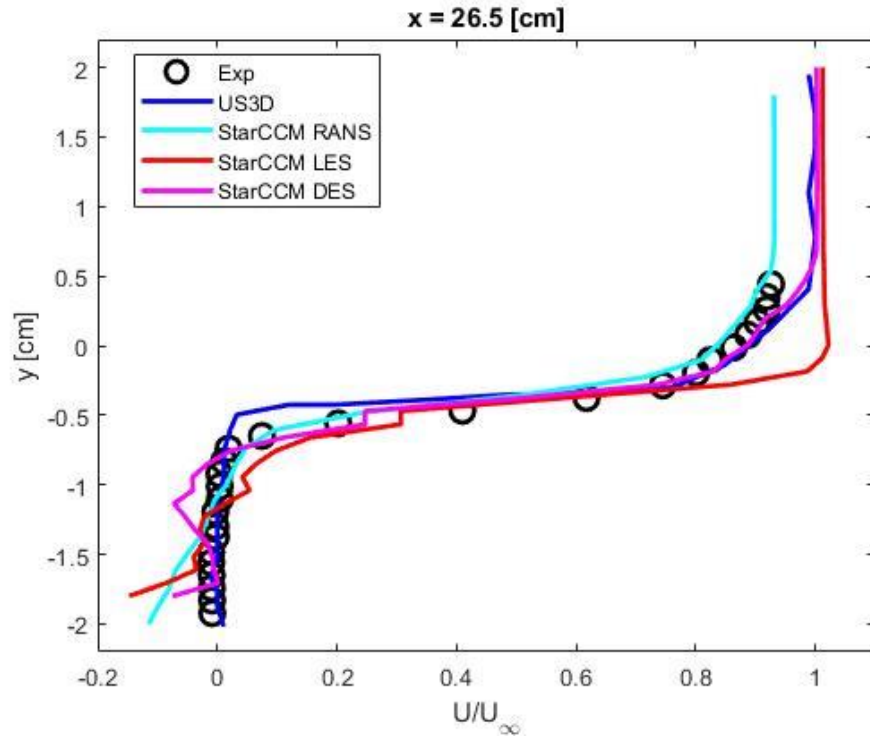

Figure 80: 25.6 cm X-Component Data for Non-Reacting DES

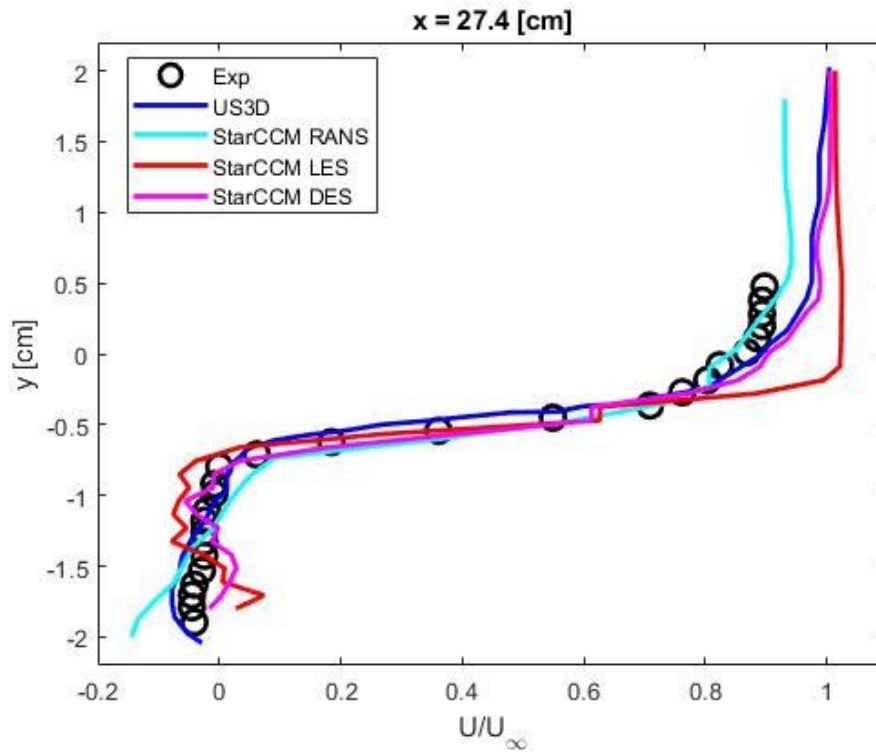*Figure 81: 26.5 cm X-Component Data for Non-Reacting DES*

Figure 82: 27.4 cm X-Component Data for Non-Reacting DES

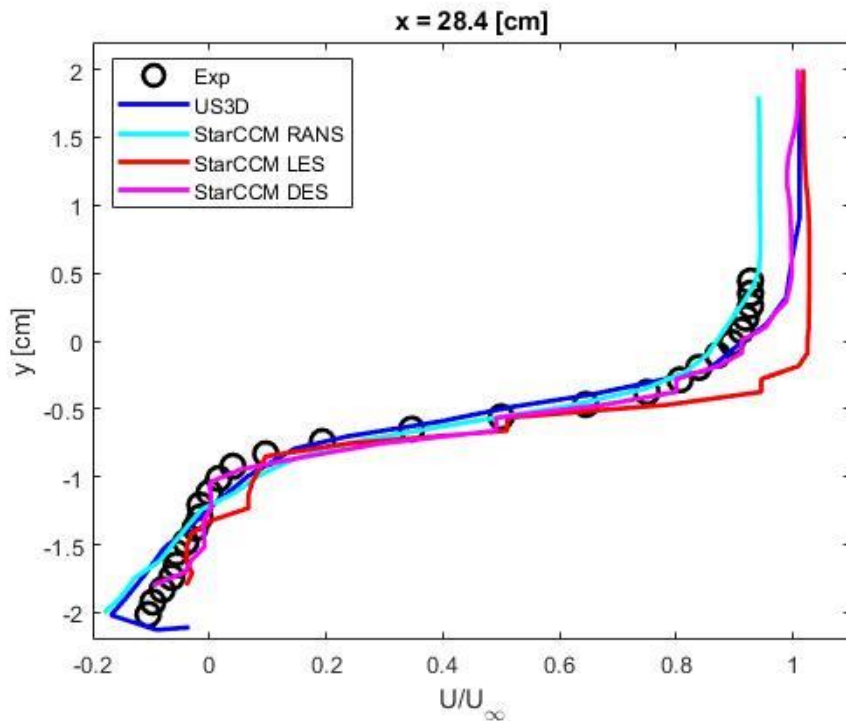*Figure 83: 28.4 cm X-Component Data for Non-Reacting DES*

Figure 84: 29.2 cm X-Component Data for Non-Reacting DES

Figure 85: 30.2 cm X-Component Data for Non-Reacting DES

Figure 86: 31.1 cm X-Component Data for Non-Reacting DES

Normalized Y-Component RANS Graphs

Figure 87: 25.6 cm Y-Component Data for Non-Reacting DES

Figure 88: 26.5 cm Y-Component Data for Non-Reacting DES

Figure 89: 27.4 cm Y-Component Data for Non-Reacting DES

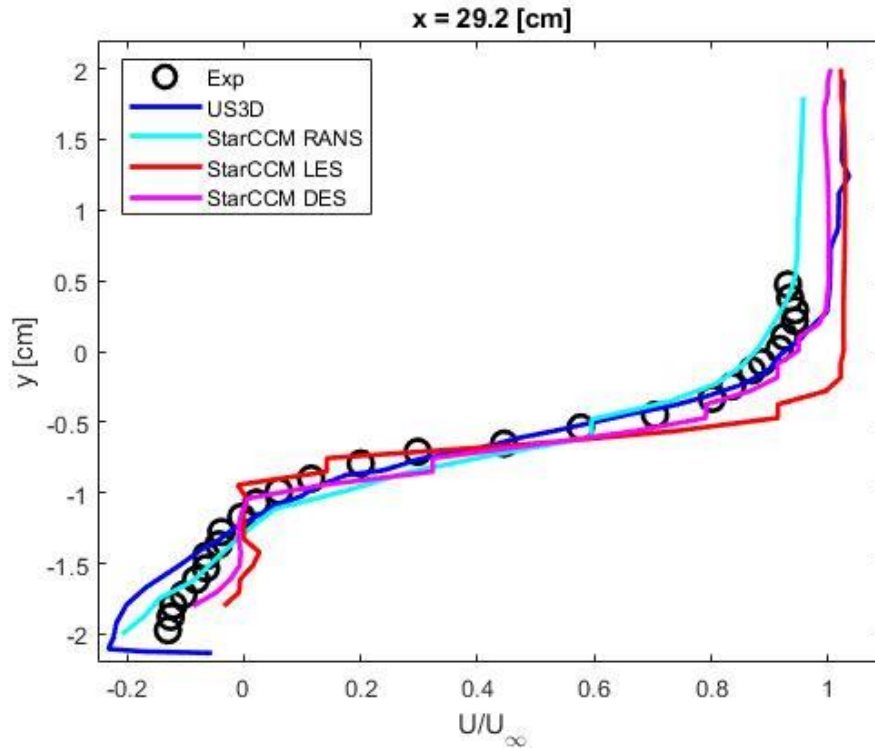*Figure 90: 28.4 cm Y-Component Data for Non-Reacting DES*
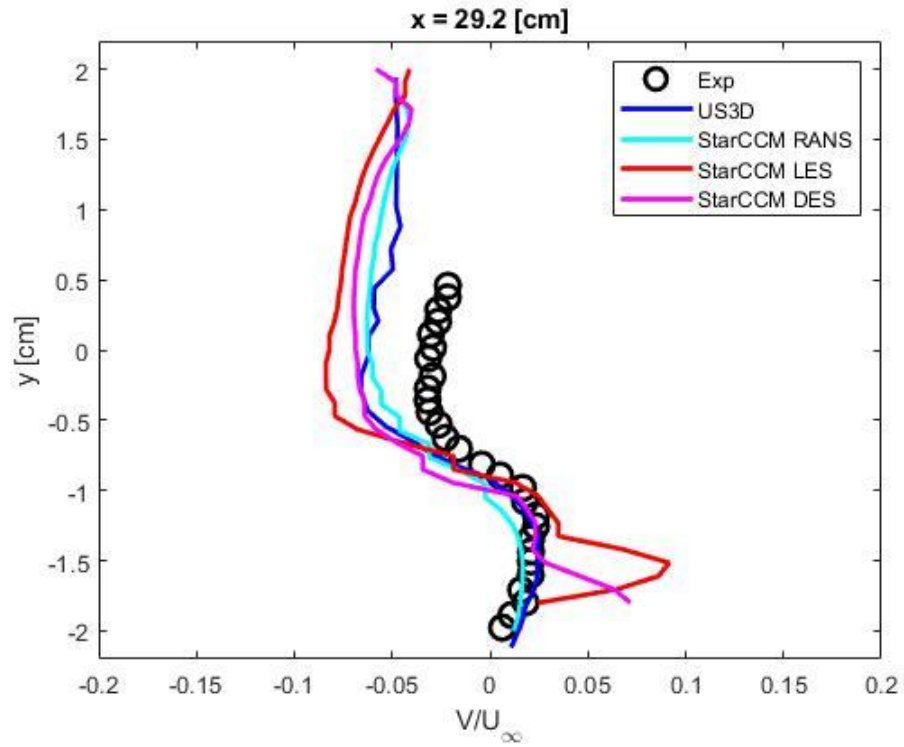
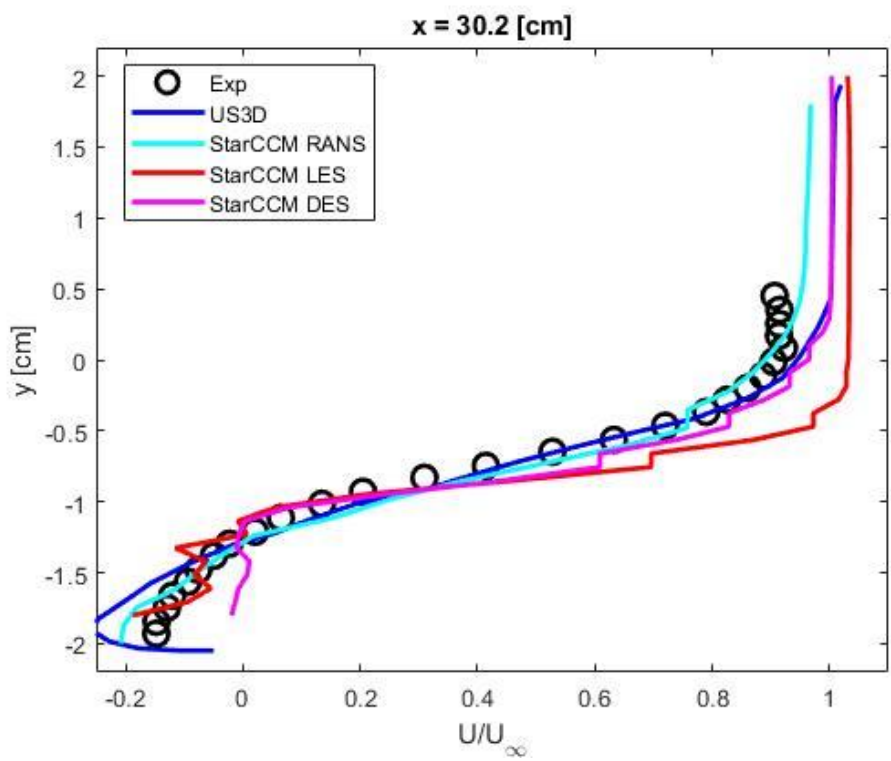*Figure 91: 29.2 cm Y-Component Data for Non-Reacting DES*

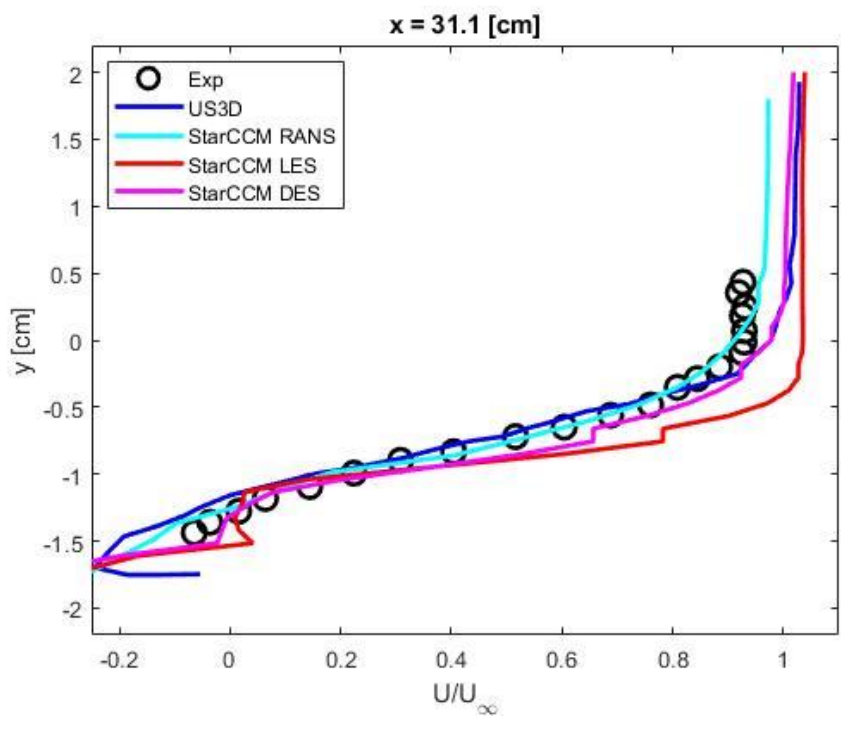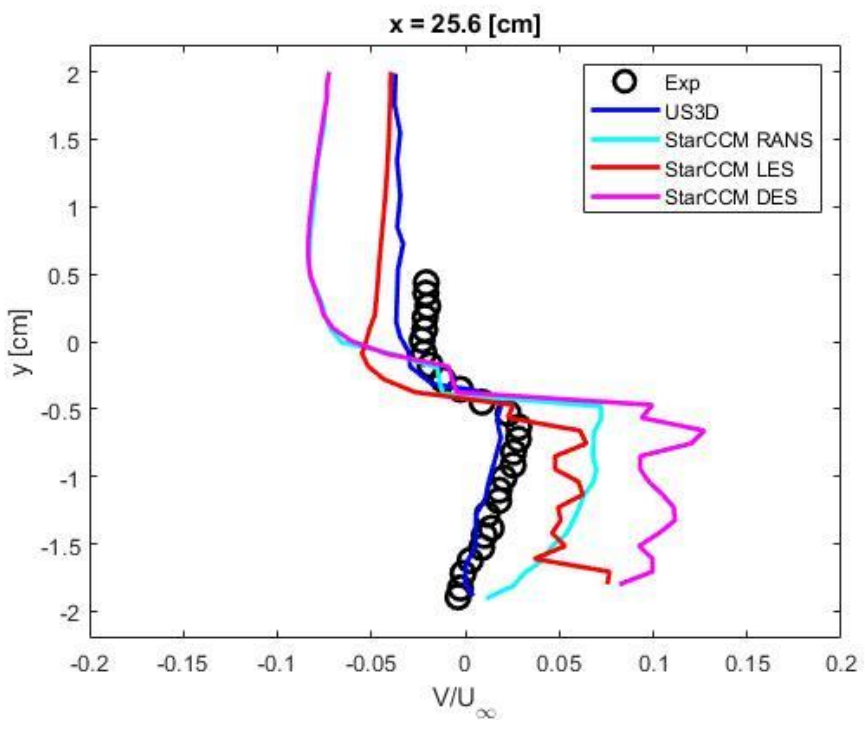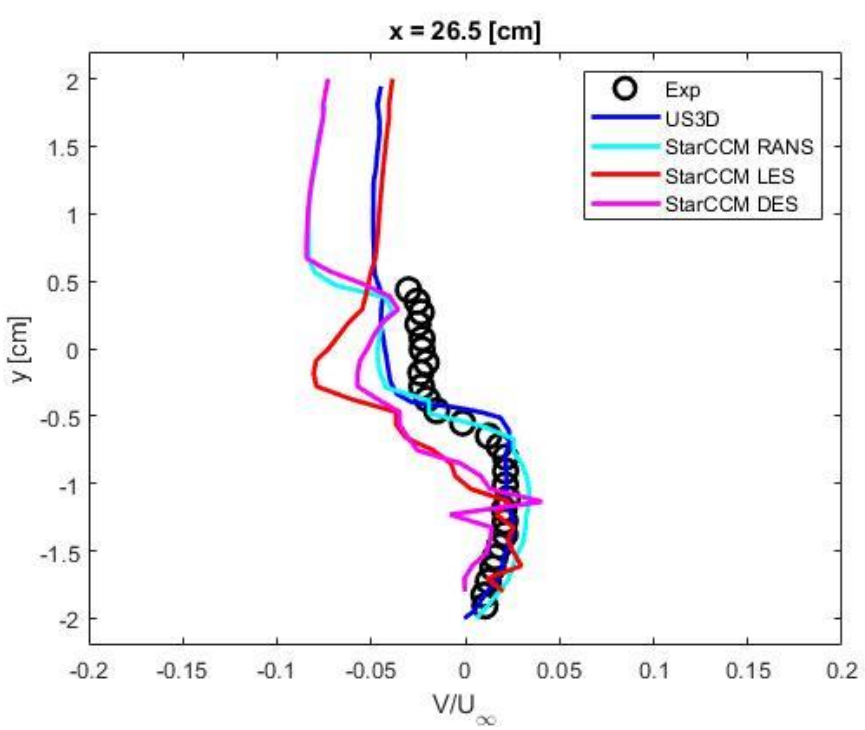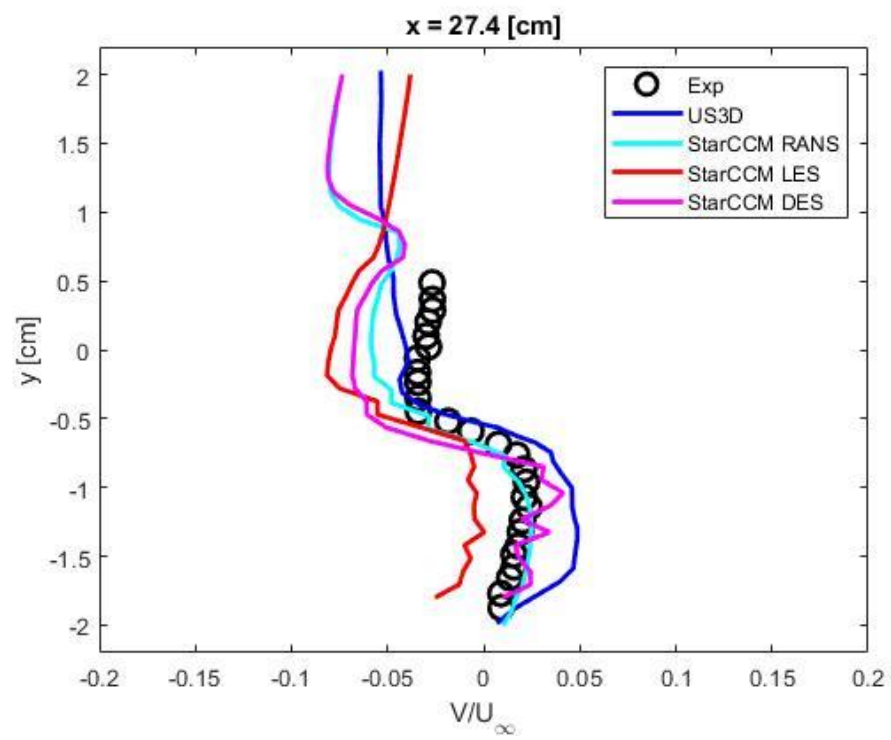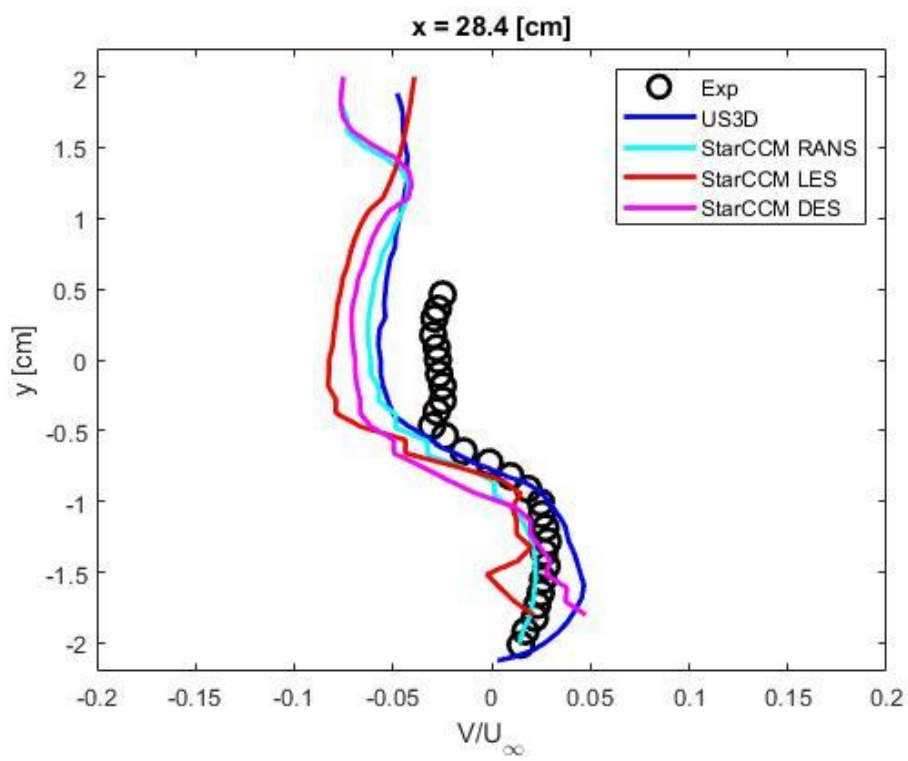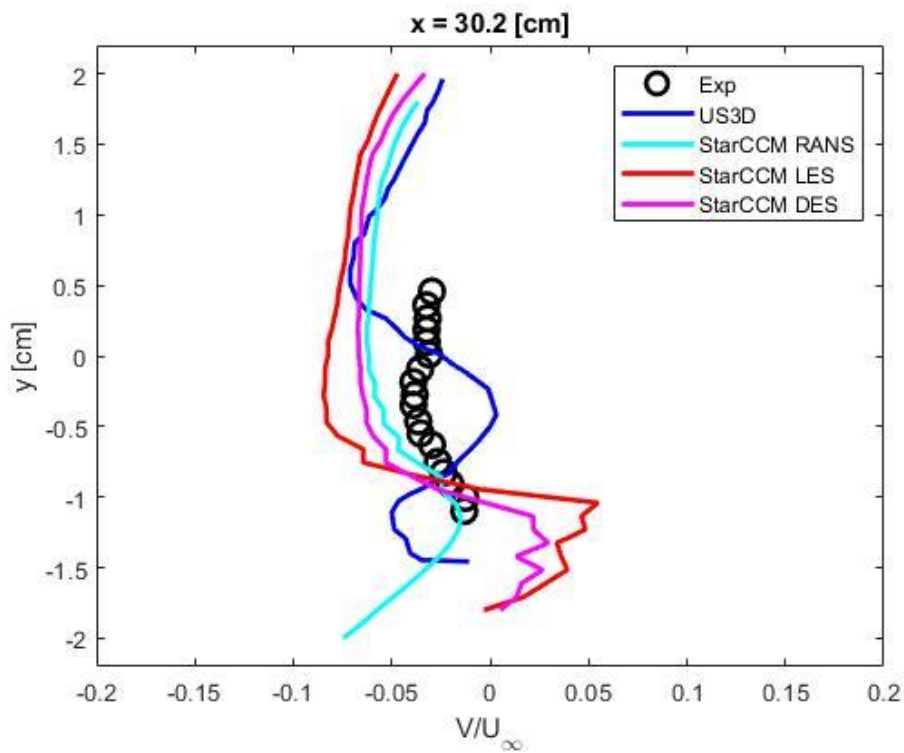*Figure 92: 30.2 cm Y-Component Data for Non-Reacting DES*
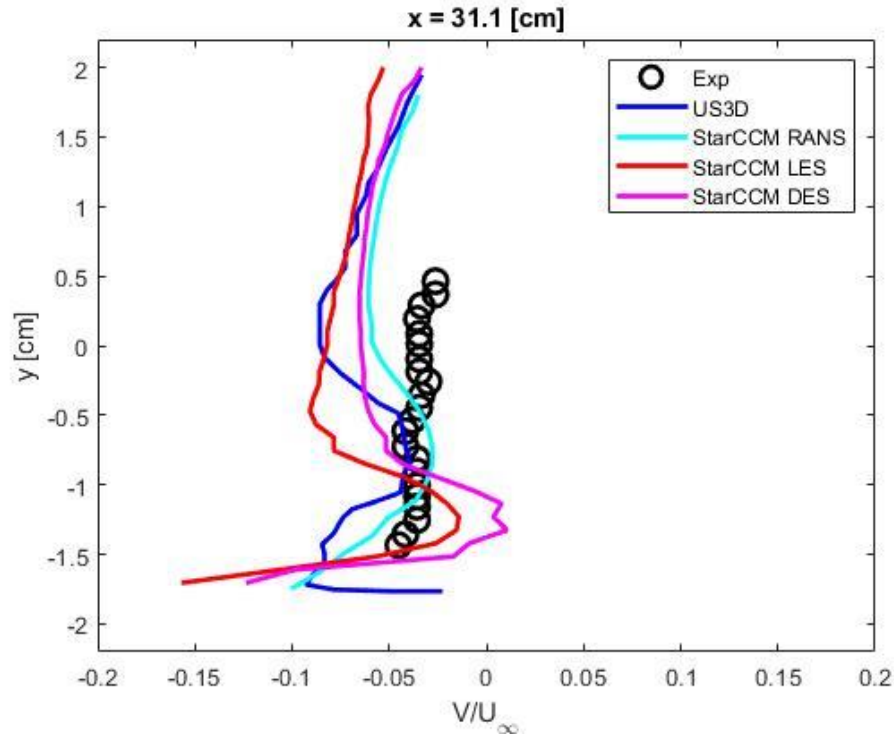
Figure 93: 31.1 cm Y-Component Data for Non-Reacting DES

Looking at the visualized results, the temperature and velocity profiles are remarkably similar to previous RANS and LES simulations. The passive scalar scene does appear to be a hybrid of the RANS and LES results, more closely resembling the shape from the LES simulation. Figure 79 shows the theoretical region where combustion will occur. The black is the lowest concentration, and the white is the highest concentration. Currently, StarCCM does not have a terrific way of depicting this region where combustion will occur.

When comparing the extracted data to publish and experimental data for the x component normalized velocity, the DES data matched up quite well with the US3D data. This should be the case as both are hybrid RANS-LES physics solvers. As previously stated, LES has trouble accurately capturing the physics of near-wall treatments. The DES does a better job of accurately modeling the physics. This can be seen by looking at the graphs in the region

with a normalized velocity close to zero and a y distance of -2 to -1 cm within the cavity flame holder. In addition, the DES simulation better captures the freestream velocity when compared to the LES model. The RANS does the best job of capturing the freestream velocity when compared to experimental data, which is expected due to the nature of RANS.

When comparing the extracted data to publish and experimental data for the y component normalized velocity, the DES data matched up quite well with the US3D data for cavity locations of x = 26.5 cm through x = 29.2 cm. For the cavity regions that are close to the walls, x = 25.6 cm, and x = 31.1 cm, StarCCM had difficulties capturing the physics which was expected. As found in earlier simulations, there are some difficulties accurately capturing the physics near the walls due to grid resolution, fuel injection, and turbulence modeling. Comparing the data from all three StarCCM solvers, the DES does appear to give results between the RANS and LES models for most locations within the flame holder cavity. The DES model is fairly new and shows promising signs, but it is evident that there are still some improvements that could be made to more accurately model supersonic flows.

 Overall, the DES simulation agrees with the experimental and published data. It offers a good median between RANS and LES simulations for accuracy and simulation run time.

Summary of Results

Comparing all simulations amongst each other offers good comparison for the various turbulence models and CFD software. Both OpenFOAM and StarCCM RANS models show the capability to model supersonic flows for a cavity flame holder. Both compare well with experimental and published data but do have some limitations. As evident from

earlier, StarCCM and OpenFOAM struggle some with capturing the near-wall and freestream physics. Further research should be done to improve the turbulence modelling of these solvers in supersonic flow. Even the hybrid US3D code had issues accurately matching the experimental data. Figures 94 and 95 show the combustion location for both softwares. As evident, the location is very similar if not the same.

Looking at non-reacting LES simulations, both StarCCM and OpenFOAM gave promising results. Extracted data compared well to the experimental and published data for the middle regions of the cavity flame holder but had some limitations at the near-wall and freestream locations. When comparing the simulation results to previously published data, the same issue was present; as of now, CFD turbulence models have some issues present when trying to solve supersonic flows close to walls. This is an area for further research growth. Figures 96 and 97 show the combustion location for the LES case for both StarCCM and OpenFOAM. As evident, the exact location of combustion is slightly different between the two. StarCCM predicts combustion to occur further right in the cavity region than does OpenFOAM. OpenFOAM predicts a combustion location more similar to the RANS model. StarCCM should be the more trusted result, as the plotted data better agrees, and research has shown that OpenFOAM LES turbulence modelling needs some improvements.

Lastly, when utilizing a hybrid RANS-LES turbulence model, the Detached Eddy Simulation, very promising results were obtained. Again, only StarCCM utilized this solver. OpenFOAM has issues with this solver, so further research could be done to develop an accurate DES solver in OpenFOAM. StarCCM had very comparable results to both the experimental data and the published hybrid RANS-LES data. This validates that

StarCCM will work for supersonic flows and that the passive scalar results are correct for showing theoretical combustion location. Figure 98 shows the combustion location for the DES case in StarCCM. As evident, the passive scalar profile is very similar to the LES case in StarCCM.
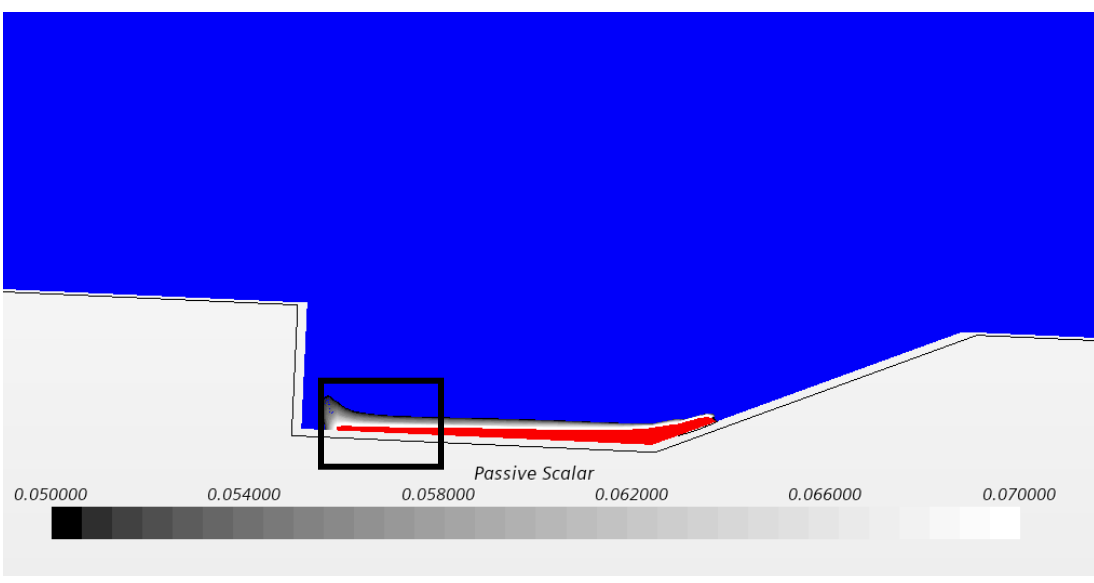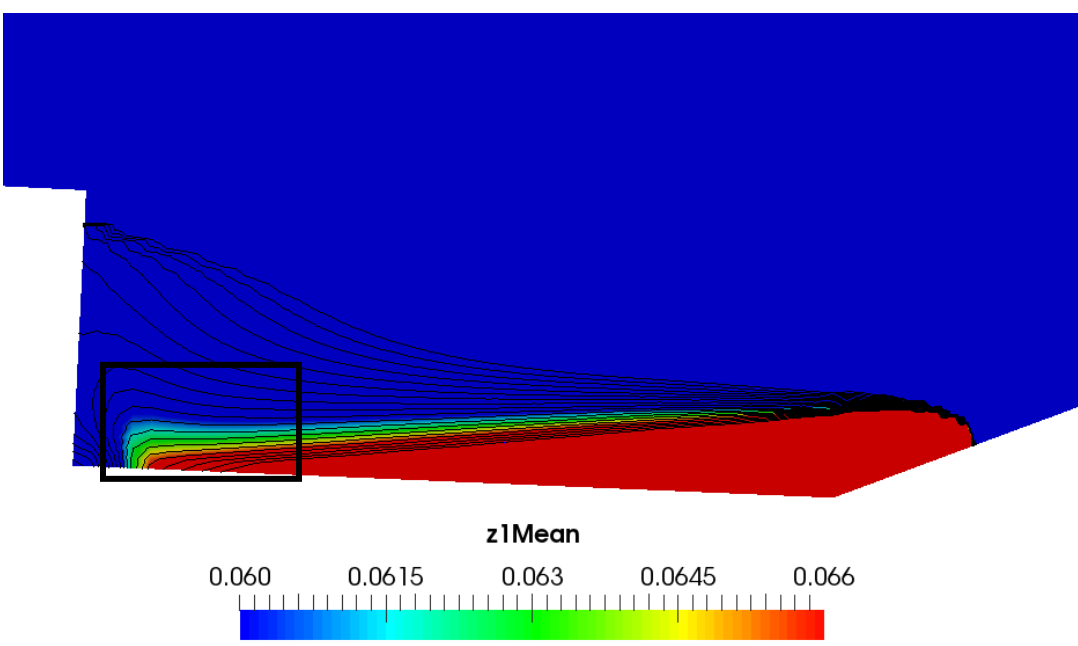

Figure 94: StarCCM Combustion Location using RANS

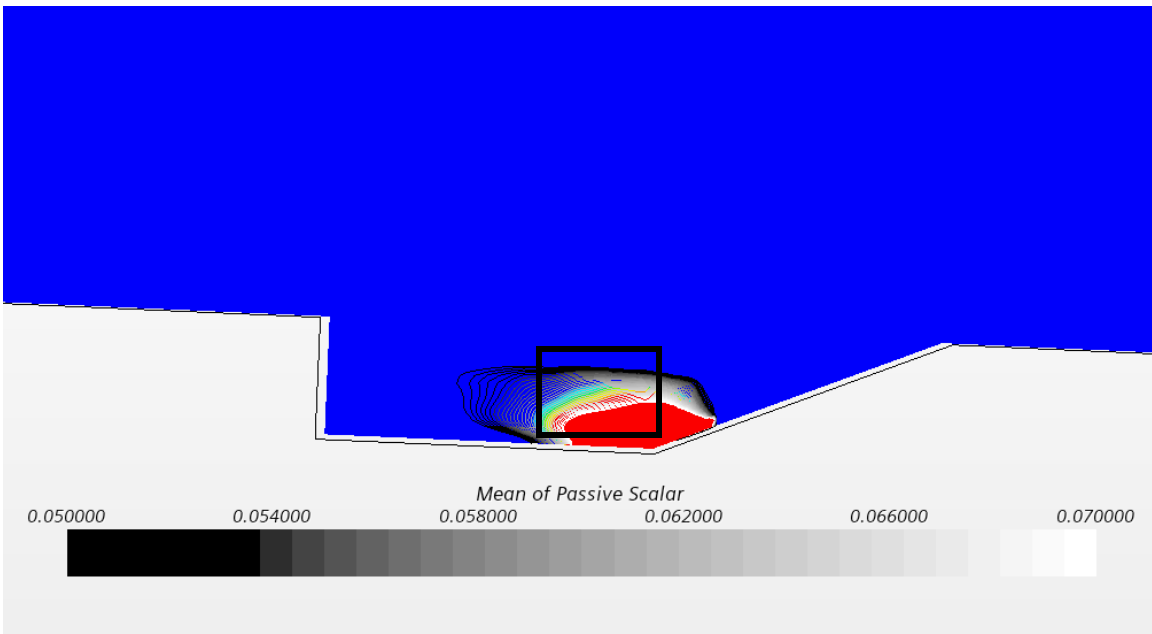*Figure 95: OpenFOAM Combustion Location using RANS*
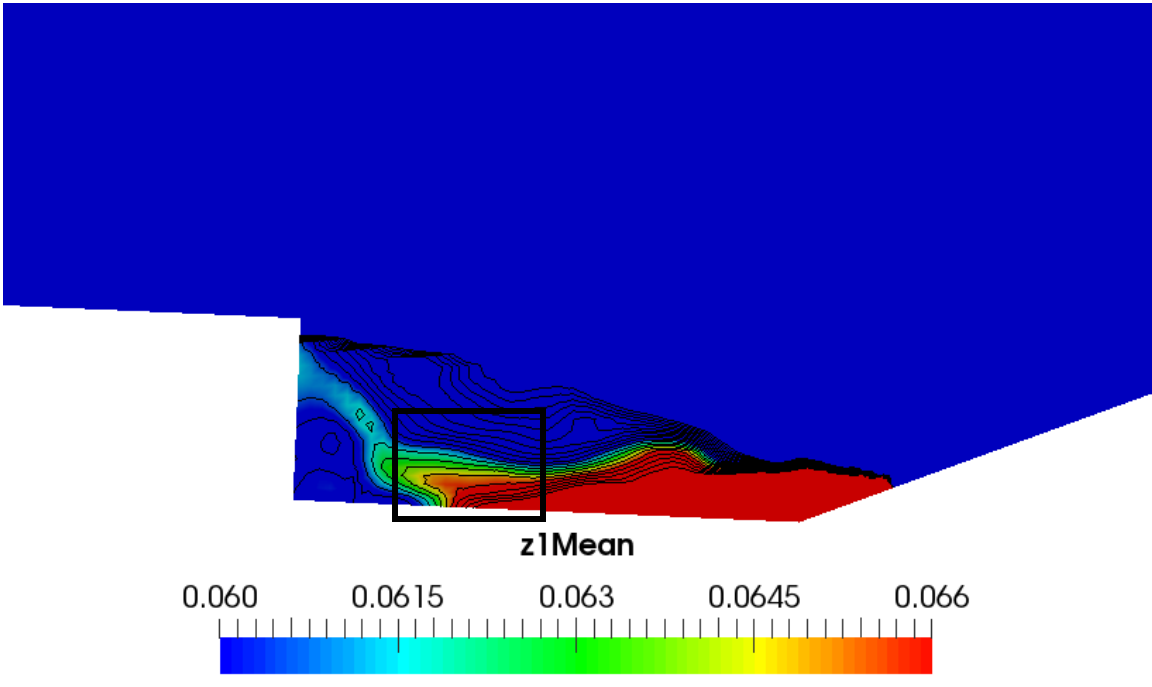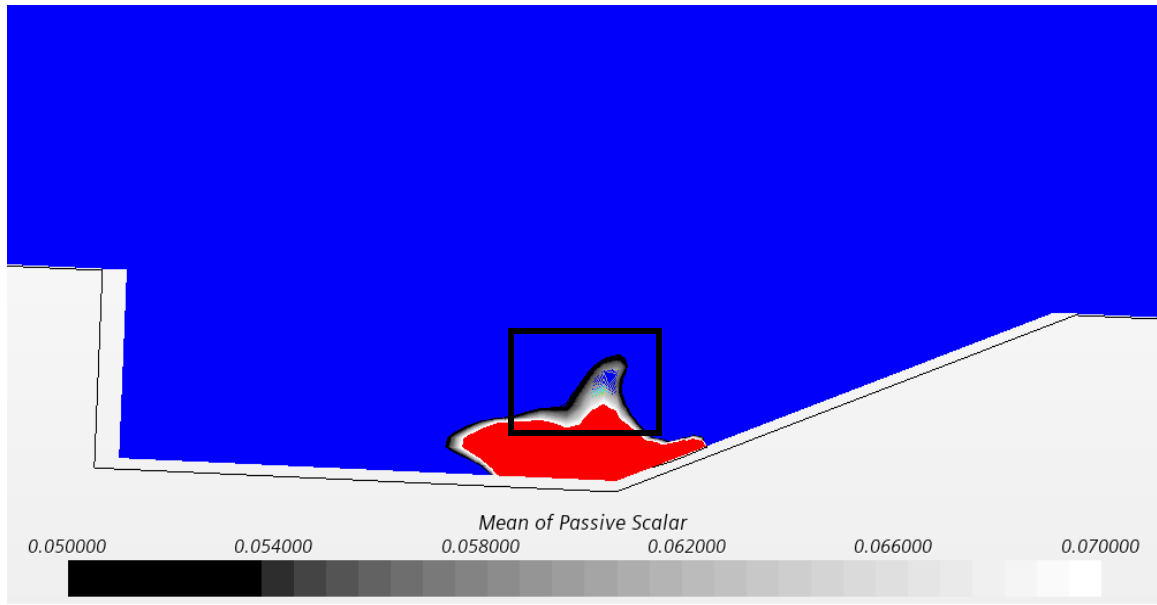
Figure 96: StarCCM Combustion Location using LES

Figure 97: OpenFOAM Combustion Location using LES

Figure 98: StarCCM Combustion Location using DES

Research Contribution

For the first time, this present research study contributes to the analysis of the passive scalar in a supersonic cavity flame holder. In this study, the passive scalar was analysed in both StarCCM and OpenFOAM and a comparison of the two was performed. The results are compared amongst the two CFD softwares, in addition to being compared to experimental data from the AFRL and previously published findings. The CFD approach was employed to accomplish this research using three-dimensional Navier-Stokes Equations. Looking at the numerical results, it is evident that the passive scalar can be used to give a simplified model of combustion within a supersonic cavity flame holder, but further research should be done to improve some of the solver physics for both StarCCM and OpenFOAM when trying to perform supersonic simulations.

The overall goal of this research was met. Effective RANS, LES, and DES models were built and found to be in good agreement when compared to experimental and published

data for both the normalized U and V velocity components. The DES offered a good middle ground for run time and accuracy. The LES model should give the most accurate results, but there are some physics solver issues present with the LES model when close to walls. In addition, grid resolution affects the results as well. The RANS model offers good insight but does not capture the eddies that are present. Overall, when compared to experimental data, all three models agreed with previous findings and prove that the passive scalar is a good alternative for showing fuel injection and combustion location. The OpenFOAM simulation results also proved to agree with the experimental and published data. Only RANS and LES cases were run in OpenFOAM. The RANS model gave slightly less accurate results than StarCCM but still compared well to previous findings. Looking at the LES model used in Open FOAM, the results slightly underpredicted the normalized U component freestream velocity but still agrees. As mentioned in previous research [4], LES cases, especially in OpenFOAM do have some difficulties capturing all physics. Although there are some discrepancies in the data, OpenFOAM offers promising results for the use of passive scalar, especially with a RANS case. Further research needs to be done to improve the LES physics modeling and further developing of the DES modeling.

CHAPTER 5: CONCLUSION AND FUTURE WORK

The conclusion of the thesis in this section provides some suggestions for future work in this area. Comparison of the passive scalar in StarCCM and OpenFOAM solvers were performed by numerical simulation using the typical operating parameters. The results obtained are summarized as follows:

- OpenFOAM, an open-source CFD code, does have the capability to solve supersonic flows but has its limitations. The LES solver could use some improvements and a DES solver needs more research to be fully developed.

- StarCCM and OpenFOAM both show that the passive scalar can be used to simplify and quicken the combustion process to determine where theoretical combustion will occur which allows for different fuel injection schemes and cavity shapes to be tested.

- The LES solver for both StarCCM and OpenFOAM has some success when solving supersonic flows, but more research needs to be conducted to fix some issues that include grid resolution and accurately capturing near-wall treatments.

This thesis has been mainly focused on analyzing passive scalar for a non-reacting case of ethylene in a supersonic cavity, leaving other supersonic cavity flame holder topics outside the scope of the thesis. The following ideas could be tested:

- Perform an in-depth analysis of the reacting case for both StarCCM and OpenFOAM, especially with StarCCM flamelet modeling.

- Perform further research to improve LES and DES models in OpenFOAM.

- Experiment with differing cavity geometries and injection schemes.

- Perform further research to assess a lighter fuel such as Hydrogen that has fewer equivalent properties to air.

- Perform simulations on a full-width geometry to assess results as periodic boundary conditions can get difficult.

REFERENCES

1. Milestones in the history of Scramjets. UQ News. (2002, July 27). Retrieved January 20, 2022, from https://www.uq.edu.au/news/article/2002/07/milestones-history-of-scramjets

2. Conner, M. (2016, April 4). X-43A (hyper-X). X-43A (Hyper-X). Retrieved January 20, 2022, from https://www.nasa.gov/centers/armstrong/history/experimental_aircraft/X-43A.html

3. Scramjet Engine - TD. ISRO. (n.d.). Retrieved January 20, 2022, from https://www.isro.gov.in/launcher/scramjet-engine-td

4. NASA. (n.d.). Branches. NASA. Retrieved January 20, 2022, from https://researchdirectorate.larc.nasa.gov/branches/

5. Peterson, D. M., & Hassan, E. A. (2016). Numerical predictions of mixing in a supersonic cavity flame holder. 54th AIAA Aerospace Sciences Meeting. https://doi.org/10.2514/6.2016-1899

6. Peterson, D. M., & Hassan, E. A. (2017). Hybrid reynolds-averaged and large-eddy simulations of combustion in a supersonic cavity flameholder. 55th AIAA Aerospace Sciences Meeting. https://doi.org/10.2514/6.2017-0339

7. Peterson, D. M., & Hassan, E. A. (2018). Hybrid Rans/Les of combustion in a supersonic cavity flameholder at mach 2 and mach 3. 2018 AIAA Aerospace Sciences Meeting. https://doi.org/10.2514/6.2018-1144

8. Wang, H., Sun, M., Yang, Y., & Qin, N. (2015). A passive scalar-based method for numerical combustion. International Journal of Hydrogen Energy, 40(33), 10658–10661. https://doi.org/10.1016/j.ijhydene.2015.06.148

9. Zang, B., US, V., Lim, H. D., Wei, X., & New, T. H. (2018). An assessment of openfoam solver on RANS simulations of Round Supersonic Free Jets. Journal of Computational Science, 28, 18–31. https://doi.org/10.1016/j.jocs.2018.07.002

10. Hassan, E., Boles, J., Aono, H., Davis, D., & Shyy, W. (2013). Supersonic jet and Crossflow Interaction: Computational modeling. Progress in Aerospace Sciences, 57, 1–24. https://doi.org/10.1016/j.paerosci.2012.06.002

11. Brodetsky, M. D. (2003). Experimental Study of Supersonic Flow Around Truncated Cones at Incidence. Journal of Applied Mechanics and Technical Physics, 44, 640–647.

12. Ruan, J. L., Domingo, P., & Robert, G. (2020). Analysis of combustion modes in a cavity-based scramjet. Combustion and Flame, 215, 238–251. https://doi.org/10.1016/j.combustflame.2020.01.034

13. Sebastian, R., Lürkens, T., & Schreyer, A.-M. (2020). Flow field around a spanwise-inclined jet in supersonic crossflow. Aerospace Science and Technology, 106, 106209. https://doi.org/10.1016/j.ast.2020.106209

14. Peltier, S., & Carter, C. D. (2015). Response of a mach 3 cavity flameholder to a shock-induced distortion. 53rd AIAA Aerospace Sciences Meeting. https://doi.org/10.2514/6.2015-0883

15. Qi, Y.-Y., Zhu, L., Liu, W.-L., Xu, B.-J., Ge, J.-R., Luo, F., & Jen, T.-C. (2017). Numerical investigation of various fuel injection angles on interaction in cold kerosene-fueled supersonic flow. Procedia Manufacturing, 7, 66–71. https://doi.org/10.1016/j.promfg.2016.12.018

16. Xiong, Y., Qin, J., Cheng, K., & Wang, Y. (2020). Influence of water injection on performance of Scramjet engine. Energy, 201, 117477. https://doi.org/10.1016/j.energy.2020.117477

17. Li, J., Zhu, G., Zhang, S., Yan, O., Li, W., & Qin, F. (2020). Two-stage fuel injection performance of RBCC under Scramjet Mode. Aerospace Science and Technology, 105, 106062. https://doi.org/10.1016/j.ast.2020.106062

18. Kummitha, O. R. (2017). Numerical analysis of passive techniques for optimizing the performance of Scramjet Combustor. International Journal of Hydrogen Energy, 42(15), 10455–10465. https://doi.org/10.1016/j.ijhydene.2017.01.148

19. Cao, D., Brod, H. E., Yokev, N., & Michaels, D. (2021). Flame stabilization and local combustion modes in a cavity-based scramjet using different fuel injection schemes. Combustion and Flame, 233, 111562. https://doi.org/10.1016/j.combustflame.2021.111562

20. Mastorakos, E., Bariaud, T.A., Poinsot T.J., "Numerical simulations of autoignition in turbulent mixing flows," Combustion and Flame, vol. 109, (1997) 198-223.
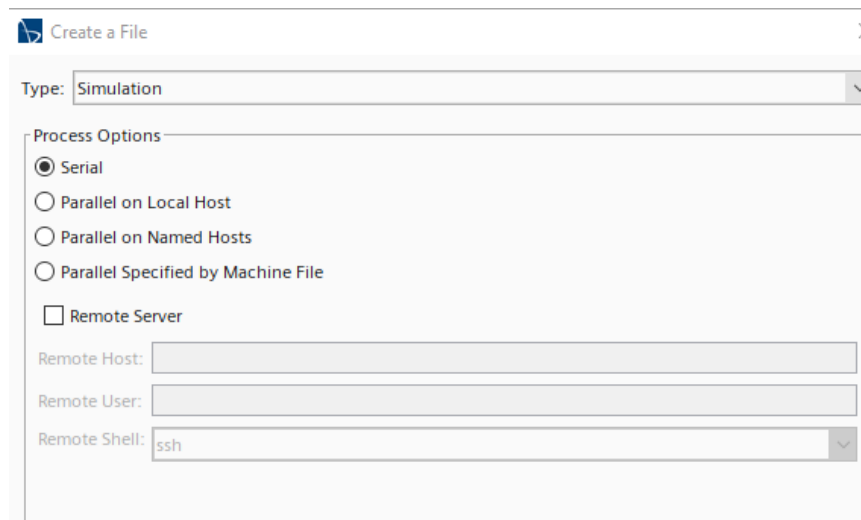
APPENDIX

Simulation Procedure for StarCCM+

The instructions with pictures provided below will briefly go through the steps of running

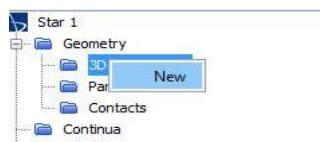the successful CFD simulation in StarCCM+ software.

Step 1: Create a new file

Select the type of processor, serial or parallel. If using parallel, choose the number of
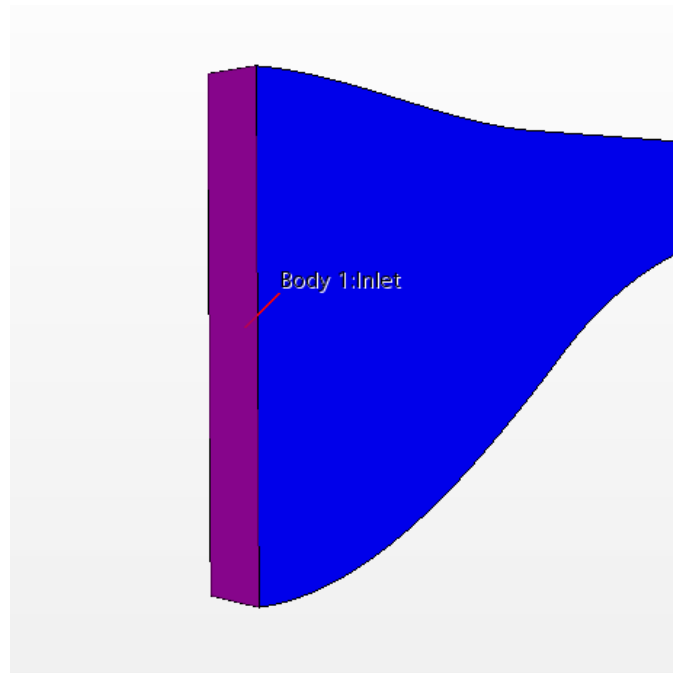
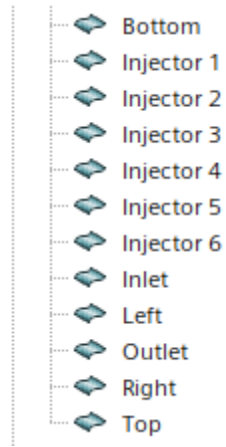processors. Click OK.

Step 2: Make a new CAD Geometry

After clicking new, a sketch is drawn to make the geometry, or a previously designed

CAD model can be imported. To import a CAD model, select import instead of create

sketch. In the case of this study, lines from a csv file were imported.
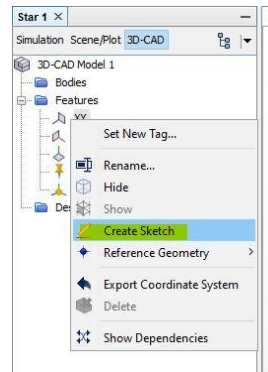
Step 3: After completing the CAD model, all the faces of the model must be named.

Step 4: Create Regions for the new CAD Model
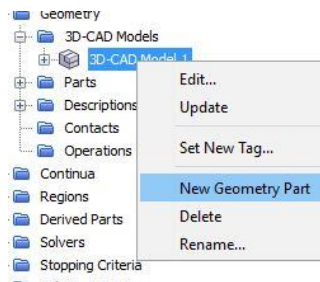
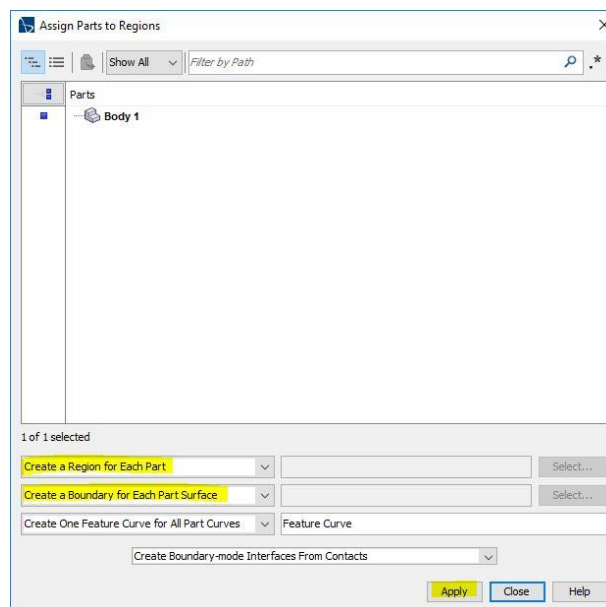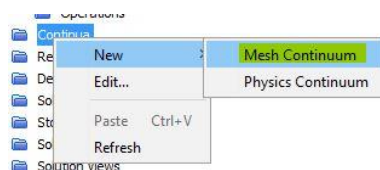The picture below will pop up. Typically, just use the default settings. Click OK.
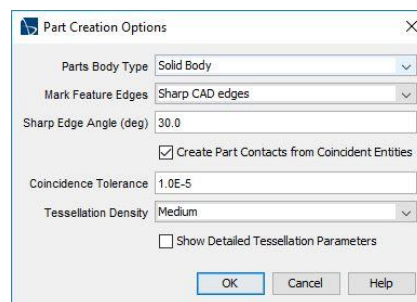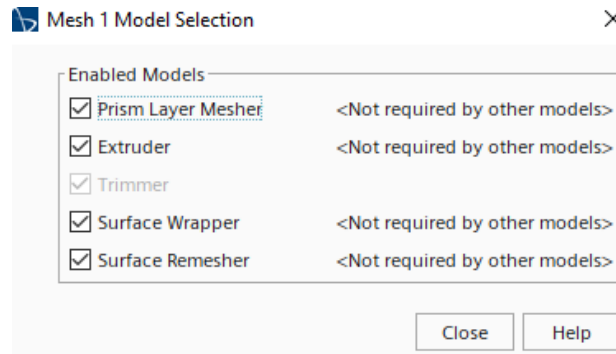
Step 5: Assign Parts to Regions
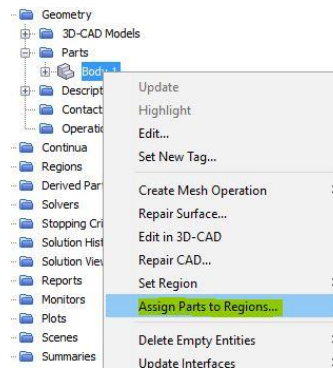
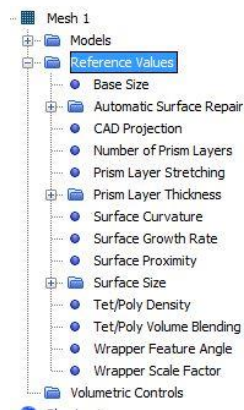Click one region for each part and one boundary for each part surface.

Step 6: Choose the Meshing Models
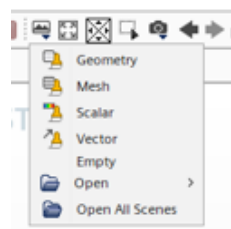
Step 7: Edit the meshing controls

Here the base size can be changed, as well as the number of prism layers, and so on.

Step 8: Click on the 'Meshed Cube' to generate a volume mesh for the CAD model.
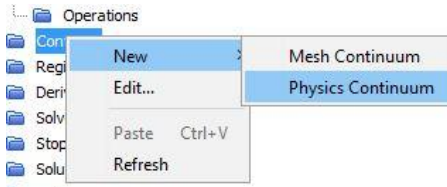

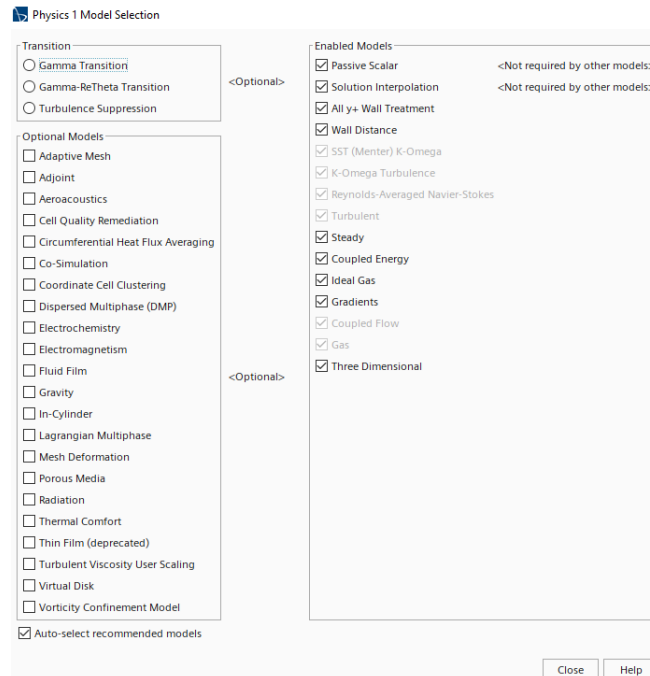Step 9: Create a Mesh scene to visualize the generated mesh of the CAD model.

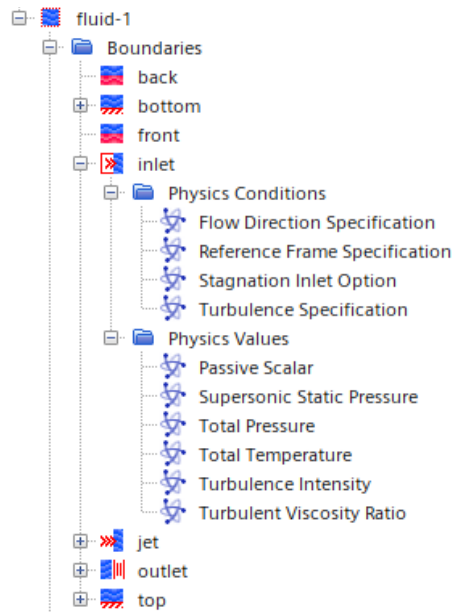Click the picture with the mountains and select mesh.

Step 10: Choose the proper Physics models

Select the appropriate physics models and click close.

Step 11: Control the physics for each region of the CAD model.

Right-click on each region to change the physics, boundary conditions, and set the values.

Step 12: Initialize the solution by clicking the green flag.

Step 13: Run the Simulation by clicking the picture of the man running.